DOTTORATO DI RICERCA IN CHIMICA

Convenzione tra
UNIVERSITÀ DEGLI STUDI DI TRIESTE
e
UNIVERSITÀ CA' FOSCARI DI VENEZIA

CICLO XXX

COVALENT FUNCTIONALIZATION OF GRAPHENE DERIVATIVES FOR NOVEL CARBON INTERFACES

Settore scientifico-disciplinare: CHIM06

DOTTORANDO / A
MANUEL VÁZQUEZ SULLEIRO

COORDINATORE
PROF. MAURO STENER

SUPERVISORE DI TESI
PROF. MAURIZIO PRATO

ANNO ACCADEMICO 2016/2017

Acknowledges

I have to write this acknowledges far from home, but the farther away you are the closer you feel to people.

First of all I would like to thanks to the person who gave me the opportunity to write these acknowledges, to learn as a scientist and growth as person: my supervisor Prof. Maurizio Prato. Thank you, I will be always grateful.

I am especially thankful to Dr. Alejandro Criado, professionally, I could not imagine a perfect lighthouse for this PhD as perfect as you, your guide and advise was essential to develop this work, personally I will always remember your stories and party-conversations. It was a pleasure.

Of course also thanks to ''Criados Jr.'' Arturo and Juampe my road trip labmates of this amazing world of graphene, the help and support that you provide me is invaluable. The countless talks about science and specially life I will always remember them. A large part of this PhD is yours. Thank you.

Thanks to all the collaborators during this PhD: Prof. Ester Vázquez and Dr. Jose Miguel González for their advices and help on the ball-milling exfoliation of graphene, Dr Elisabet Prats for the measurements of the electrical properties of graphene, Dr Victoria Bracamonte for being patient, nice and introduce me in the amazing world of the electrochemistry. I am also very grateful to GRAPHENEA S.A, especially to Alba Centeno and Amaia Zurutuza for all the help and support with CVD graphene. Collaboration is a fundamental step for human development.

I want to show all my gratitude to the technicians from University of Trieste and CICbiomaGUNE, their help and support is fundamental, you are heroes. Judith Langer for the Raman help, Marco Moller for the support of TEM/SEM images, Luis Yate for his help and kindness in XPS and a huge number of people who participate indirectly with their help: Michela, Franco, Manuela, Ricardo, Luigi, Javi, Prof. Mauro Stener, and of course Prof. Tatiana Da Ros due to your personality, always taking care of the people.

I am also grateful to the University of Trieste, CICbiomaGUNE and the European Union.

Personally, my hearth during this period is divided in two places, the wonderful Trieste ''*Go girado per giorni e notti per veder tutte le contrade, tutti i loghi dove passavo in un'età che purtroppo mai più ritornerà*.'' and the green Donostia. I met such a wonderful people, which helped me a lot.

In Trieste, thank you for the family group of Prof. Maurizio Prato, the great teatime with Ana, Arturo, Valentina, my crazy Agnieszka, and my amazing labmate Tanja, you gave me laughs and beautiful moments. Jose and Caroline for your advices, Ana and Dani for helping and hosting me all the time. Francesco for all the italian immersion that I learned. Iro and Panos for the great moments, María (happiness in person, thank you) and many others: Angela, Andrea, Davide, Cristina, Susanna, Zois, Luka, Francesca, Eva, Michele, Vicky, Federico, Alexa, Lorenzo… Also thank you to other people outside the lab, especially Mauro (the great man), Martu and Barcola colleagues.

In Donostia, thank you for the members of the group of Prof. Maurizio Prato, Blanca and Huilei (''XieXie''). Neils group, you are amazing as group and as persons, I enjoyed the coffees as much as paying futmondo clauses, to the funny Cris, the adorable Anna or many other members of the Biomagune family; Dorleta, Susana, Idoia, Carolina, Bea, Anabel, Ricard, Elena… thank you. Special mention to a ''little cute person'' for all the time we spent together, Nuria, I am sure you have a promising future. I cannot forget about my brother from the south, Antonio, en este mundo hace falta más personas como tú.

To the ''Compostelanos'', because I did not understand the meaning of friendship until I met you, even in the distance, I feel you close every day. To Iago, Anxo and Yolanda, you are simply great. Also to my bagpipe friends to bring me feelings that I only experience through the music. I should write a PhD about all of you.

I also want to thank my previous group from CIQUS. Thank you to my supervisor Dolores (contigo empezó todo) thank you to Sara, Sabela (the sweetest person I ever met) Manuel, García and Lojo. Thanks to my friends of the degree.

Y ya finalizando, quiero agradecer especialmente a una persona muy válida que me ha enseñado unos valores de trabajo y lucha en este PhD, a mi ''gatocán'' particular, mi eterna compañera de laboratorio, de piso, de viajes, pero sobre todo, a mi amiga. Siempre te has portado muy bien conmigo pero tu apoyo en esta última etapa ha sido indescriptible. En ocasiones me has enseñado luz cuando yo solo veía sombras. Muchísimas gracias **Jénnifer**.

He compartido un tercio de mi viaje con una mujer muy, muy importante; las circunstancias de la vida a veces une y separa caminos a su antojo, pero cuando llegamos al final no seríamos nadie sin las personas que nos han acompañado, especialmente por alguien que ha dado todo por mi. Hoy escribo esto sabiendo que gran parte de que esté aquí es por ti: muchas gracias **Paula**, ningún agradecimiento estará jamás a la altura de todo lo que me has dado.

E por último quero ter a oportunidade de agradecer a miña terra "terra donde m'eu criei" lugar de ledicia e morriña e de momentos únicos. O especial que me sinto ó ter unha familia que me deu tanto cariño e apoio. E máis particularmente moitas grazas **papá** por ser un exemplo en vida e moitas grazas **mamá** (a de antes e a de agora) por esa dulzura e cariño. Non teño palabras. GRAZAS

Time is pasing quickly but your remembers will be with me forever. Thank you very much to everybody

Manuel

A miña terra,
o meu fogar

Abstract

Graphene is an allotrope of carbon material with a unique set of properties. Since its discovery in 2004, the number of publications about this material grew significantly fast. In the first chapter of this work, a general introduction of these topics, an overview of this material and relevant characterization techniques are described.

Chemical functionalization of graphene is a topic of paramount importance, because it allows for the fine-tuning of material's chemical and physical properties. An additional challenge in graphene functionalization is the surface modification in a controlled way, in order to create novel carbon interfaces to introduce functional biomolecules, like DNA or proteins, which are commonly used in biosensors and bioelectronics.

This work discusses the exploration of conventional routes for the preparation and functionalization of graphene, with special emphasis in the underexplored aryne cycloadditions. Besides, the selection of a suitable graphene material for the setting of an electrochemical functionalization of graphene electrodes with future application as biosensor platforms was performed. Moreover, the development of an early-stage essay biosensor of a modified graphene electrode for the electrochemical detection of oligonucleotides. By last, the study of a novel, fast and scalable non-conventional functionalization under microwave irradiation that can solve common problems of the conventional modifications of carbon materials.

The present results could open a range of possibilities for the scientific community, paving the way to new functionalization protocols with fast, efficient, large-scale and green procedures to obtain more user-friendly graphene materials and to create novel organic interfaces on diverse graphene derivatives for the manufacture of future biosensors and bioelectronic devices.

Riassunto

Il grafene è un allotropo di materiale di carbonio con un insieme unico di proprietà. Dalla sua scoperta nel 2004 il numero di pubblicazioni su questo materiale è cresciuto molto velocemente. Nel primo capitolo di questo lavoro, viene descritta una introduzione generale di questi argomenti, con una panoramica di questo materiale e delle tecniche di caratterizzazione pertinenti.

La funzionalizzazione chimica del grafene è un argomento di fondamentale importanza, poiché consente di modificare le proprietà chimiche e fisiche del materiale. Un'ulteriore sfida nella funzionalizzazione del grafene è la modifica della superficie in modo controllato, al fine di creare nuove interfacce di carbonio per introdurre biomolecole funzionali, come il DNA o le proteine, che sono spesso utilizzate in biosensori e bioelettronica.

Il Capitolo 2 discute l'esplorazione delle vie convenzionali per la preparazione e la funzionalizzazione del grafene. Con particolare enfasi nelle cicloaddizione di aryne. Inoltre, la selezione di un adatto materiale di grafene per l'impostazione di una funzionalizzazione elettrochimica di elettrodi di grafene con applicazioni future come piattaforme di biosensori. Peraltro, lo sviluppo di un biosensore di un elettrodo di grafene modificato per il rilevamento elettrochimico di oligonucleotidi. Infine, lo studio di una funzionalizzazione non convenzionale nuova, veloce e scalabile sotto irradiazione a microonde che può risolvere problemi comuni delle modifiche convenzionali dei materiali di carbonio.

I risultati attuali potrebbero aprire una serie di possibilità per la comunità scientifica, aprendo la strada a nuovi protocolli di funzionalizzazione con procedure veloci, efficienti, su larga scala e verdi per ottenere materiali di grafene più *user-friendly* e per creare nuove interfacce organiche su diversi derivati di grafene per la produzione di futuri biosensori e dispositivi bioelettronici.

Index

List of abbreviations

AFM: Atomic-force microscopy

AIBN: 2,2-Azobis(2-metylpropionitrile)

CNMs: Carbon nanomaterials

CNTs: Carbon nanotubes

CV: Cyclic voltammetry

CVD: Chemical vapour deposition

CVDG: Chemical vapour deposited graphene

DI: Deionized

DMF: N,N-dimethylformamide

DNA: Deoxyribonucleic acid

DWCNTs: Double-walled carbon nanotubes

EDC: 1-Ethyl-3-(3-dimethylaminopropyl)-carbodiimide

Eq: Equivalents

FD: Functionalization degree

FLG: Few-layers graphene

GCE: Glassy carbon electrode

GICs: Graphite intercalation compounds

GO: Graphene oxide

IT: Interfacial tension

ITO: Indium tin oxide

MAC: Microwave-assisted chemistry

MW: Microwave

MWCNTs: Multi-walled carbon nanotubes

NHS: N-hydroxysuccinimide

NMP: N-methyl-2-pyrrolidone

NMR: Nuclear magnetic resonance

ODCB: *Ortho*-dichlorobenzene

PBS: Phosphate buffer saline

PET: Petroleum ether

REF: Reference

rGO: Reduced graphene oxide

RNA: Ribonucleic acid

SEM: Scanning electron microscope

STM: Scanning tunnelling microscopy

SWCNTs: Single-walled carbon nanotubes

TEM: Transmission electron microscopy

TFA: Trifluoroacetic acid

TGA: Thermogravimetric analysis

THF: Tetrahydrofurane

UV-Vis: Ultraviolet-visible

XPS: X-ray photoelectron spectroscopy

1. INTRODUCTION

Carbon, the sixth element of the periodic table, is one of the most abundant elements in the universe[1] and in the earth crust.[2] Carbon atoms can be found in different forms or allotropes.[3] In the last decades, many allotropes of carbon have been discovered, each one having different chemical and physical behaviours: the cheapest of the carbon materials is graphite, which it is opaque and black; the most expensive is diamond, which is, on the other hand, the most transparent less conductive allotrope. To explain these properties, it is important to remark the good flexibility of carbon to form chemical bonds, *i.e.* the good capacity to accommodate in different hybridizations.

In this thesis, our main goal is to understand the chemistry of a member of the family of carbon nanomaterials: graphene, which is the one of the most recently discovered allotropes of carbon with interesting and amazing properties for electronics and biomedicine.

1.1 Carbon nanomaterials

Carbon nanomaterials (CNMs) are one of the allotropic forms of carbon with at least a single unit sized in the nanoscale. Many allotropic forms of carbon are known nowadays (Figure 1).

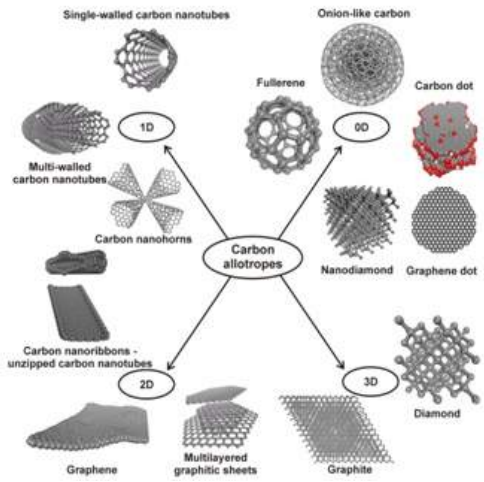

Figure 1. The classification of carbon nanomaterials depending on the number of dimensions that are confined to the nanoscale size. Adapted from Gerogakilas *et al.*[4]

In 1985, the revolution of carbon nanomaterials began with Kroto, Curl and Smalley. The three scientists discovered a spherical organic molecule

composed of sixty sp^3-sp^2 carbon atoms, named Buckminsterfullerene or C_{60},[5] with a powerful use in solar cells.[6] Several years later, in 1991, Iijima[7] discovered another member of the family, the carbon nanotubes, a rolled-up layer of sp^2 carbon atoms. The direction that the polyaromatic layer is rolled-up determines the properties of the carbon nanotube: from metallic to semiconductive. Within the carbon nanotubes, we can distinguish between multi-walled carbon nanotubes (MWCNTs), double-walled carbon nanotubes (DWCNTs) and single-walled carbon nanotubes (SWCNTs), depending on the number of layers they are produced. In any case, this material has excellent thermal, mechanical and electronic properties.[8]

Beside all the applications, a new revolution in the carbon nanomaterials field designed the guidelines of the future researchers. It started in 2004 with the discovery of graphene by Novoselov and Geim.[9] Graphene can be represented as a single layer of his parent carbon allotrope, graphite. This was the first time than a 2D structure was isolated, a concept that was previously considered as thermodynamically unstable. The discovery of this material implied a new field within the material science: the 2D materials. The number of publications about graphene grew exponentially (Figure 2), especially after the Nobel Price given to the discoverers in 2010 and the financial efforts that the public institutions gave to the study of graphene.

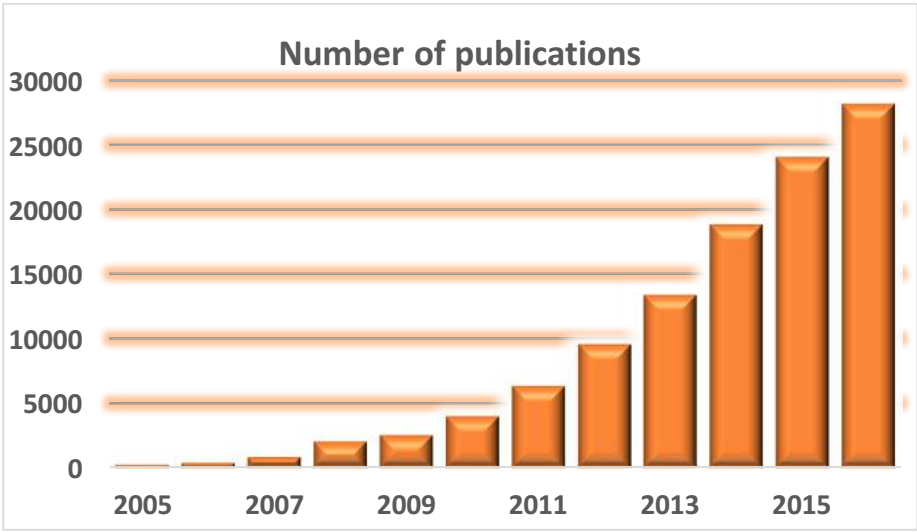

Figure 2. Number of publications of graphene during the last years.

This PhD thesis made all the efforts to understand better (the chemical behaviour of) this material and to give solutions to some of the problems and limitations that involve graphene science.

1.2 Properties of graphene

All graphene atoms are displayed in a planar aromatic structure, thus being equivalently accessible to interact with the media or any reagent. Graphene has unique properties, being remarkable their mechanical, optical and electronic behaviours, although they could vary depending of the defects present on the surface of the material.

Even though graphene is a light material (0.77 mg m^{-2}), its mechanical properties, obtained with the Atomic Force Microscopic (AFM) technique, showed a stress-strain curve of 130GPa and a Young modulus of 1 TPa, one of the largest values of the materials.[10] This Young modulus value indicates that graphene has large elasticity and it could withstand high pressures without any deformation or rupture; such resistivity comes from the net of double bonds from the sp^2.

The electrical properties of graphene come from its structure. Several studies, indicate that graphene is a semiconductor with a zero band gap, *i.e.* the difference between the valence and the conduction band is zero without overlapping. The presence of π bonding orbitals and π antibonding orbitals is so high than the resulting bandwidth is 0 eV. The combination of the atomic orbitals generates delocalized orbital states with a Fermi level of energy. The electronic mobility on graphene as high as 10^6 ms^{-1}, and its behaviour is defined by Dirac equation. The charge mobility[11] is defined as $2 \cdot 10^5$ cm^2 V^{-1} s^{-1} with a high concentration (10^{12} cm^2).[12] This makes graphene a material with low resistivity (10^{-8} Ω·m). Due to these unique and extraordinary properties, graphene becomes an exceptional substitute for silicon in the fabrication of nanodevices.

Graphene has the thickness of a single atom; this means a high optical transparency. Light transmittance is a good measurement to detect the thin films of graphene materials. Figure 3 shows an example of the variation in the transmittance between one and two layers of graphene.[13] This high transparency, together with its high conductivity, makes graphene as an ideal material for the fabrication of transparent electrodes for photovoltaic cells,[14] LEDs screams[15] and touch displays.[16]

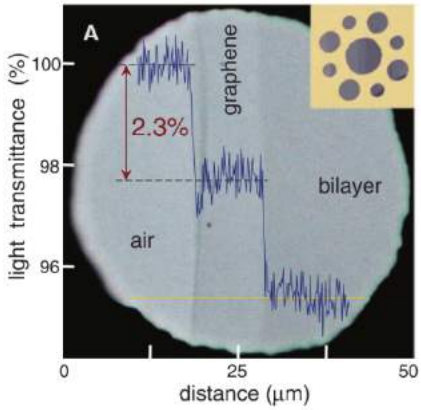

Figure 3. Optical microscopy looking through one-atom-thick crystal, a metal support structure with several apertures with graphene crystallites placed over them where 97,7% of transparency is observed. Adapted from Nair *et al*.[13]

Regarding the thermal properties of graphene, it has been determine that this material has the higher thermal conductivity of all known materials so far: 5000 W m^{-1} K^{-1}.[17] Thus, it becomes an ideal candidate for the fabrication of thermal devices with high thermal conductivity. The main drawback in the use of graphene in any device is the low interaction of the material with the substrate attached, what comes from the limited heat transfer in the *z* axis due to Van der Waals forces.

In summary, all the graphene properties make it a suitable material for a large variety of applications as it showed Ferrari *et al.* (Figure 4).

Figure 4. Properties and applications of graphene. Adapted from Ferrari *et al.*[18]

1.3 Characterization methods of graphene and CNMs

For a good understanding and confidence in the production and functionalization of CNMs, a well characterization of the material becomes an essential tool. It is worthy to note that material science, as opposed to conventional organic synthesis, needs a combination of a larger number of different techniques for a reliable result. Here, we report a summary of the main techniques commonly used to characterize CNMs.

1.3.1 Raman spectroscopy

Raman spectroscopy is a powerful and important technique for CNMs, specially for carbon nanotubes and graphene. The singular function of this spectroscopy is based on the inelastic scattering of monochromatic light irradiation, which is a unique fingerprint of each material and gives information of their defects, stacking of layers or crystalline size.[19]

All carbon materials, due to their similar chemical structure, display a similar Raman spectrum. Graphene shows significant bands: (i) the graphite band (G band), which appears at 1580 cm^{-1} and is common on all graphitic nanomaterials, is associated to the longitudinal optical phonon mode; (ii) the D band, appearing around 135k 0 cm^{-1}, is caused by the breathing modes of sp^2 carbon rings and requires a defect for its activation; (iii) the 2D band,

observed between 2500 to 2900 cm^{-1}, is a second-order mode that is related to the number of graphene layers. The intensity of the D band related to the G band is commonly used to determine the level of defects of graphene materials. The increase of the I_D/I_G ratio between pristine graphene (graphene without modifications) and functionalized graphene (graphene after modifications) indicates the covalent functionalization due to the introduction of sp^3 atoms in the carbon lattice , (Figure 5A).[20] The position of the bands varies with the energy of the laser and its shape with the number of stacked layers.

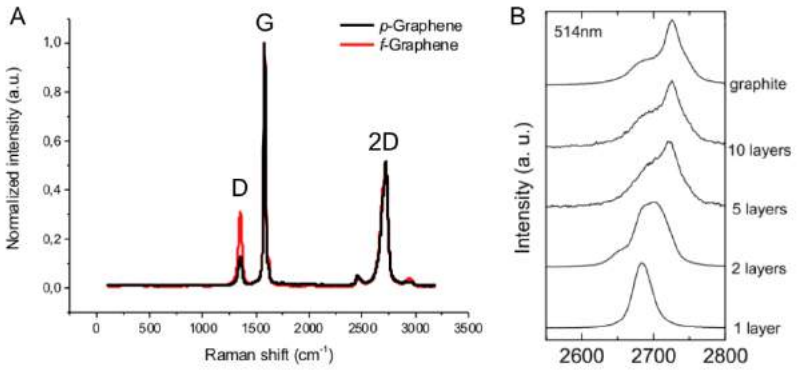

Figure 5. A) Raman spectra of pristine graphene (*p*-Graphene) and functionalized graphene (*f*-graphene). B) 2D band of different stacked layers of graphene. Adapted from Ferrari *et al*.[21]

Figure 5 shows how 2D band can give additional information: the width, the shape and the intensity have a direct relation on the number of stacked graphene layers. Thus, monolayer graphene presents a homogeneous 2D band with higher intensity than the G band, bilayer graphene has similar intensity than the G band and an amorphous shape, and few-layers graphene (FLG) presents broader and decreased intensity (similar as for graphite). Moreover, it is also known that doping onto the graphene surface does have an influence in the intensity of this 2D band.[22]

Other materials, such as carbon nanotubes, show other characteristic peaks as the RBM (between 100-300 cm^{-1}). These peaks appear due to their cylindrical shape, which causes vibrations in the radial direction of the tube.[23]

1.3.2 Thermogravimetric analysis

Thermogravimetric analysis (TGA) is an important characterization technique for carbon-based nanomaterials. In general words, TGA is based on a high-resolution balance that measures very precisely the weight variation of a sample along the time while increasing the temperature due to its combustion. The analysis can be carried out under different atmospheres, being N_2 and air the most common ones. Under air, all carbon-based materials are degraded, giving information about the quantity of metallic residues, while under inert atmosphere they are stable up to high temperatures (*ca.* 800 ºC). In any case, when functionalized they are less stable since the bonds formed in the functionalization process are more labile. Thus, by comparing the pristine with the functionalized CNM, we can determine a degree of functionalization (Figure 6) [24]

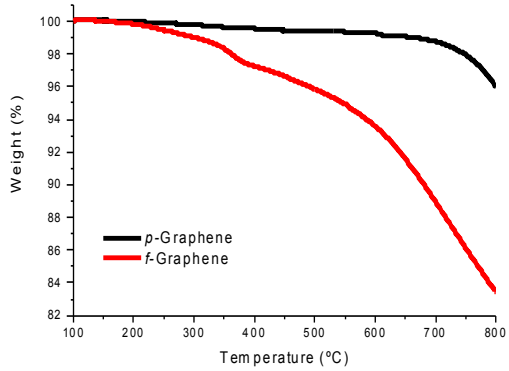

Figure 6. TGA profile of *p*-Graphene (black) and *f*-Graphene (red) under N_2.

1.3.3 X-ray photoelectron spectroscopy

X-ray photoelectron spectroscopy (XPS) is a very powerful technique to obtain information about the chemical composition of the surface of the analysed material. The sample is irradiated with an X-ray gun causing the emission of photoelectrons that are able to pull out the core level electrons of the sample. This X-ray gun is able to penetrate deep into the sample (10 nm depth).[25] After the quantification of the core electrons, the resultant energy (eV) is characteristic for each compound, being thus possible to elucidate the composition of the sample. This tool is important when new molecules are introduced to carbon-based samples through functionalization; in our case, we are able to quantify in the *f*-graphene the new compounds attached to the surface of the material. With high

resolution equipment and mathematical data processing, we can get information not only on the atomic composition of the surface, but also on the chemical identity of the corresponding atom.

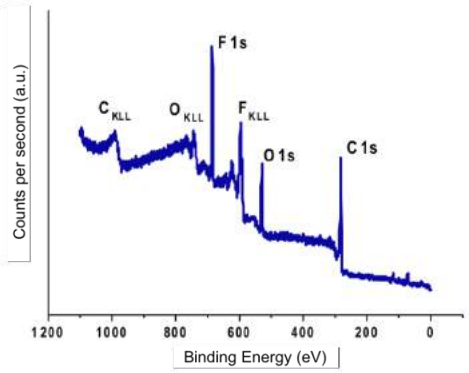

Figure 7. Survey of a functionalized graphene with fluorine-containing molecules.

1.3.4 Microscopy techniques

The size scale of nanomaterials needs a nanometric resolution microscopy. Morphological information as diameter, length and thickness of graphene (number of layers) can be determined by these techniques:

- Atomic force microscopy (AFM) is a technique that slightly interacts with the surface of the sample through a thin tip and due to piezoelectric behaviour. the corresponding tip can do nanometer-sized movements giving a precise scanning of the surface roughness.[26]

- Scanning electron microscopy (SEM) is a technique used to study the surface topography of a conductive material at the micro and nanoscale. The sample is irradiated with an electron beam and the image is generated from the scattered electrons of the sample. For non-conductive samples, a previous treatment of sputtering is needed.

- Transmission electron microscopy (TEM) gives a nanometric resolution. Samples are irradiated with a beam of electrons that directly passes through them. The detected signal by a camera is automatically processed by a software to create a 2D image of the corresponding structure. The interaction of the sample with the beam depends on the electron density; thus, metals provide good contrast and are easy to

identify, while organic matter can decompose during the laser irradiation.

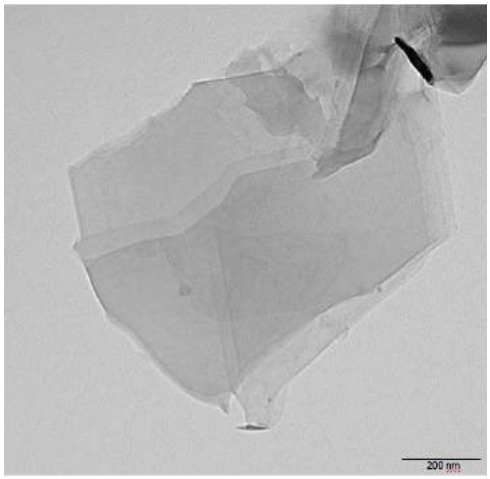

Figure 8. TEM image of a FLG.

1.4 Production of graphene

The production of graphene is a topic of paramount importance. On one hand, development of synthetic methods for obtaining GBMs for research purpose is almost enough.[27,28] On the other hand, after thousands of research publications, the industry of graphene is still in an early stage. Some companies are able to employ scalable and efficient GBMs production methods.[29] However, the preparation of high-quality graphene has still a lack in the production, not only because it requires large-scale procedures and high-cost methods, but also because they currently present different problems as reproducibility, homogeneity and long time.[30]

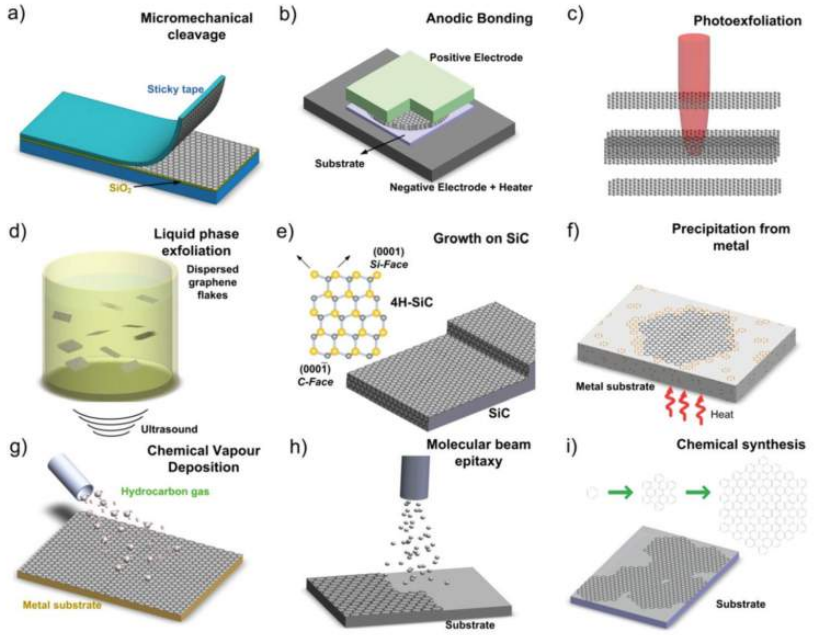

Figure 9. Schematic illustration of the main experimental procedures to produce graphene. Adapted from Ferrari *et al*.[18]

The production of graphene can be obtained by bottom-up approaches, as for example chemical synthesis of size-controlled nanographenes;[31,32] or by top-down methods techniques from bulk material,[33] for instance, graphite exfoliation. Usually, graphene needs the combination with other materials for its production stabilization, including support materials for its maintenance. The first synthetic method used was micromechanical cleavage (or mechanical exfoliation, Figure 9a), which has a fundamental use in research. It has the advantage of an easy identification of the flakes by elastic and inelastic scattering (Figure 10), although is not feasible for a large-scale production since the maximum sample size is around 1 mm. Micromechanical cleavage is usually supported onto silicon substrates. This represents the starting proof of principle for graphene-based devices, since graphene onto silicon substrates are still extensively studied due to the simple and easy production of this material.

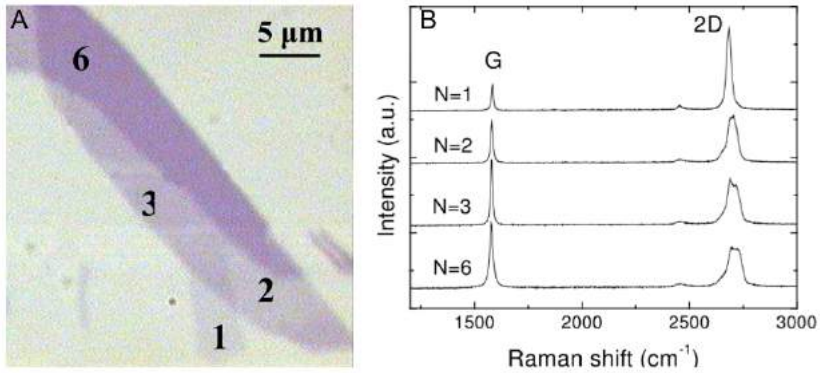

Figure 10. Optical image of mechanically exfoliated graphene where the number of flakes is easy to identify (A) and Raman spectra of graphene with different number of layers(N) (B). Adapted from Casiraghi *et al.*[34]

The extraction of layers of graphite is possible due to the use of graphite in liquid environments and the use of ultrasounds for the exfoliation of the bulk material.[35] Liquid phase exfoliation (Figure 9d) represents an easy and low cost method. It has three main steps: dispersion of the material in an optimum solvent, exfoliation under sonication and purification or separation of the resulting dispersion. The separation usually requires ultracentrifugation.[36,37] The yield of this procedure (which represents the ratio between dispersed graphitic material and starting graphite) is low, and could be determined by optical absorption spectroscopy using the Lambert-Beer Law.[37]

The exfoliation of graphite *via* ultrasonication can be controlled by hydrodynamic shear-forces.[38] The ideal solvents for the exfoliation are those that minimize the interfacial tension between the liquid and graphite layers. The interfacial tension (IT) is an important factor to take in account: high IT values results in high tendency of the layers tend to adhere to each other, being then higher the energy required to separate two flat surfaces in contact, thus the graphene layers.[39] Liquids with high surface tension are the best solvents to form stable suspensions of graphene and graphitic layers due to the minimization of the IT between graphene and solvent. The most common solvents used in this type of exfoliation are NMP, DMF and ODCB.[37] The use of perfluorinated aromatic compounds were also described as solvents giving good yields. [40]

Despite the advantages of this approach, its principal drawback is the use of large volume of solvent, which are usually highly toxicity. As an alternative,

aqueous media approaches became an eco-friendly approach,[41] although it requires the addition of surfactants. Another alternative is the use of mixed-solvents, two mediocre solvents could be combined into good solvents for the exfoliation and convert the procedure in a facile and green preparation with the use of solvents like water or acetone.[42]

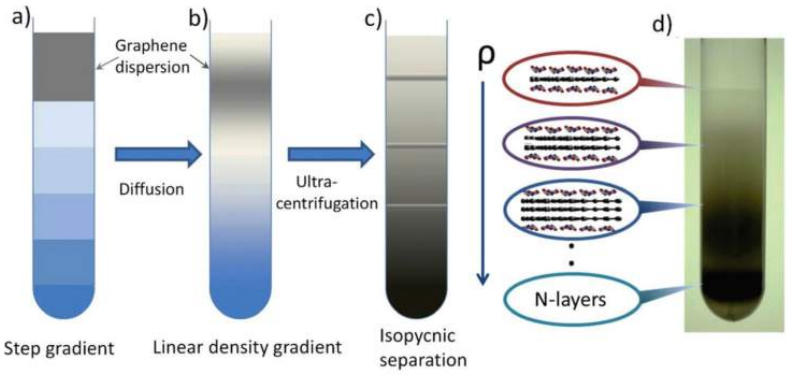

Figure 11. Description of the behaviour of the graphene dispersion with the use of surfactants and it separation. Adapted from Ferrari *et al.*[18]

Liquid phase exfoliation becomes an easy and scalable process. The resulting dispersion can be is feasible for the deposition of graphene thin layers onto different rigid and flexible substrates through drop casting, spin coating or vacuum filtration, thus giving rise to a wide range of applications that include conducting inks,[43] thin films[37] and composite materials, among others.[44] However, its main disadvantage is the low quality of the obtained material, in terms of number of layers.

A higher quality graphene is the chemical vapour deposited graphene (CVDG). Chemical vapour deposition (CVD) is a chemical process where a substrate is exposed to a volatile precursor which decomposes and is deposited on the substrate surface.[45] The main difference between the diverse CVD methodologies is the gas delivery system. The first studies were focused on the catalytic and thermodynamic activity of the metal surfaces in the presence of (amorphous) carbon. In 2004 the focus shifted to the growth of graphene. Some attempts were performed like the use of ethylene precursor over the Ir steps edges.[46] However, the first large area of CVD growth graphene was described in 2009 by Xuesong *et al.*[47] on polycrystalline Cu foils, using thermal catalytic decomposition of methane. The use of Cu became a cheaper approach.[48] In 2010, this methodology was

scaled-up in a production of CVDG up to 30 inches by Bae *et al.* (Figure 12).[16]

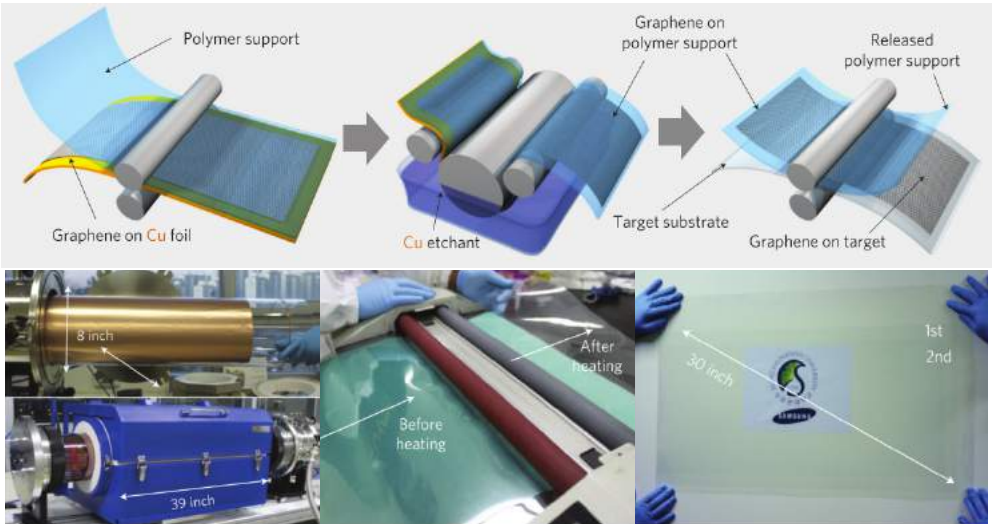

Figure 12. Protocol of the roll-production of graphene films by CVD. Adapted from Bae *et al.*[16]

In summary, the growth mechanism could be explained as a decomposition of carbon atoms from hydrocarbons which nucleate and grow on Cu in large areas.[49] The growth factor can be controlled by the temperature and the pressure: low pressures and temperatures around 1000 ºC are ideal for large single crystal domains.[50]

In general, the growth on Cu and metals has a main disadvantage: the formation of grain boundaries due to the difference in thermal expansion coefficient between Cu and graphene.[51] This fact favours the formation of undesired wrinkles[52] on the surface of graphene, easily detectable by different microscopies,[49] that cause significant device degradation due to the defect scattering (Figure 13).

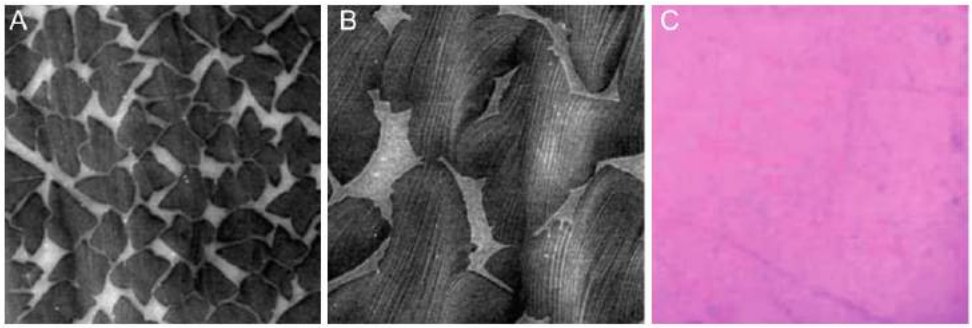

Figure 13. (A and B) SEM images at different temperatures and pressures. (C) Optical image of the wrinkles. Adapted from Li *et al.*[49]

The presence of the supporting substrate modifies the graphene properties. There is a lack in the literature about how this interaction affects directly to the electrical behaviour of graphene and a deeper study to fulfil this gap is still needed.[53] These interferences can be solved by the application of some surface treatments that can provide control on the graphene properties. For that reason, it is important to know the material requirements and the specific application to control factors as the growth conditions, substrate choice and pre-treatment. Some studies about the reactivity of CVDG were published, although more research on this field is still to be done.[54]

For applications of CVDG, the transfer of the graphene layer to a particular substrate, different than the Cu, is mandatory. For that reason, transfer methods became a critical point in the preparation process. The procedures are time consuming, expensive and nonenvironmental friendly. Normally they consist in the protection of graphene with a polymer mask, followed by the etching of the metal catalyst in solution to release the graphene film in the liquid to then transfer it to the target substrate.[55] However, this method leaves residues on the graphene surface (dopants) that can affect to its reactivity and properties and requires handling skills affecting the yield and the reproducibility. Up to date, few studies showed new systems for an automatic transfer of CVDG,[56] by using vacuum and high temperatures,[57] thus minimizing the polymer residues.[58] The development of new strategies for the stabilization of the dopant agents on the graphene surface is needed for a standard commercialization. CVD is a powerful technique to produce graphene, but the development of reliable, environmentally friendly, fast and economic approaches for large scale production of this material is still on demand.

A third method to produce graphene is the thermal decomposition of SiC, where a direct-growth process on a semiconductor surface is performed. This approach allows an extent control on the number of layers, quality and uniformity. However, it is an extensive method and has size limitations.[59]

In conclusion, there are several methods to produce graphene in different qualities and costs. It is important to know what kind of application is the material going to be used in to choose the best method to manufacture the desired device, considering the quality and the price ratio of the material (Figure 14).[60]

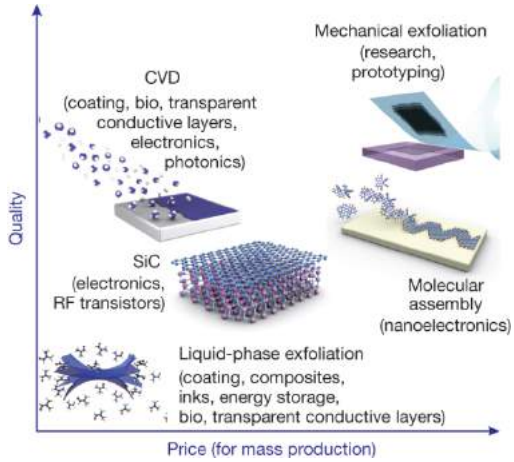

Figure 14. Classification of several production techniques of graphene. Adapted from Novoselov *et al*.[60]

1.5 Graphene oxide and reduced graphene oxide

The combination of graphite with strong oxidants and concentrated acids results in graphene oxide, well-known oxidation since 1958.[61] Some proposals about its structure determined the presence of several oxygenated functional groups: most of the oxygen functional groups come from epoxy and hydroxyl groups on the basal plane, and phenol, carboxy, carbonyl, lactone and quinone at the edges of the sheet. These studies proposed an approximately structure, but the precise atomic structure is difficult to elucidate. The relative size of the sheets depends on the grade of oxidation. GO contains a large number of defects, and Raman spectroscopy shows high and broad D bands. Because of the loose of aromaticity and the presence of oxygenated groups, water dispersibility of the material is

significantly improved with respect the pristine graphene, making it a very promising material for a different set of applications, including drug delivery and biosensing.[62,63] On the other hand, the electron transfer occurs at the edges or at the defects points, but not at the basal plane as for pristine graphene sheets.[64]

GO can be also used as a starting material for the synthesis of a new kind of CNM, called reduced graphene oxide (rGO).[65] Using the thermal, chemical or electrochemical reduction of GO, the partial recover of sp^2 carbon atoms can be achieved.[66]

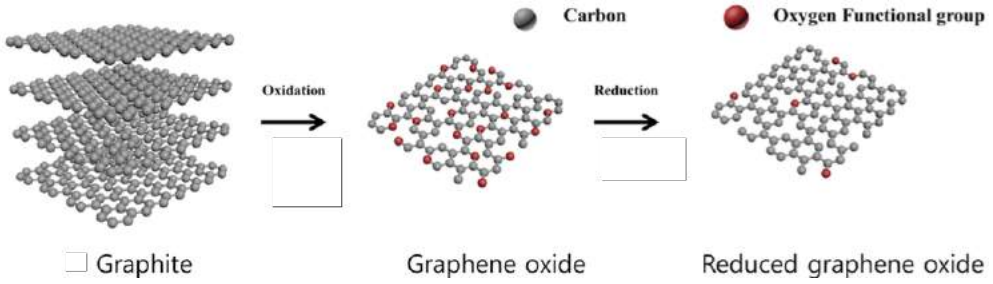

Figure 15. Scheme of the production of GO and rGO. Adapted from Byung *et al.*[67]

Both GO and rGO materials are highly used in electrochemical application and represent a new generation of electrodes.[68] In this thesis, we will study their preparation, handling, understanding and modification of these derivatives of graphene, since they can provide new opportunities for further applications or the improvement of the stablished ones.

With all mentioned above and due to increasing number of publications of graphene derivatives, scientific community demanded a global classification method with a precise vocabulary for the family of GBMs. In 2014,[69] Wick *et al.* reflected on the use of the term *graphene* and how was not always used in a precise way by scientists. For that reason, they developed a nomenclature model considering three parameters: the number of layers, average of the lateral dimensions and atomic carbon/oxygen ratio. This classification framework gives a starting point for a categorization of different GBMs (Figure 16).

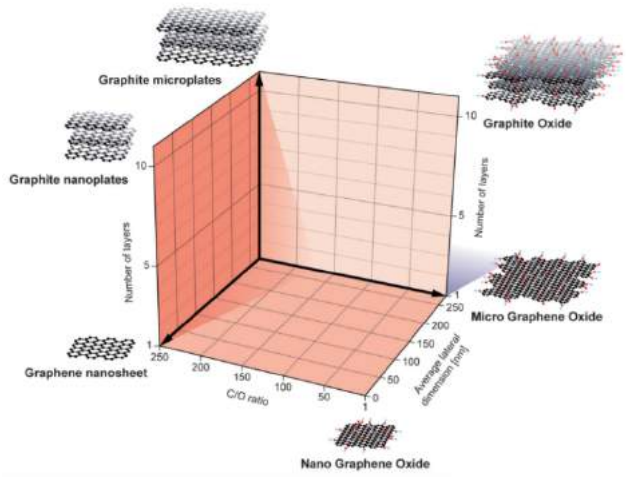

Figure 16. Classification of different graphene derivatives. Adapted from Wick *et al.*[69]

The chance to locate different materials into the graph described in Figure 17 is possible through the characterization methods described above. The number of layers and the thickness can be obtained from the TEM,[70] AFM,[70] Raman spectroscopy[71] and optical absorbance measurements.[72] The atomic C/O ratio can be calculated through XPS analysis [73,74] and elemental analysis (ICP-MS).[75] Finally, TEM,[70] SEM[70] and AFM[76] can complete the information about the lateral size of the material. This methodology of classification improves the terminology for the structural characterization. Besides, it gives a global overview of the multiple carbon allotropes.

1.6 Functionalization of graphene

Since the discovering of graphene, the scientific community and the press pointed it as the most promising material in the forthcoming years. However, pristine graphene seems to be an inert material without strong interactions with the media, since its long aromatic character give rise to a high chemical stability. Over the years, the production of large quantities of graphene was settled, so the research community interest was directed to perform several chemical functionalization to adapt the properties of the graphene to a specific application. Mainly, the inspiration of this novel functionalization comes from the already-known nanomaterials: fullerenes and carbon nanotubes.

The two main categories of functionalization of graphene are the covalent and the non-covalent derivatizations. In the covalent modification, the

surface, thus the hybridization of the C-atoms, is modified, what have stronger effects on the properties of the material. However, in the non-covalent functionalization the π character of the material plays a strong role without suffering any modification of the sp^2 carbon atom of the pristine material.[77] Depending on the required application, a functionalization strategy has to be chosen, considering its advantages.

1.6.1 Covalent functionalization

Usually the reactivity of graphene is affected by the inherent properties of the material, and vice-versa. A clear example comes after functionalization, where the existence of sp^3 carbon atoms in the edges of the material and some defect sites, decreases the number sp^2 carbon atoms and, thus, the aromaticity and conductivity of graphene. During the reaction the number of C=C bonds decreases, and, in consequence, the reactivity increases during the reaction. The reactivity also comes from the natural curvature of the graphene sheet.

The introduction of organic molecules onto the graphene surface has two factors worthy to consider. On one hand, the main disadvantage is the disruption on the aromatic character, which has a direct impact on the electronic and mechanical properties. Additionally, depending on the reaction, the formation of side products could be generated, thus making difficult the purification of the functionalized material. For that reason, it is important to control the functionalization using different procedures depending on the desired application. On the other hand, the addition of organic molecules make new hybrids of graphene with different properties and functionalities, such as the enrichment of the physicochemical properties or the anchoring of new target molecules for bioapplications.[78] With the covalent functionalization we improve the dispersibility, mechanical strength or stable introduction of biomolecules, drugs, polymers, etc. All these modifications can be characterized by the several techniques explained above.

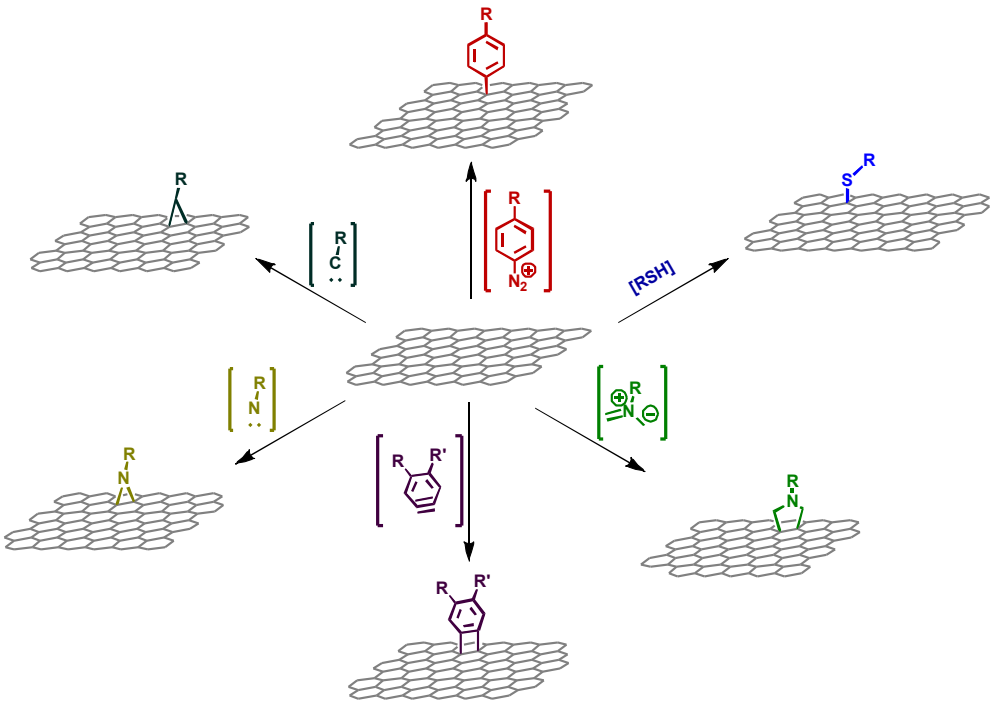

Figure 17. Schematic representation of the general covalent functionalization reactions of graphene.

1.6.1.1 Radical reactions

Radicals, frequently generated in the gas phase, are aggressive species that attack very easily sp^2 carbon atoms. The most used radical reaction for nanomaterials and other different surfaces is the diazonium salt reaction (Figure 18). Researchers employ it for their applications due to its simplicity, easy functionalization and high yields, resulting in high intensity D bands.[79] The mechanism involves the reaction between an aryldiazononium salt with hydroxide, producing a diazotate.[80] The reaction then evolves to diazotate that reacts with another aryldiazonium salt, leading to the formation of a diazanhydride, which, after decomposition, releases N_2 producing an aryl radical. This aryl radical reacts with the carbon surface creating an aryl-graphene-radical intermediate that links with another radical. After the delocalization of this radical, a second coupling can occur in the adjacent or different position.

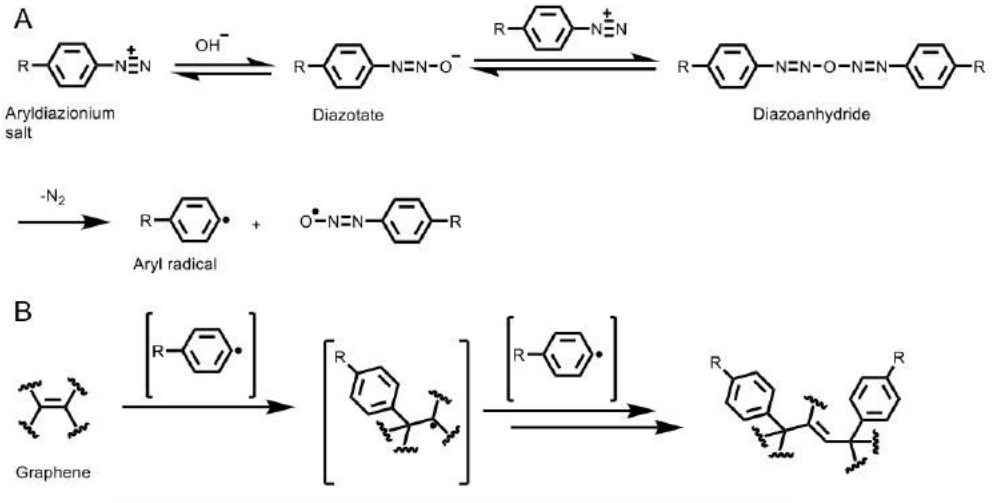

Figure 18. Mechanism of aryldiazonium radical addition. (A) Aryl radical formation from diazonium compound. (B) Radical addition to a carbon surface.

The modification of the electronic properties of graphene derivatives was deeply studied using this modification. Tour *et al.* described the reaction observing a decrease in the conductivity of the graphene, which was dependent on the duration of the radical addition. The introduction of this molecules can offer to graphene semiconducting properties, converting this approach in a facile route for bandgap engineering of graphene.[81]

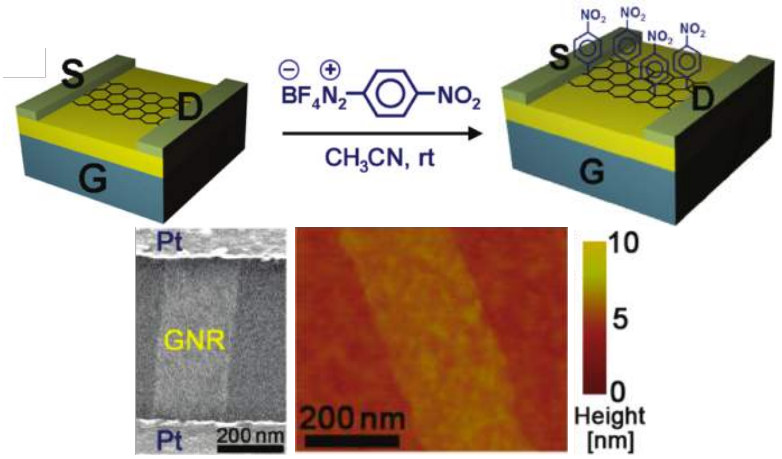

Figure 19. Addition of *para*-nitrophenyl radical on a graphene transistor capable to measure the conductivity of functionalized graphene. Adapted from Niyogi *et al.*[81]

With this functionalization and with an accessible condition to perform the reaction, different studies can be done to determine the properties of graphene. Strano *et al.*[82] described the different reactivity of the monolayer, bilayer and multilayer graphene, describing also anomaly large reactivity in the edges of the material (Figure 20).

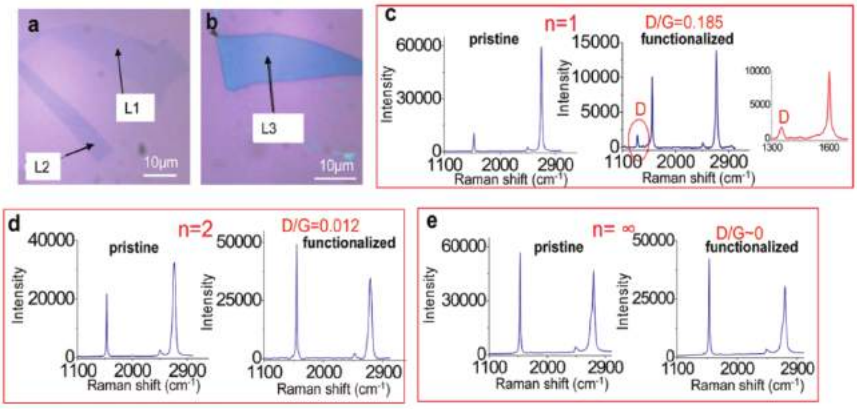

Figure 20. Reaction of diazonium coupling with graphene. (a, b) Optical images of a single and multilayer graphene. (c, d, e) Raman spectra of *p*-graphene and *f*-graphene for single, bi and multilayer graphene, respectively. Adapted from Strano *et al.*[82]

Modifications of aryl diazonium salts in *para* position makes easily accessible by synthetic routes since several groups can be introduced. For example, Pumera *et al.* performed several reactions of different diazonium salts containing various halogen atoms, observing the modification of the electrical properties, being the resistivity strongly dependent on the electronegativity of the halogen introduced (Figure 21).[83]

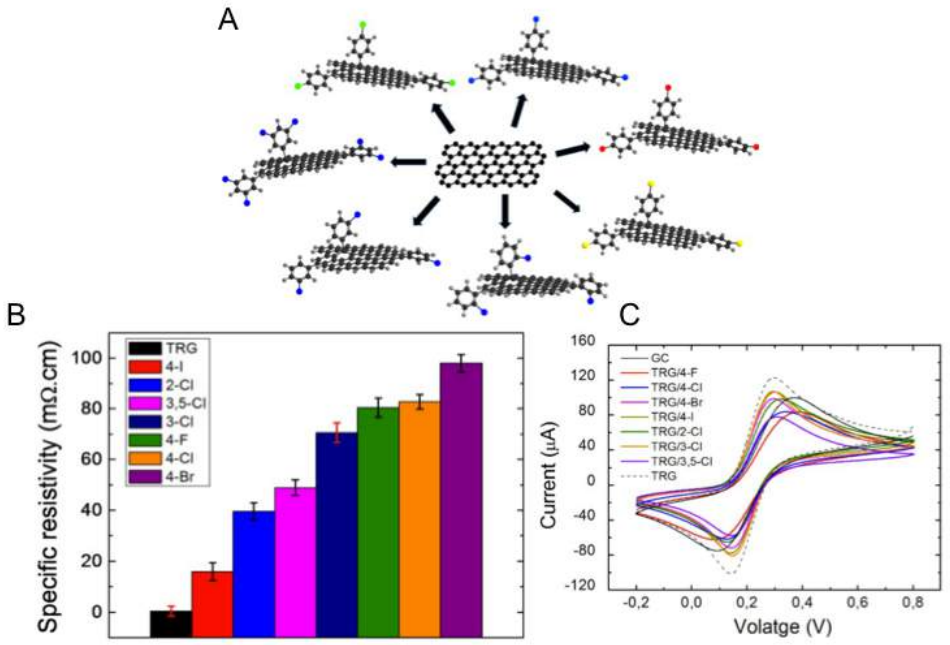

Figure 21. (A) Functionalization with several diazonium salts. (B, C) Resistivity and cyclic voltammograms of functionalized graphene. Adapted from Pumera *et al*.[83]

Other research groups introduced carboxyl groups by phenyl radical additions. The surface modification of carboxy phenyl groups became attractive for biosensing applications since the functionalized graphene could be easily modified through esterification or amidation in order to covalently attachment other target biomolecules.[84–86]

As conclusion, radical reactions, particularly, diazonium coupling reactions, were widely used for modifying graphene properties, pattering and for further modifications for biorecognition.

1.6.1.2 Cycloadditions

Cycloaddition reactions are pericyclic chemical reactions where some unsaturated molecules forms a cyclic adduct with a net reduction in the bond multiplicity. These approaches can offer reversible modifications and mild conditions.

1,3 Dipolar cycloaddition

The reaction between a 1,3-dipole with a dipolarophile is the 1,3 dipolar cycloaddition. The final formation of a five-member ring is a soft approach for a covalent functionalization. In this case, graphene has a role of dipolarophile. The 1,3 dipolar cycloaddition with azomethine ylide (i,ii) leads to the formation of perpendicular pyrrolidine rings to the graphene surface. This approach allows two paths for the introduction of specific organic groups on the graphene structure. The corresponding substituent R_n added could come from the N-methyl glycine (i) in the N-position or from the aldehyde (iv) in the C2-position of the pyrrole ring.

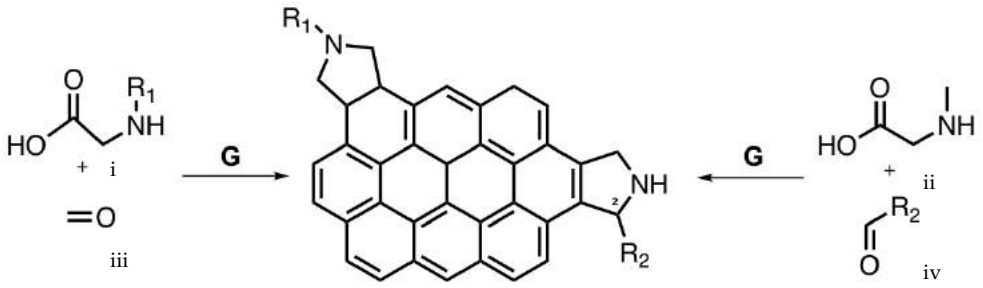

Figure 22. Reaction of 1,3-dipolar cycloaddition of azomethine ylide with a representation of graphene. The introduction of different substituents (R_n) could be performed through two paths.

Both paths were widely studied.[87] Prato *et al*.[88] performed a successful functionalization of a protected *alpha*-amino acid and paraformaldehyde followed by the deprotection of a Boc group. They easily integrated AuNRs as a contrast marker for identifying the reactive sites and creating a new nanocomposite material for diverse applications (Figure 23).

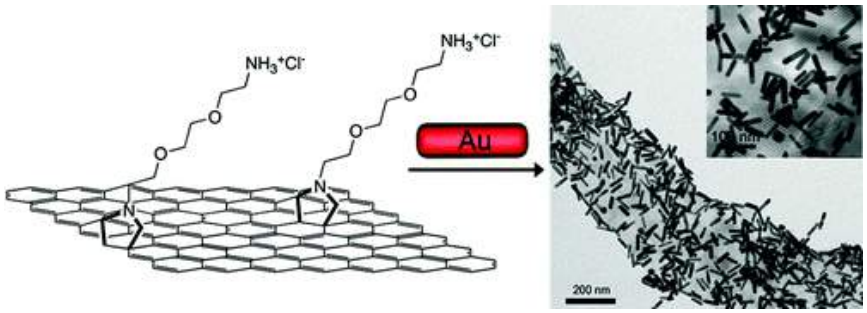

Figure 23. Schematic representation of aminated functionalized graphene and TEM image of the new nanocomposite formed by the corresponding functionalized graphene and AuNRs. Adapted from Prato Prato *et al*.[89]

Diels-Alder

The Diels-Alder cycloaddition is a well-known reaction in organic synthesis. The reaction occurs between a conjugated diene and a substituted dienophile, forming a substituted cyclohexene system. Graphene can act as diene or dienophile because of its polyaromatic character. Haddon *et al.* showed this behaviour making several Diels-Alder cycloaddition reactions using different dienes and dienophiles (Figure 24).[90] The reaction was performed at room temperature leading to the formation of six member rings perpendicular to the graphene sheet. This chemical reaction has a reversible character; thus, graphene can recover its initial electronic properties.

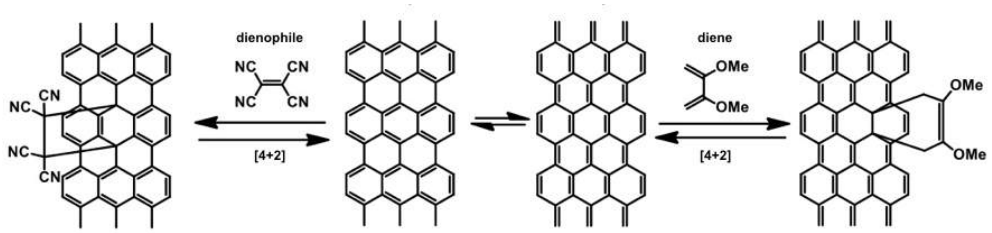

Figure 24. Diels-Alder reaction between graphene and diene or dienophile.

Arynes are highly reactive organic intermediates produced by the removal of two *ortho* substituents of phenyl derivatives. Up to date, aryne cycloaddition reactions with diverse carbon nanomaterials have been reported. One example is the benzyne cycloaddition with C_{60} fullerene that leads to [2+2] adducts.[91] Nevertheless, there is not yet experimental evidence of the exact structure of the adduct obtained from reactions performed on carbon nanotubes,[92,93] carbon nanohorns,[94] and graphene[95] derivatives there

is no experimental evidence as yet about the exact structure of the adduct obtained. Several theoretical studies suggest that the kind of benzyne cycloaddition onto carbon nanotubes (i.e., either [4+2] or [2+2]) depends on different parameters, mainly the type of carbon nanotube (*i.e.*, number of walls, chirality, etc.) and its diameter.[92,96,97,98,] In the case of graphene, theoretical studies argued that the reaction with benzyne on a graphene fragment of 4 x 4, 6 x 6 and 8 x 8 unit cells is more energetically favourable through [2+2] cycloaddition, although also the [4+2] can occur.[98,99] Other theoretical calculations suggested that cycloaddition reactions occur in edges and defect areas,[100,101,102] even though they have been reported on defect-free epitaxial graphene.[103] However, there is no experimental evidence of reactions performed on graphene with arynes as yet about the exact structure of the obtained adducts.

This functionalization is reported as a great tool to remarkably increase the dispersibility by the incorporation of a large variety of different groups in the phenyl molecule. In 2010, Ma *et al.* described a methodology based on the decomposition of 2-(trimethylsilyl) aryl triflate as starting material for the production of the aryne in presence of graphene,[95] (Figure 25). In 2012, Kalugin *et al.* performed the benzyne functionalization of epitaxial graphene and graphene under mild conditions.[104] In 2016, Martín *et al.* described the formation of a C_{60}-aryne building block that reacted with the graphene surface.[105]

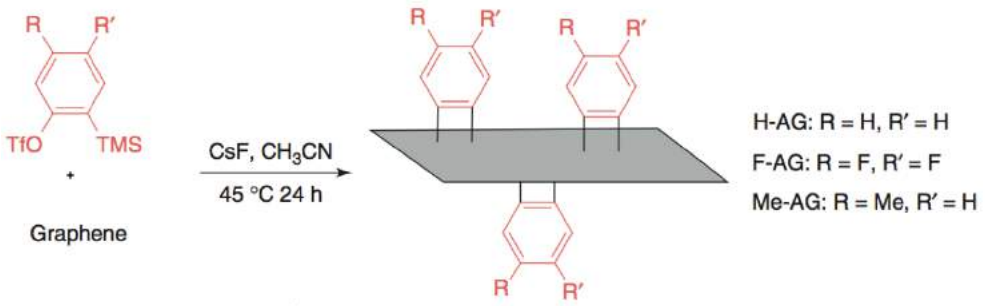

Figure 25. Aryne addition on graphene surface. Adapted from Ma *et al.*[95]

The interaction between functional groups of the biomolecules and pristine graphene, at first glance, is unfavourable due to absence of organic moieties, or anchor points on the surface of graphene. For this reason, the development of methods for the graphene functionalization with organic functional groups has been of great interest. In addition, the large surface area of graphene leads this material with great potential for the attachment of molecules with, for instance, sensitive abilities for the detection of

particular disease indicators. In the literature, there are many examples related to this field. In 2010, Lim *et al* described a DNA and pH sensor detector by the addition of oxygenated defects on epitaxial graphene.[106] Other example was done by Jung *et al.,* who developed a novel graphene based immune-biosensor for highly, selective and rapid detection of virus.[107]

1.6.2 Non-covalent functionalization

The non-covalent modification of graphene is a non-destructive approach where the properties of graphene are only slightly modified. It consists on the physical adsorption of different molecules based on π-interactions and Van der Waals forces. It is a common method to functionalized graphene when the application needs not to alter the electronic network of the material.[80] The interactions of the organic moieties with graphene are weaker than in the covalent functionalization, being this approach less stable.

The main organic molecules employed in this kind of adsorption are pyrenes. Several studies showed the irreversible binding of pyrene anchor to the surface of graphene.[108,109] The synthesis of pyrene derivatives can be performed, introducing the desired terminal groups that can be used for the attachment of different functionalities through amines and nucleophilic substitutions.[110] A higher surface modification was reported by Mann *et al.* using a tripodal molecule with three pyrenes. The functionalization was confirmed by electrochemical signals from $Co(tpy)_2$, observing higher attachment in the tripodal pyrene moiety than in the individual pyrene.

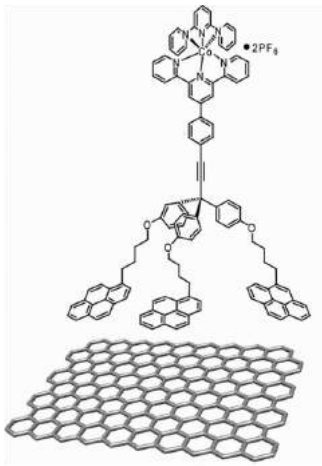

Figure 26. Non-covalent functionalization of tripodal pyrene derivative.

In 2017, Güryel *et al.*[111] developed an analysis of the role of non-covalent interactions of polymers with graphene, considering that the overall interaction was strongly influenced by the specific polymer conformation and the functional groups, being attractive interactions with the graphene sheets. This study constitutes a base for modelling design of new nanomaterials.

1.6.3 Non-conventional functionalization

In general, modifications of graphene derivatives require big efforts. However, numerous successful modification processes of graphene have been reported.[112] Some of these procedures have disadvantages. For instance, the main handicap of conventional functionalization of graphene is the lack of solubility, which converts graphene into a material with unstable and non-homogeneus suspensions that can hind the chemical manipulation.[37,36] In addition, the use of high amount of solvents at low concentrations or long-time reaction procedures are other disadvantage that impede the functionalization.[87]

Therefore, it is mandatory to obtain new chemical routes for the modification of graphene, with low reaction rates, scalable processes and the reduction of amount of solvents to obtain affordable and green procedures.

The use of alternative tools for manipulation and functionalization of carbon materials becomes an attractive topic.[113] For instance, the

functionalization *via* photochemical reactions,[114] where the use of solvents and reagents are limited, the generation of radical anions are easily performed under UV irradiation among others. In 2017 Chen *et al.* developed the formation of hexahapto graphene complexes with transition metals through a simple photochemical route. Some of the complexes presented significantly enhanced conductivity, being a myriad of opportunities for new graphene derivative materials with diverse properties (band-gap engineering, magnetic materials and conductivity).[115]

Another non-conventional representative option is the chemical bulk functionalization.[116] Longer-time reactions are performed but this approachgenerates highly reactive graphene; in addition, the protection of the graphene layers are achieved to avoidreaggregation and solvent induced doping. Another general problem of conventional reactions above-mentioned is the low degree of functionalization on graphene, being challenging to determine unambiguously the success of reactions. The planar structure of graphene makes an inert material for diverse functionalization approaches. In order to overcome this problem, Hirsch *et al.* described a new concept of graphene functionalization that lead to a large variety of covalent adducts with high degree of functionalization.[116] The key point is the application of negatively charged graphites or graphenides (negatively charged graphene sheets), this process is called graphite intercalation compounds (GICs), generally, with potassium (placed in the sheets of graphite). The advantage of this approach is the improved dispersion in solvents and the chemical activation due to the generated negative charge by a reduction process.

Figure 27 describes the *in-situ* reduction through sodium/potassium alloy (NaK_3) in 1,2-dimethoxyethane as alkalyde stabilizing solvent. The addition of diazonium salt dispersion was performed to reduce and functionalize graphene sheets. Annealing of the reaction products (up to 1000 ºC) led to the complete regeneration of carbon framework and restauration of graphite. This study confirms the reversibility on covalent modifications of graphene.

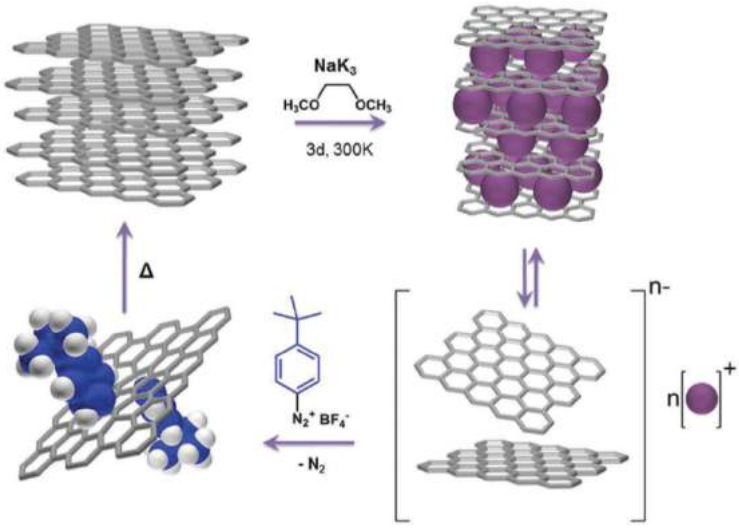

Figure 27. Reductive covalent functionalization of GICs with phenyl diazonium tetrafluoroborate. Adapted from Hirsch *et al.*[116]

In 2017 Abellán *et al.* developed a huge screening of benchmark in reductive covalent functionalization graphene routes unifying different experimental conditions, providing important insights into the understanding on the principles of these approach.[117]

A novelty procedure which involves the transformation of mechanical energy into driving force for the chemical modification is the mechanochemistry, a well-known method in the industry. Many examples have been reported about this methodology with carbon nanostructures.[118] A representative one was reported by Hang *et al* in 2010. They described one-step procedure for preparation and functionalization of graphene through ball milling preparation.[119]

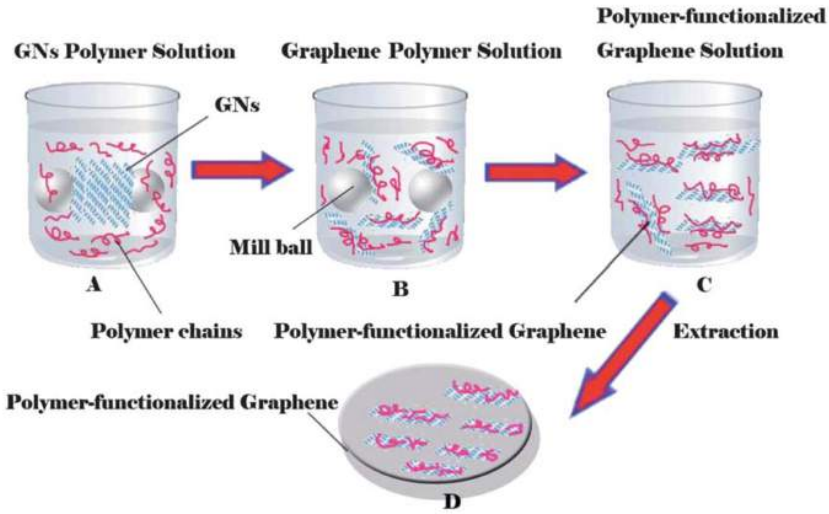

Figure 28. Schematic illustration preparation and functionalization of graphene through ball milling. Adapted from Hang *et al*.[119]

Solvent-free procedures have great interest to modernize classical procedures making them more clean, safe, affordable and easy to perform. Reactions on solid supports, reactions without any solvent or catalyst, and solid-liquid phase transfer catalysis can be thus employed with significant increases in reactivity, selectivity and production.[120,121] Regarding carbon-based nanomaterials, several examples of solvent-free modifications were reported to pave the way for green protocols and large-scale functionalizations.[113] For instance, a Diels-Alder reaction was reported to produce the exfoliation of graphite into efficiently functionalized graphene layers under solvent-free conditions in one-step process.[122]

An approach which introduce defects in graphene uniformly with high repeatability, single sided doping capability and the ability to change the surface without modification of bulk material is the ion beam technology.[123] Previously, ion irradiation has been used for the study of structural and electrical changes on graphene and as annealing process for the reducing of the damage in the bulk material.[124] Besides, this technique was employed for the obtaining of N-doping graphene by ion implantation on epitaxial-grown samples, demonstrating that an ordered arrangement of the nitrogen atoms occurs triggered by 6x6 modulation.[125] In 2017, Kaushik *et al.* irradiated epitaxial graphene observing increase in defect density by Raman spectroscopy.[126] The formation of sp^3 defects was controlled with the fluence intensity. This work provides new routes for the introduction of defects in controlled manner using ion beam technology.

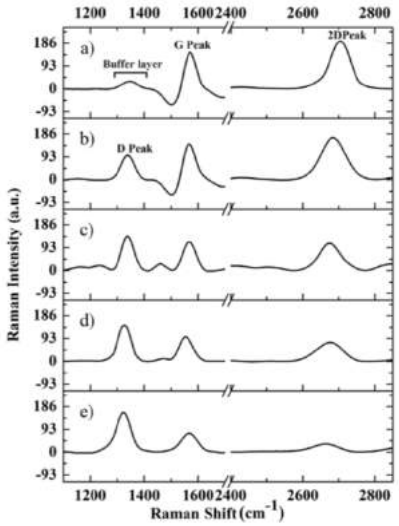

Figure 29. Raman spectrum of pristine (a) and irradiated graphene on SiC from low fluences to high fluences (b to e). Adapted from Kaushik *et al.*[126]

An effective and economical process for graphene functionalization is plasma treatment.[127] The use of different feed gasses allows the introduction of different species such as oxygen, fluorine or nitrogen onto the graphene surface. Previous research conclude that ion bombardment leads to the destruction of graphene structure.[128] However, Walton *et al.* developed a plasma based method to engineer thermal conductance through manipulation of the interface chemistry for the introduction of different functionalities using small variations on pressure and operating background.[129] Huang *et al.* report a facile plasma approach for functionalization of graphene in air and H_2O_2 solution,[130] controlling the duration of irradiation the authors confirmed *via* XPS a significant change of the atomic oxygen content.

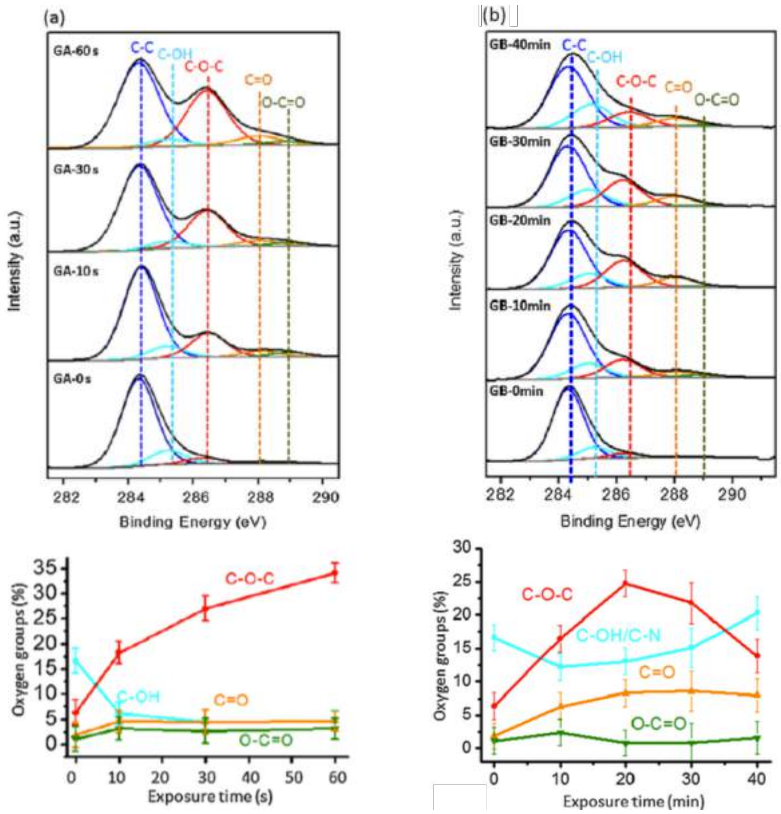

Figure 30. XPS data and oxygen group content for (a) air plasma treatment and (b) H_2O_2 solution. Adapted from Huang *et al.*[130]

An emerging methodology at the beginning of the 21st century is the microwave-assisted chemistry, (MAC) which has revealed as valuable alternative in the synthesis of organic compounds, polymers, inorganic materials, and nanomaterials.[131] Important innovations in MAC now enable chemists to prepare catalytic materials or nanomaterials and desired organic molecules, selectively, in almost quantitative yields and with greater precision than using conventional heating. In particular, MAC is an important tool in the field of carbon-based nanomaterials. They are extensively used as microwave (MW) matrices because of their capacity to absorb MW with high efficiency, rapidly generating high surface temperatures.[132,133,134] For instance, different methods for the preparation of graphene derivatives has been recently reported by using MW irradiation.[135,136]

Other approaches of non-conventional surface modification of graphene are focus on the possibility to functionalize with extremely high yield and high selectivity. The atomically controlled chemical functionalization has broad

interest for the modification of mechanical, optical and electronic properties. To achieve this goal, Pérez *et al* used cyanomethyl radicals ($CH_2CN\bullet$) in presence of graphene grown on Ru.[137,138] Acetonitrile was homolytically broken by electron bombardment, getting radicals that react with the nanostructured graphene with atomic-level selectivity. (Figure 31)

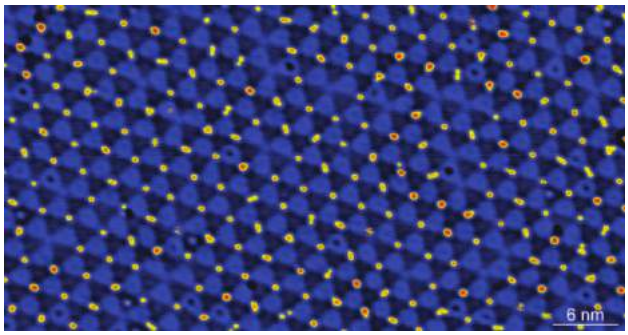

Figure 31. STM image of radical reaction of Graphene/Ru with cyanomethyl radicals, red dots show the selective atom of the covalent functionalization. Adapted from Emilio *et al* [138]

In 2018, Kyhl *et al.* demonstrated a route for the functionalization of graphene using the excitation of H_2 molecules. The authors observed a functionalization in highly ordered manner being a viable tool for band gap engineering.[139]

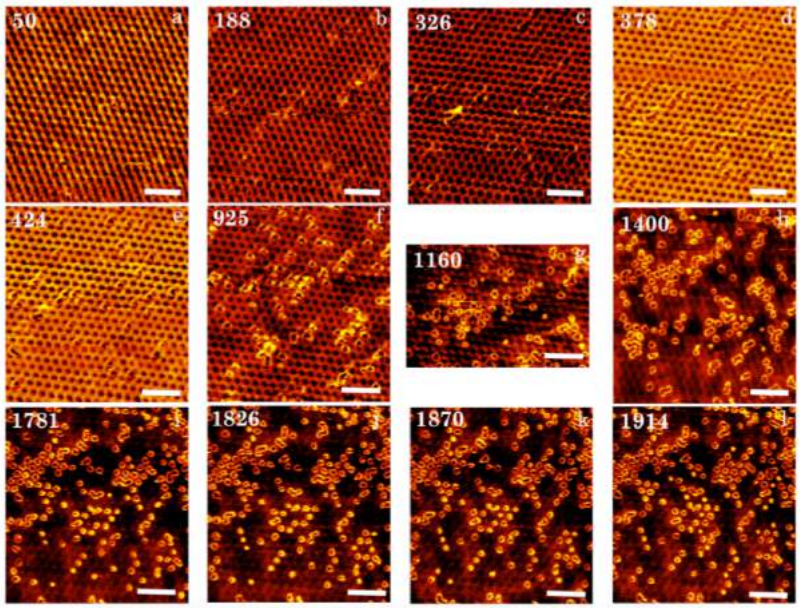

Figure 32. STM images of graphene in Ir(111) exposed to vibrational excited H_2 at different exposure times (indicated in seconds in the left corner), scale bar are 100 Å. Adapted from *Kyhl* et al.[139]

In conclusion, the exploration of non-conventional methodologies mentioned above, become an important tool for the adoption of alternative methods for surface modification of graphene, obtaining new reactivity profiles that can improve functionalization or even allows access to impossible conventional reactions with graphene.

1.7 Production of interfaces on graphene by chemical modification for biosensing and bioelectronics

The creation of interfaces on graphene by its modification is highly important for incorporating this carbon material in a variety of applications, including electronic devices and biosensors. In particular, the chemical modification of the surface of graphene leads to enhance the biocompatibility, reactivity, sensing properties and the most important feature, the binding capacity to attachment sensing molecules.[140,141] Generally, the introduction of small molecules, drugs, antibodies enzymes or genetic material is performed in two steps: an initial modification to introduce specific points, and as second step, the attachment of proper biological elements through the anchor points. Chemical groups as carboxyl, hydroxyl, amine or maleimidic moieties are commonly introduced for the corresponding link of the bioactive molecule by covalent and non-

covalent functionalization.[142] Currently, both strategies are being investigated for the construction of biomedical devices. Covalent functionalization necessarily perturbs the sp^2 structure of graphene resulting in defects, which alters its electronic properties. In contrast, non-covalent methods do not disrupt the sp^2 network of graphene, thus its electronic properties are unaffected. For that reason and its large versatility, non-covalent modifications are more preferred in current research. However, the high stability of covalently modified graphene, is a more useful strategy for biomedical devices which works under harsh conditions.

1.7.1 Non-covalent modification

Non-covalent functionalization of graphene on surfaces include different driving forces such as polymer wrapping, π-π interactions, electron ionic interaction, hydrogen bonding, and van der Waals forces. Non-covalent functionalization of graphene derivatives for different applications has recently been reported in detail by Zboril and co-workers.[143] For biomedical applications, π-π interactions are clearly the most used derivatization due to their chemical versatility. Although many different aromatic compounds have been described for functionalization of graphene derivatives,[142] pyrene derivatives containing functional groups are the most used molecules in this field, since they allow introducing all above-mentioned biomolecules. For instance, Duesberg *et al.* have used pyrene derivatives highly efficient surface plasmon resonance (SPR) immunosensor.[144,143] They functionalized a CVD graphene on Au with coordinated Cu^{2+} ions with a pyrene derivative, for the subsequent Cu-S coordination of biotinylated specific antibody cholera-toxin. However, non-covalent modification of graphene is not only useful for introduction of biorecognition elements. In nanopore-based biosensors for sequencing DNA, and hydrophilic modification of graphene surface by interaction with pyrene ethylene glycol was performed, to reduce the nanopore closure due to the hydrophobic interaction between DNA nucleotides and graphene surface.[145,146] In another example, Guo *et al.* have showed an electrochemical sensor for detection of thrombin by non-covalently functionalizing rGO on a glassy carbon electrode with other kind aromatic molecule, the dye Orange II.[147,148] This adsorption of electroactive dye on rGO surface not only prevents the agglomeration of graphene layers but also acts as *in-situ* probe for the detection of the target protein by variation in its electrochemical signal. By other non-covalent method, graphene surfaces, especially GO and rGO surfaces, can be decorated with metal nanoparticles, *e.g.* Au or Pt, *via* electrostatic interactions.[149,150,146] These nanoparticles are useful as anchor points for biomolecules, as well as

transducer components for signal improvement. After the introduction of specific anchor sites, the coupling of biomolecules is required. The immobilization approaches that are widely performed are: covalent attachment, cross-linking, and electrostatic interactions.[151] Besides, various biomolecules are also used as anchor points for bounding biorecognition elements. The strong biotin-avidin interaction is a very useful technique for nucleic acids and antibodies, due to the exceptional affinity between these molecules. For this approach, a previous functionalization with avidin protein on graphene surface is crucial. A GFET for DNA analysis was developed based on a biotin–streptavidin-binding strategy on BSA adsorbed onto CVDG on silicon.[152,146] The direct adsorption of biomolecules and on graphene can be considered a non-covalent functionalization. However, the interaction is not fully understood and is non-specific: aromatic residues of biomolecules can interact with aromatic rings of graphene, charged residual groups can be adsorbed on GO or rGO surfaces because are negatively charged structure, or even hydrophobic structures may support a physical adsorption by van der Waals forces. The direct adsorption of recognition bioelements on graphene without interaction with previously introduced specific sites is also widely used in biosensors, which are mainly based on hybridization or unwinding events.[153,143] For instance, the group of Marin Pumera have developed different electrochemical sensing platforms non-covalently functionlalized with recognition bioelements on the graphene-modified electrodes, such as DNA and antibodies.[154,155,151]

Related to graphene-modified surgical implants, there is an important lack of functionalization approaches in the literature. However, very promising results have been recently reported in the field of biomedical applications. A prosthesis made by a titanium alloy coated with rGO was functionalized with an osteogenic drug of dexamethasone *via* π-π interactions on graphitic domains, resulted in a drug-loaded material that significantly improve osseointegration.[156,140] Another promising example was the non-covalent functionalization GO-coated implant with the bone morphogenetic protein-2 and the stem cell recruitment agent Substance P for dual delivery.[157,158] This modified material showed the greatest bone regeneration for titanium implants.

1.7.2 Covalent modification

Covalent modification of graphene is attractive for its applications, since of its robust nature as well as its higher ability to significantly change the

electronic properties of graphene derivatives. Multiple covalent modifications were described for graphene on different substrates that allows introducing diverse chemical moieties.[159] However, in the manufacture of graphene-based chemical devices, only typical grafting strategies of surfaces based on free-radical addition and aggressive oxidation processes materials are used up to date. Besides, strong oxidations by acid treatments of graphene materials and mild and controllable methods for oxidation of graphene on surfaces have been reported. The latter methods allow the introduction oxygenated groups avoiding high damages of the graphene structure in comparison with the classical oxidation methods. For instance, the controlled electrochemical oxidation of epitaxial graphene using HNO_3, allows its oxidation with the introduction of low number of defects.[160] The exposure of graphene on silicon surface to oxygen under ultra-high vacuum conditions leads to a homogenous modification of graphene with oxygenated groups.[161] The oxidation degree of this method is tunable by controlling the exposure time of oxygen. Another example is the Ar/O_2 plasma treatment of epitaxial graphene, which led to the incorporation of different oxygenated groups.[162] In this process, the functionalization degree is once more controllable by tuning the working pressure.

Among the many different possibilities of modification of graphene surfaces reported in the literature for the introduction of chemical moieties,[159] only the well-known free radical additions are used as the covalent modification for biomedical devices. In this line, aryl diazonium salts with different functionalities have been successfully employed. The phenyl radical addition can be performed under mild conditions by thermal decomposition or electrochemical reduction. Johnson and co-workers have developed a biosensor based on arrays of hundreds of graphene-based GFETs for opioids that consists in an engineered μ-opioid receptor protein chemically bonded to the graphene surface through diazonium coupling.[163,143]

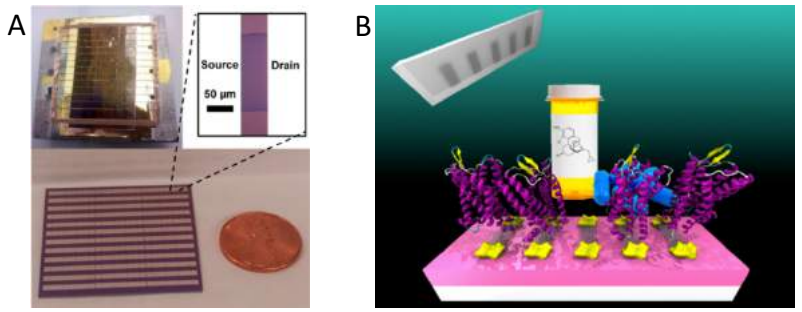

Figure 33. (A) Example of the fabricated transistor. (B) Representation of the biosensor based on arrays of graphene. Adapted from Johnson *et al*.[163]

The stable biofunctionalization yielded a biosensor that exhibits high selectivity and sensitivity (detection limit of 10 pg/mL) for the target naltrexone (an opioid receptor antagonist) based on the concentration-dependent shift of the Dirac Point of graphene.

More recently, a similar strategy based on a controlled electrochemical modification method for graphene surfaces was reported, in order to develop biosensing platforms.[164,151] The covalent functionalization of CVD monolayer graphene by electrochemical reduction of carboxyphenyl diazonium salt allows introducing carboxyl groups. This approach is a more controllable modification than the thermal decomposition because the functionalization degree can be easily controlled by the number of cycles of the electrochemical process. The produced sensor allowed the detection ovalbumin with high specificity after anchoring ovalbumin antibodies trough amide bond in the previously introduced carboxyl groups.

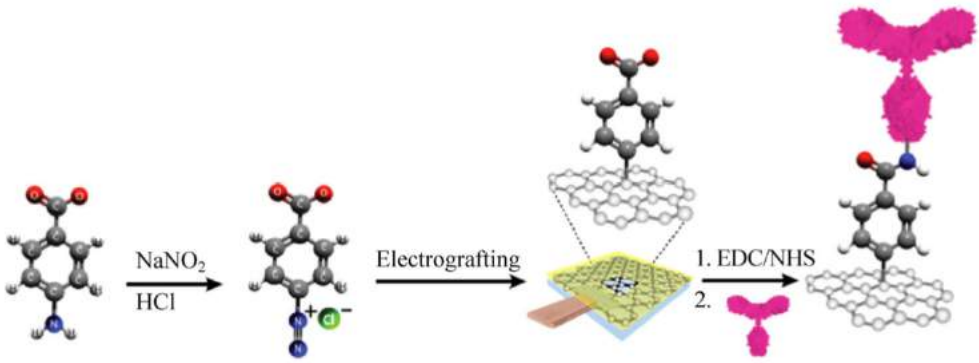

Figure 34. Schematic representation of CVD graphene biosensor. Adapted from Eissa *et al*.[164]

Another investigated covalent modification on graphene on surfaces was the radical polymerization on graphene. [165,159] Although it has not been widely explored, it opens a large number of possibilities for modified graphene surfaces. In contrast to most of the covalent modifications of CVD graphene, polymerization hardly introduces additional defects in the graphene structure, as showed by the unchanged D-band in the Raman spectra, since radicals probably react with exiting defects in the pristine material. In addition, the possibility of using different monomers or conductive polymers allows the introduction of diverse specific groups or improvements in the electric properties of the corresponding graphene device, respectively.

1.8 Chemistry of arynes

Due to the wide use of arynes in this PhD thesis, a concise explanation about aryne generation and chemistry is explained for a better understanding. Arynes[166] are neutral intermediates of reaction, which could be considered as derivate of aromatic systems due to the loss of two *ortho* substituents. The main member of the family is the *o*-benzyne or 1,2 didehydrobenzene (Figure 35)

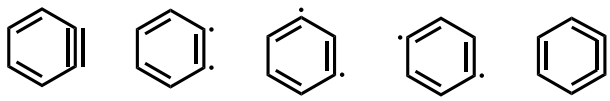

Figure 35. Structural representation of different isomers and resonances of benzyne.

Arynes have short lifetimes and highly reactive species. They have a deformation of the geometry due to the structure of a lineal bond in a six-member ring, thus becoming difficult specie for the study of their properties. Several theoretical studies[167] suggested arynes to have a strained triple bond, with some biradical character; however, Warmuth in 1997 suggested a cumulenic behaviour. [168]

The possible evidence of the arynes as intermediate of reaction was suggested at the beginnings of the 20th century, although until the 50's Robert *et al.* did not demonstrated the existence in the formation process of anilines with the reaction of aril halides and KNH_2.[169] The use of arynes in organic chemistry was limited because of the harsh conditions for its generation, but, in the last decades, many methodologies to generate arynes

were implemented, thus turning aryne chemistry a great tool for organic synthesis.

1.8.1 Methods for the generation of arynes

Due to high reactivity of these species, arynes must be generated *in situ* in the reaction media and with the use of the corresponding precursors. Figure 36 collects the most useful methods for the *in-situ* synthesis of arynes.

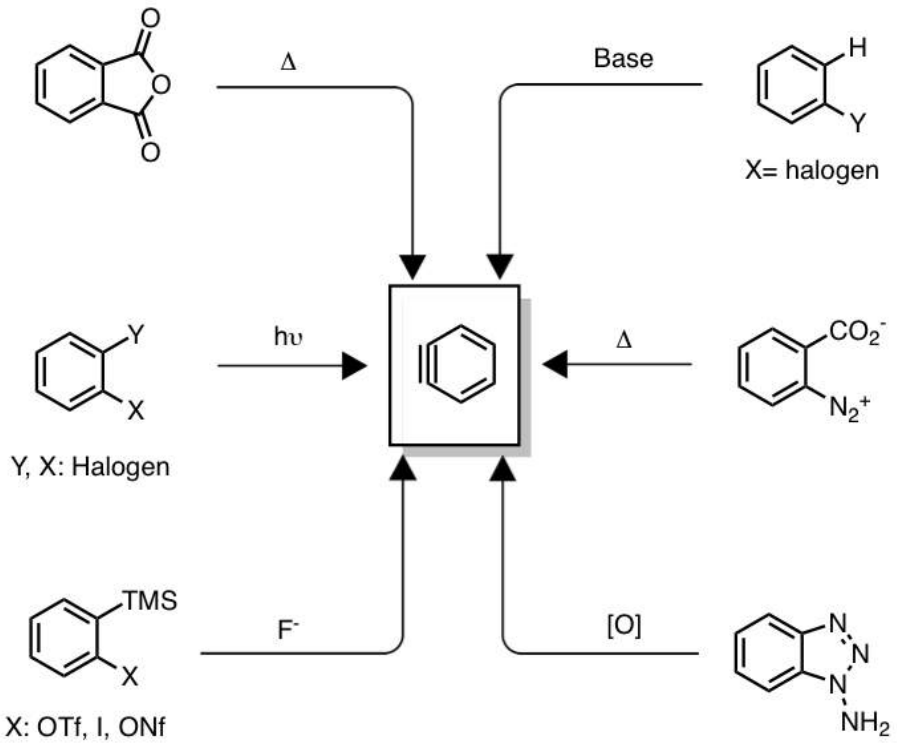

Figure 36. Methods for aryne generation.

Normally, the generation is limited to the required conditions of the reaction. The main method described for the *o*-benzyne avoids the use of strong bases and harsh conditions. It uses a triflate with a source of fluoride ion,[170] and promotes an attack over the silicon and an *ortho*-elimination of the triflate. Another method using harsh conditions is the thermal decomposition of anhydrides that leads to the liberation of CO_2 and CO.

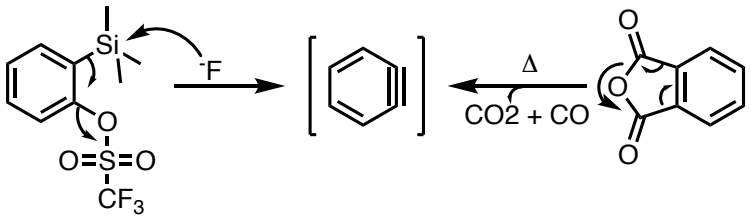

Figure 37. Schematic representation for the generation of benzyne from a triflate and from thermal decomposition.

Even though the high reactivity of these compounds, the quietly controlled reaction conditions can result in several kinds of cycloadditions [171] without large amount of undesired by-products. Thus, the use of arynes has become a great tool for the functionalization of carbon materials like graphene or carbon nanotubes. For these reasons, in this thesis we perform large efforts for the understanding and functionalization through this kind of chemistry.

1.8.2 Aryne reactivity

Arynes have high reactivity with a strong electrophilic character. The tension produced by the distortion, in an aromatic six-member ring, of the linearity in a *sp* carbon provokes the high reactivity and short lifetime. The aryne reactivity is dominated by the addition of nucleophiles to a triple bond and the participation as dienophile in cycloaddition reactions, specially Diels-Alder reactions.[172]

1.8.2.1 Nucleophilic addition

The nucleophilic attack to the benzyne creates an arylic carbanion, which could react with an electrophile, obtaining an aromatic compound with two substituents.[173,174] Arynes can react with different nucleophiles such as alcohols, amines, thiols or carbanions. Nucleophilic additions allow the formation of polycyclic systems in presence of benzyne nucleophile and electrophile as is described by Okuma *et al.*[175] (Figure 38).

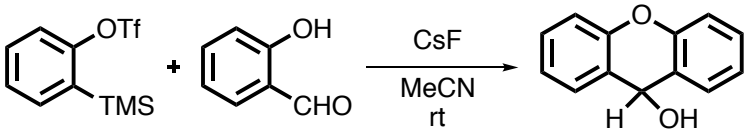

Figure 38. Schematic representation of nucleophilic addition of salicylaldehyde with benzyne described by Okuma *et al.*

1.8.2.2 Insertion of arynes on sigma bonds

Similar procedure of the addition of a nucleophile with a benzyne occurs when the nucleophile and electrophile are attached through a σ bond. The result is the insertion of aryne in the nucleophile-electrophile bond. These approaches could be performed due to the discovering of soft generation methods of arynes (described in the section 1.8.1). An example of this reactivity was performed by Guitián *et al.* where, with the generation of benzyne through *o*-(trimethylsilyl)aryl triflates with styrene oxide. The authors developed for the first time, an aryne insertion in the σ bond of strained cyclic molecules. In this case, the insertion of benzyne into a C–O sigma bond.[176]

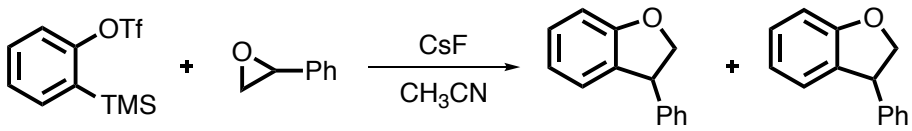

Figure 39. Schematic representation of an insertion of benzyne on sigma bond performed by Guitián *et al.*

1.8.2.3 Benzyne cycloadditions

The first aryne cycloaddition was described by Wittig and Pohmer in 1955. The authors observed a [4+2] cycloaddition between *o*-benzyne and furan with the obtaining of 1,4-Dihydro-1,4-epoxynaphthalene.[177]

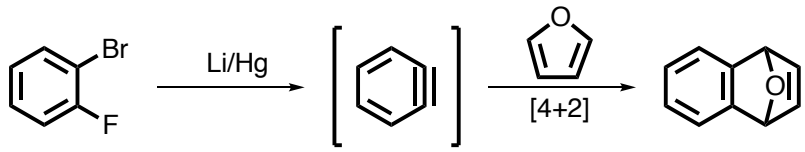

Figure 40. Schematic representation of the first described cycloaddition by Wittig and Pohmer.

Several cycloadditions were described in presence of arynes, summarized below.

[2+2] Cycloadditions

A [2+2] cycloaddition is a symmetry-forbidden regarding the Woodward and Hoffman rules.[178] The reaction should occur in several steps. In 1992 Hoke *et al.* described the [2+2] cycloaddition reaction with benzyne and fullerenes.[91] The cycloaddition occurs between benzyne and the double bond located in the six-member ring of fullerene. In summary, the C_{60} can form different adducts [C_{60} + $(C_6H_4)_n$].

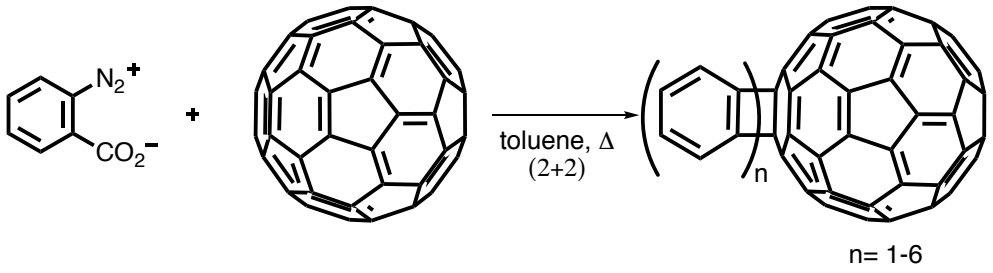

Figure 41. Schematic representation of [2+2] cycloaddition of benzyne and fullerene.

[3+2] Cycloadditions

The [3+2] cycloaddition are a good synthetic approach for the formation of heterocyclic of five-member rings to a benzene ring. The formed heterocyclic have great value due to the high biological activity (indazoles, indoles, triazoles…), an example of this cycloadditions was described by Kivrak *et al.* in 2010 where the authors obtained dihydrobenzisoxazoles by the [3+2] cycloaddition reaction of arynes and oxaziridines with interesting biological properties and pharmaceutical potential.[179]

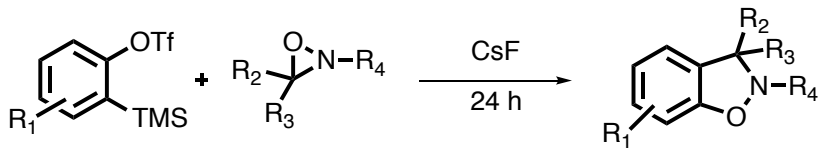

Figure 42. Schematic representation of [3+2] cycloaddition.

[4+2] Cycloadditions

In Diels-Alder reactions, arynes act as highly reactive dienophiles.[172] [4+2] cycloadditions are the most important reaction of arynes with the use of different dienes. The most favourable reaction occurs with cyclic dienes, especially with five-member rings. A high dienophile character is observed due to the possibility to react with dienes in an aromatic system. Figure 43 presents different examples of this cycloaddition with aromatic compounds, from a reaction with perylene in the bay zone,[180] to the reaction of benzyne with benzene,[181] or the addition of benzyne to the central place of anthracene, which represents the general preparation methods for triptycene derivatives.[182]

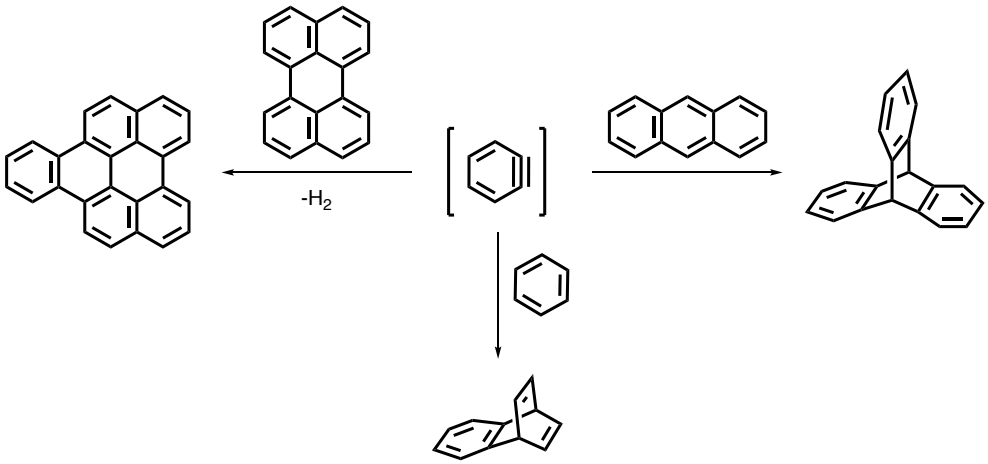

Figure 43. Schematic representation of several [4+2] cycloadditions with aromatic compounds.

2. RESULTS AND DISCUSSIONS

2.1 Aim of the work

The importance of graphene and the use in several applications has been demonstrated along the previous introduction. Moreover, the functionalization of graphene is a powerful tool for tuning their properties. For that reason, during this PhD thesis we were focused in several studies:

i. The exploration of conventional routes for the preparation and functionalization of graphene. With special emphasis in the underexplore aryne cycloadditions.

ii. The selection of a suitable graphene material obtained before for the setting of an electrochemical functionalization of graphene electrodes with future application as biosensor platforms. Moreover, the development of an early-stage essay biosensor of a modified graphene electrode for the electrochemical detection of oligonucleotides.

iii. The study of a novel, fast and scalable non-conventional functionalization under microwave irradiation that can solve common problems of the conventional modifications of carbon materials.

The research of these topics could open a range of possibilities for the scientific community.

2.2 Preparation of graphene

We developed a method described by Colleman *et al.*[37] and Tour *et al.*[183] with sonication of graphite under ultrasounds for 30 minutes. We performed two experiments, with NMP and with ODCB Figure 44).

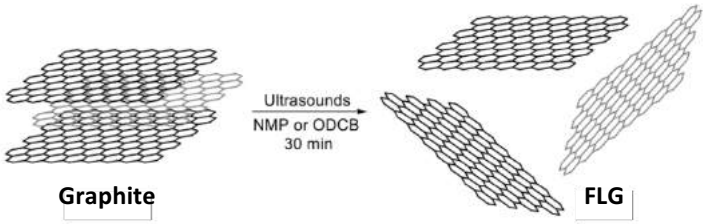

Figure 44 Exfoliation method of graphite by ultrasounds in NMP or ODCB as solvent.

The sonicated FLG showed small changes between the use of NMP or ODCB in Raman spectroscopy, with a similar 2D band for FLG. The main distinction was observed on the D band intensity which denotes a slightly higher functionalization for the NMP than ODCB as solvent.

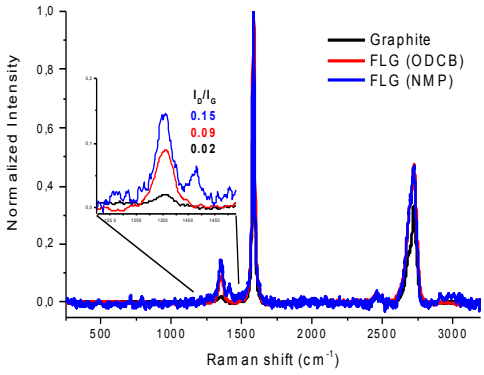

Figure 45. Raman spectra of graphite (black), sonicated FLG with ODCB (red) and sonicated FLG with NMP (blue).

In order to have a graphene-based material that can be water dispersible for reactions in aqueous media, the preparation of GO and chemical rGO was performed. A hydrophilic oxidized graphene material was synthesized from powder graphite under harsh conditions at low temperature. This methodology was described by Marcano *et al.*[184] and does not involve large

exotherm or highly production of toxic gas, in comparison with the widely used Hummer's method.[61]

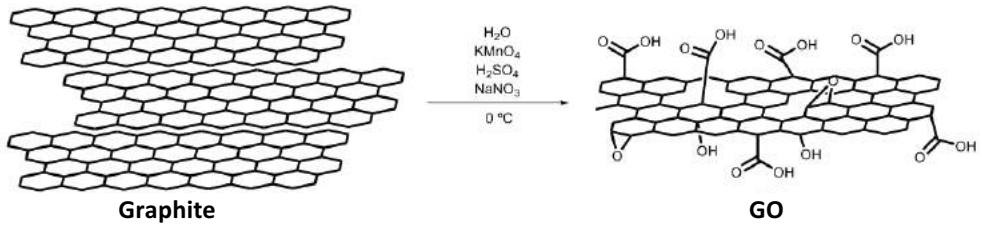

Figure 46. Scheme representation for the obtaining of GO.

The Raman spectroscopy of the oxidized material showed the characteristic bands of GO, a highly intense and broad D band (~1590 cm^{-1}) respect to the graphite spectrum. Thermogravimetric analysis showed major weight loss between 150 and 450 °C, which probably corresponds to thermally unstable oxygenated groups as CO, CO_2 (45% of weight loss), after 450 °C a slower weight loss of 5% was observed (Figure 47).

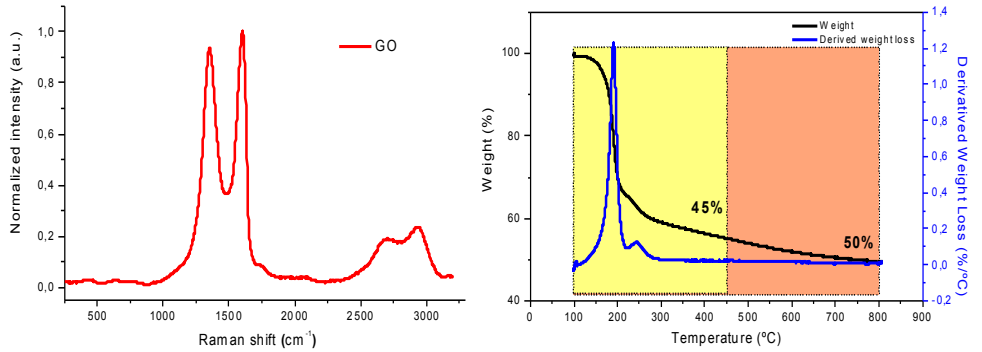

Figure 47. Raman spectrum of GO and TGA profile (black line) with the corresponding first derivative (blue line) of GO.

As we expected, the obtained GO presented higher water dispersibility because of the oxygen-containing groups. Subsequently, its chemical reduction was carried out to partially recover the aromatic structure with better electrical properties but maintaining the water dispersibility. The GO was dispersed in a basic medium containing hydrazine under high temperature. After several washes by dialysis and filtration to remove the excess of the chemical reductive agent, the rGO was obtained as a black powder.

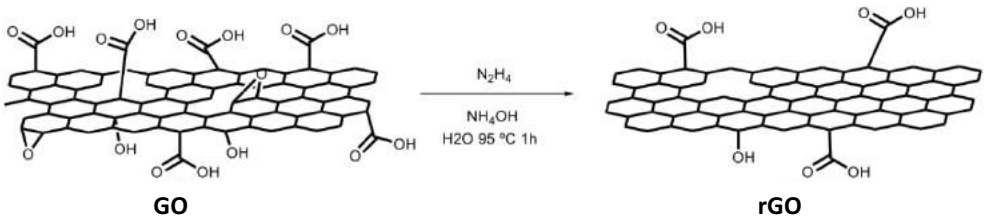

Figure 48. Scheme representation for the obtaining of chemically rGO.

The reduction of GO was confirmed by TGA. The weight loss of the material decreased from 150 °C to 450 °C decrease from 45% to 12%. In addition, the Raman spectrum showed a decrease in the fluorescence due to the abundant oxidized carbon atom regions, a decrease in the area of the D band and an increase in the D band intensity, results according with the literature.[185]

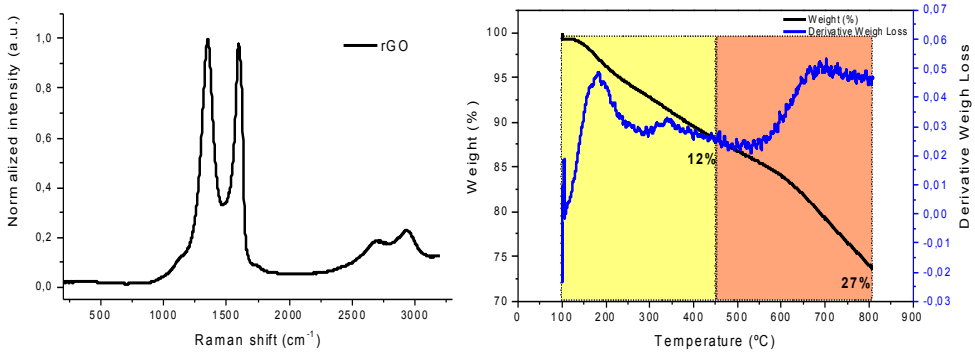

Figure 49. Raman spectrum of chemically rGO and TGA profile with its derivative.

2.2.1 Chemical Vapour Deposition Graphene

The CVDG used was supported by collaboration with the company Graphenea, an example of a general characterization is shown in the Figure 50.

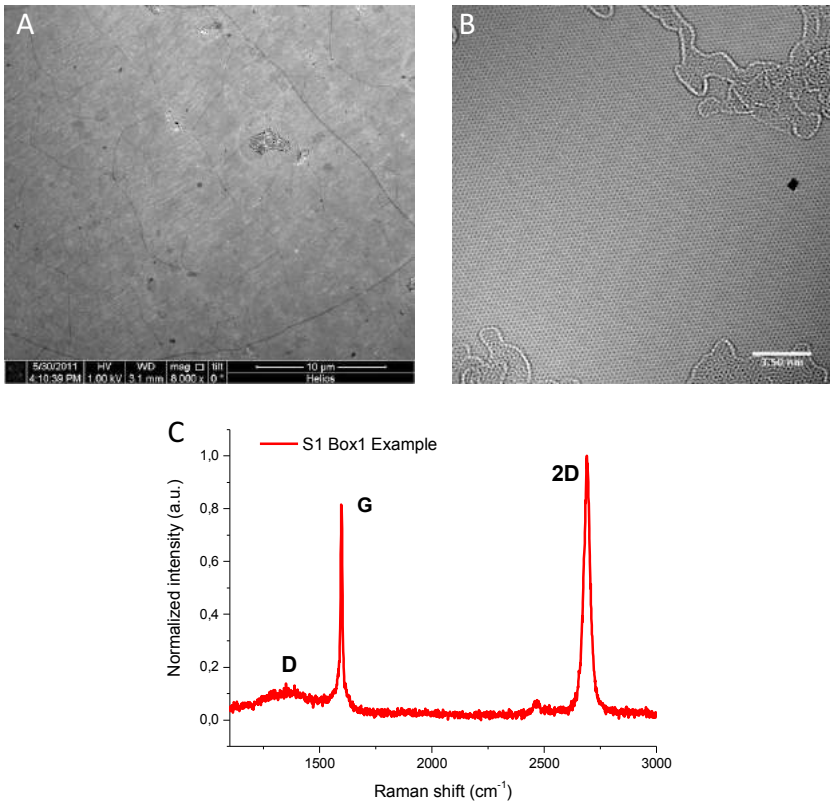

Figure 50. Characterizaton of CVD pristine graphene provided by Graphenea; (A) SEM image of graphene supported on SiO_2/Si, (B) HRTEM of suspended graphene and Raman spectrum (C).

The material was transferred onto a $1cm^2$ of SiO_2/Si, 300 nm thermal oxide on one side.

2.3 Functionalization of graphene for biosensing

2.3.1 Electrochemical functionalization for the development of new electrodes for biosensing

Biosensors are quantitative analytical tools with biological materials and physicochemical transducer, the detection of oligonucleotides becomes a powerful tool for diagnosis.[186] In particular, the electrochemistry of graphene has being extensively exploited in biosensing technologies.[187,188] This section was focused on the electrochemical modification and functionalization of graphene derivatives in a platform developed for biosensing. As final step, to prove the effectiveness of the platform, we will attempt the electrochemical detection of a small oligonucleotide as a

receptor of the desire analyte in a future biosensor. The procedure of the section is summarized in the Figure 51, with four steps, we started with the conventional glassy carbon electrode (GCE) for the deposition of graphene onto its surface, following by the electrochemical functionalization of the graphene surface with organic moieties, and as final step, the attachment of an oligonucleotide for the electrochemical detection.

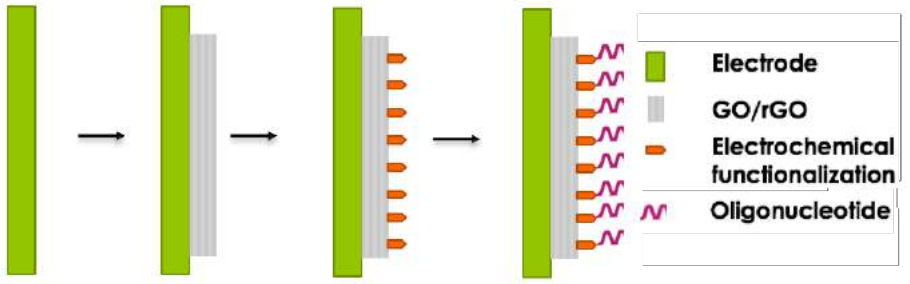

Figure 51. Scheme of the followed steps of the biosensing platform.

First of all, stable dispersions of graphene must be synthesized (see section 2.2). In electrochemistry, heterogeneous electron transfer occurs at the edges of the graphene derivative or at defects in the basal plane. GO and rGO provides abundant defect sites as well as the partial restoration of the conductance as electrode materials.[189] Besides, it contains large amounts of oxygen-containing groups, which can be beneficial to the functionalization with biomolecules for biorecognition.

The performance of the graphene-based electrode was carried out by the deposition of 10 μL of a GO aqueous suspension on a typical GCE. To avoid the detachment of the deposited graphene material, the corresponding solution was dried at room temperature for 2 hours.

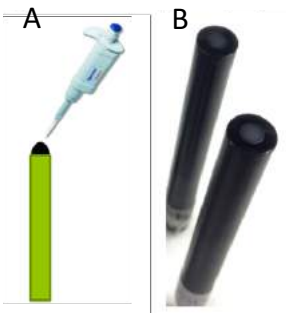

Figure 52. (A) Schematic representation of the drop casting deposition of GO onto GCE giving GCE/GO. (B) Image of two GCE/GO.

Then, the electrical properties of the resultant GCE/GO were observed to a cyclic voltammetry in presence of potassium ferricyanide in PBS. GCE allows ferricyanide to reach the electrode surface. However, after adsorption of GO, a significant decrease in the peak currents and higher separation in the peak signal was observed due to the repulsion of negatively charged of the functional groups presented in the surface of the material.

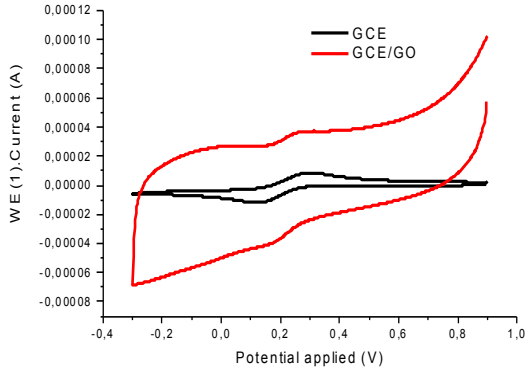

Figure 53. Cyclic voltammetry of GCE (black) and GCE/GO in presence of potassium ferricyanide.

The electrochemical reduction of GO becomes attractive due to the partial restoration of the conductance of the material. For that reason, our next step was to develop a direct electrochemical reduction of GCE/GO. Thus, a negative voltage was applied, obtaining an irreversible reduction peak starting at -0.8 V, which corresponds to the reduction of GO (Figure 54).

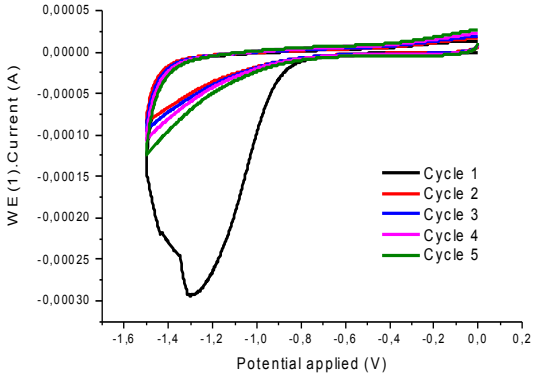

Figure 54. Cyclic voltammetry of the electrochemical reduction of GO (Electrochemical rGO).

To make possible the integration of this approach in a final sensing system, the modification of electrodes with graphene derivatives was transfer to other conductive platforms. Indium-free conductive substrates, such as Fluorine-doped Tin Oxide (FTO), are particularly promising for their increased resistance to chemical corrosion and cost reduction.[190] Thus, the development of this protocol was also performed using FTO as supporting electrode. A work area of 1cm^2 was delimited in the FTO to facilitate the characterization of the material. Optically, there was a clear colorimetric difference between GO (brown) and the electrochemical reduced graphene oxide (Electrochemical rGO) (black) on TFO (Figure 55).

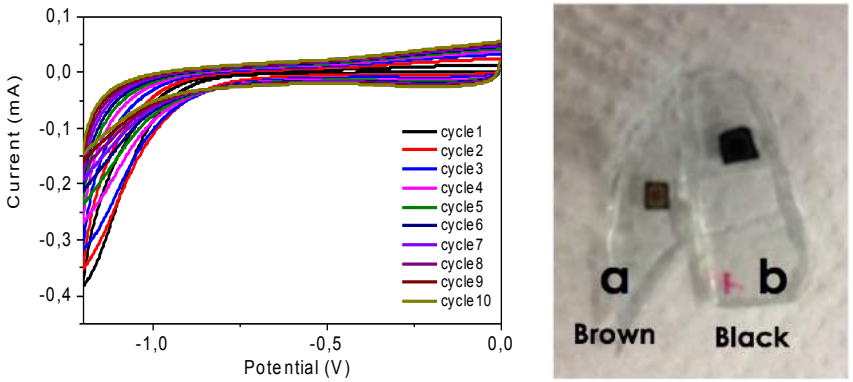

Figure 55. (Left) Cyclic voltammetry of the electrochemical reduction on FTO. (Right) Image of GO (a) and Electrochemical rGO (b).

There was a manipulation inconvenient after electrochemical reduction of the graphene material. Therefore, we decided to employ a sticky polymer to fix the GO before the reduction process. However, the detachment was only partially improved. Then, the following attempt was focused on the direct deposition of rGO on GCE. A rGO dispersion in water (10 μL, 1mg/mL) was dropped on the GCE. Then, the suspension was dried at room temperature. In the electrochemical characterization, different electrical properties of the electrodes were obtained between the nude GCE and the modified GCE/rGO. On one hand the rGO improved significantly the electrochemical behaviour in comparison with GO due to the partial remove of organic moieties during the reduction process. On the other hand, the ferricyanide signals presented small differences between redox peak potentials. In addition, GCE/rGO showed a good homogeneity of the drop deposition and reproducibility.

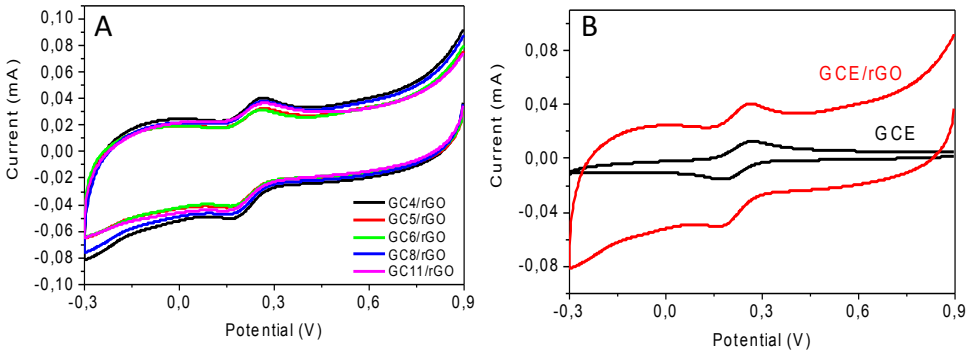

Figure 56. (A) Homogeneity on the cyclic voltammetry in presence of potassium ferricyanide for GCE/rGO. (B) Cyclic voltammetry in presence of potassium ferricyanide of GCE and GCE/rGO.

The covalent functionalization with aryl diazonium salt was performed as a next step in the construction of a sensing platform. Particularly, carboxylic groups will be introduced to increase the binding capability of the graphene surface in the attachment of sensing biomolecules. Therefore, 4-carboxybenzene-diazoinium tetrafluoroborate (4-CBD) was used to enrich the graphene surface with carboxyl groups for future attaching of biomolecules.

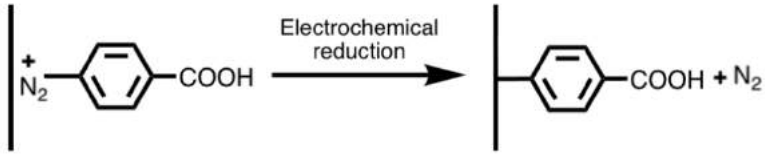

Figure 57. Scheme of the CBD coupling onto the surface of the modified electrode.

The GCE/rGO was immersed in a solution of 4-CBD (10mM). The electrochemical reduction was done thoroughly cyclic voltammetry. A band at 0.4 V was observed, being the highest transfer charge, which corresponds to the graphene functionalization (Figure 58) The electrochemical functionalization occurs in the first cycle of the reaction.

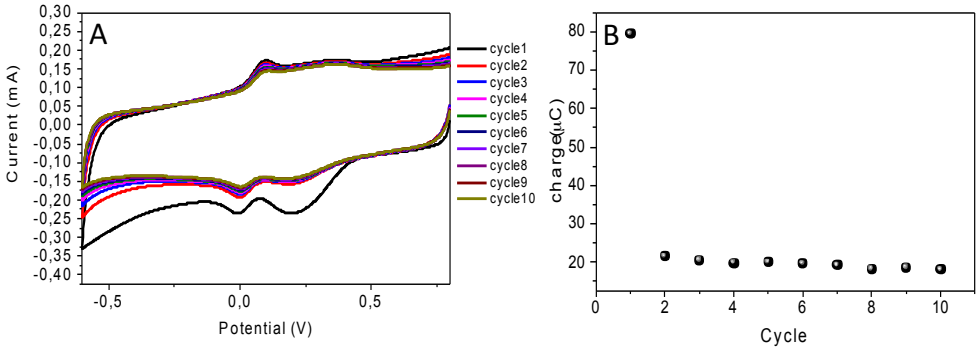

Figure 58. (A) Cyclic voltammetry for electrochemical functionalization of GCE/rGO. (B) Charge dependent in the number of cycles involved in the functionalization.

Electrochemical Impedance Spectroscopy showed significant differences in the profile of GCE/rGO and GCE/rGO/CBD. A high resistivity is observed in the functionalized electrode, confirming the successful covalent modification.

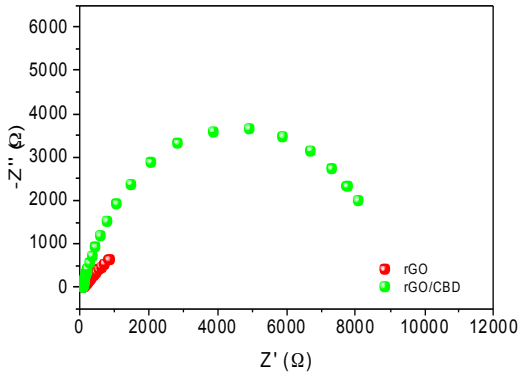

Figure 59. Impedance profiles of GCE/rGO and GCE/rGO/CBD.

With all the above-mentioned steps, we developed a modified platform based on a graphene material, which could be useful as biosensing platform.

There is emerging interest in transducing systems based on graphene derivatives, because possess a high conductivity and a preferably low electron transfer resistance on their surface. Furthermore, it is also beneficial if there is a large surface area for immobilizing biomolecules.[141] In particular, electrochemical polynucleotide sensors offer high sensitivity, high selectivity and low cost for the detection of selected DNA or RNA

sequences or mutated genes associated with human disease, and promise to provide a simple, accurate and inexpensive platform of patient diagnosis.

One of the most used sensing protocols for DNA and RNA analysis in graphene-based sensors is based on the electrochemical detection of the recognition event of aptamers (*e.g.* single-stranded DNA (ss-DNA) or ss-RNA) with the corresponding complementary analyte.[191] For instance, Zhou *et al.* reported an electrochemical DNA sensor is composed by a modified electrode with rGO where a ss-DNA is covalently inmobilized.[192] The sensing protocol was based on the passivation of the electrochemical signal of the free bases of immobilized DNA when the hybridization event occurs with the target polynucleotide, yielding a double-stranded DNA.

As proof of concept, our next step was focused on the attachment of amino oligonucleotide on the modified graphene surface by amide bonds, as recognizing element in a final sensor. The selected oligonucleotide is composed by 5 Guanine bases because their oxidation is easily detected in cyclic voltammetry when they are free.[62] For the attachment of amino 5-Guanine oligonucleotide carrying an amino group was mandatory the activation of the carboxylic acids present in our graphene electrode through the well-known cross-linking reaction with 1-ethyl-3-(3-dimethyl-aminopropyl) carbodiimide hydrochloride (EDC) and N-hydroxy-succinimide (NHS).

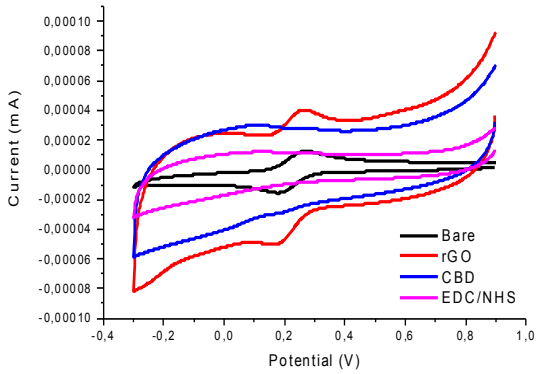

Figure 60. Cyclic Voltammetry profiles in the presence of potassium ferricyanide of all the modification processes of the graphene-based electrode.

Subsequently activation of carboxylic acid, 20 µL of amino 5-Guanine oligonucleotide were added to the electrode at different concentrations and

time. After washing, the measures of current against potential were performed to know the resistance of the modified electrode GCE/rGO/CBD/5G. Significant differences were observed as shown in Figure 61, where a higher concentration and longer time of the oligonucleotide with graphene, showed a higher resistivity of the electrode. It means that a higher attachment of the oligonucleotide is happening on the biosensing platform.

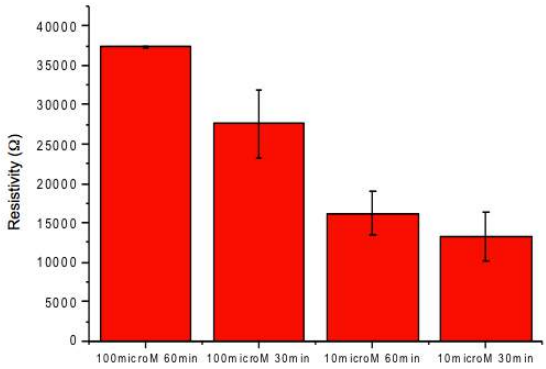

Figure 61. Resistivity values of a 5Gs oligonucleotide at different concentrations.

We were able to observe differences in the introduction of oligonucleotide to our system GCE/rGO/CBD. However, we were not able to detect the redox peak of free Guanine in the cyclic voltammetry of the system, loosing great value for the use of this platform as biosensor. The possible explanation is the formation of polymer in the diazonium reaction[193,194] that can passivate the graphene surface. Therefore, it will be necessary to find controllable modifications for graphene derivatives.

2.3.2 CVD graphene functionalization for biosensing

Graphene has demonstrated indisputably the potential as next generation electronic material, however, nowadays monolayer graphene cannot stand alone, it needs a supporting substrate for a desired application.[195] The examples in the literature for supporting substrates for this material is varied: metals,[196] semiconductors,[197] polymers, or also liquids make the called next generation hybrid devices a powerful tool for applications.[198] This combination with other aspects can modify the morphology, structure, interaction and properties of graphene.[199,200] For that reason, the understanding of the behaviour of graphene on surface and its modification

become a highly interest research topic.

The introduction of graphene onto a holding support brings new characteristics to the hybrid device, the interface between graphene and substrate plays a dominant role, for the obtaining of a good quality graphene. All this mentioned above has direct impact onto graphene reactivity. Chemical functionalization of graphene on substrates is a topic of paramount importance, the surface modification of the material can allow the tuning on the physical and chemical properties.[201,202] Small roughness of the substrate,[52] doping,[203] or induced curvature of graphene,[204] make different reactivity and behaviour, being necessary the search of new conditions for surface modification of the material.

2.3.2.1 Diazonium coupling reaction

A well-known and widely employed modification of CVDG for biosensing is through diazonium coupling reaction (mentioned in section 1.7). Among different reported strategies Strano and co-workers reported the use of surfactants for a suitable modification of CVDG with diazonium salts in diverse surfaces. We considered the functionalization of CVDG on SiO_2 immersed in a 1% aqueous solution of SDBS (Figure 54). However, this approach was incompatible with our CVDG samples on SiO_2, because the anionic surfactant facilitates the detachment of the graphene material.

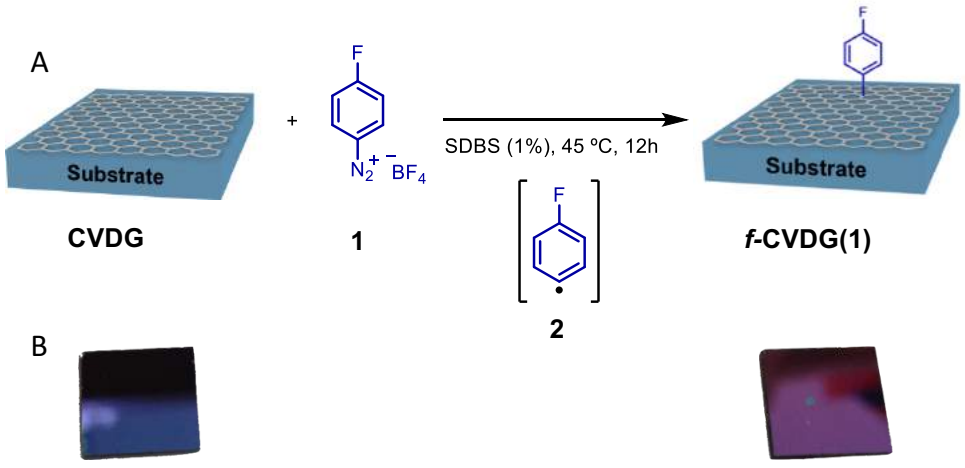

Figure 62. Scheme of diazonium coupling reaction (A). Photo of the pristine substrate, and of the substrate after detachment(B).

In order to reduce the detachment and obtain a reproducible graphene functionalization, the modification of reaction parameters as time and

temperature were checked. The optimal conditions are summarized in the Figure 63.

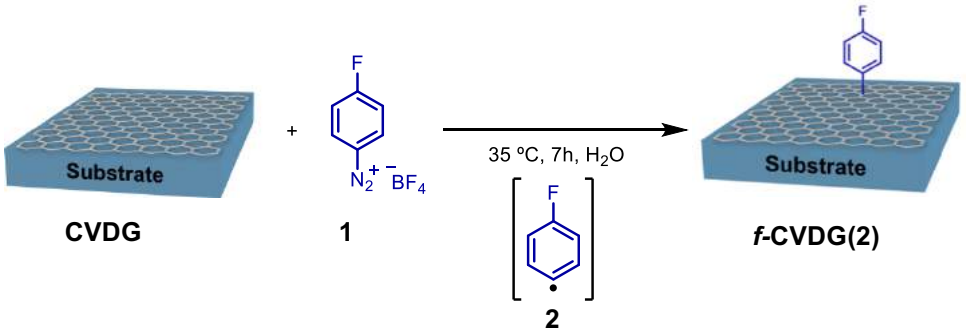

Figure 63. Conditions for the diazonium coupling reaction.

In our methodology, the key point to avoid the detachment was the concentration of the diazonium salt **1**. A deep study of the influence of the concentration determined that $1.6x10^{-4}$ M is enough to obtain high degree of functionalization with very low detachment. Figure 64 shows how the detachment began in the edges of the substrate, we can assume that probably the interaction substrate-graphene is lower in the edges than in the centre of the sample.

Figure 64. Partial detachment of graphene (5%) in the edge of the f-CVDG(**2**) supported on SiO_2 sample.

Raman spectroscopy confirmed the high degree of functionalization for this reaction. The Raman mapping of D band intensity in a representative graphene region of the sample indicated the increment of sp^3 carbon atoms in the graphene structure due to the covalent functionalization.

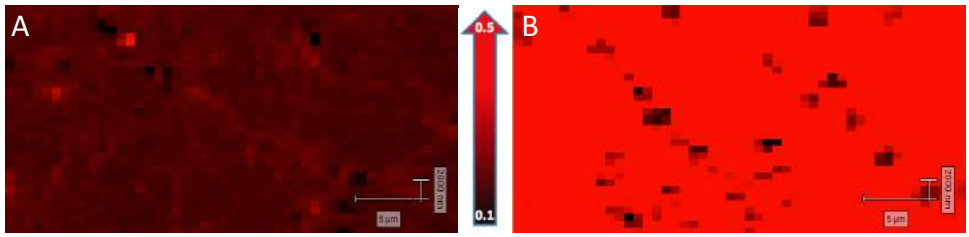

Figure 65. Raman mapping of the I_D/I_G before (A) and after the diazonium salt reaction (B).

After the optimization of diazonium salt modification with CVDG samples, we addressed the introduction of functional groups on the diazonium moiety. These functional groups can be tailored by organic chemistry to allow various chemical characteristics to be coupled to the graphene. In particular, we decided to anchor on graphene primary amine as active group. To this end, the diazonium salt **3** was synthesized, carrying a protected amine with a tetrafluorophthalamide unit as protecting group. The presence of the fluorine atoms will allow to confirm by XPS analysis, the covalent modification of graphene and the subsequent amine deprotection. Thus, a graphene-based electrode composed by CVDG on ITO was modified by diazonium coupling reaction. Figure 66 shows the first step performed for the introduction and deprotection of the diazonium salt. The thermal decomposition and generation of the radical reaction was done *in situ* from corresponding aniline with isopentyl nitrite.

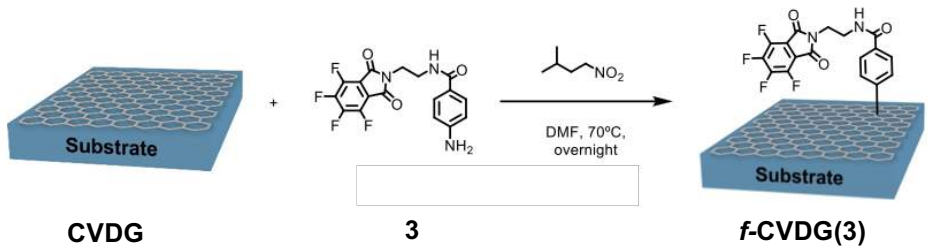

Figure 66. Scheme of surface modification of CVD graphene electrode through diazonium reaction.

Raman spectra showed high variations on the D band intensity between pristine graphene and functionalized (*f*-CVDG(**3**), this result is in concordance with XPS analysis, where F and N was detected onto the surface of *f*-CVDG(**3**).

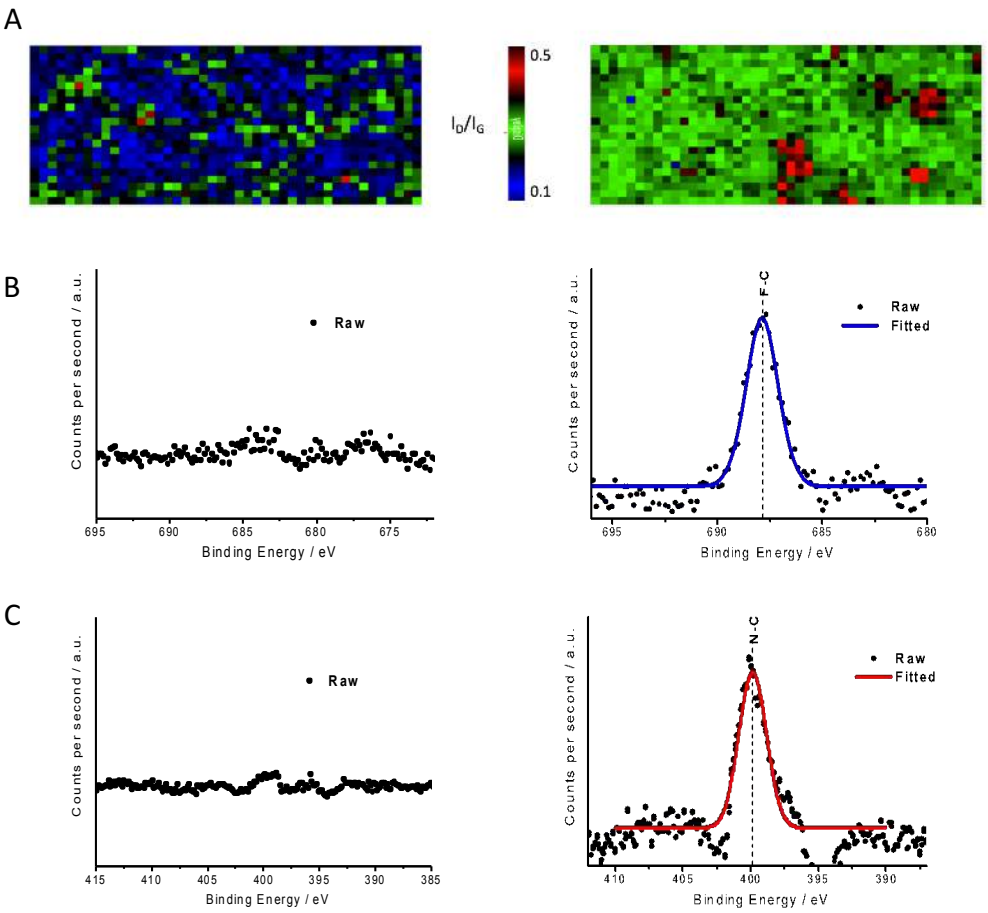

Figure 67. (A) Raman mapping of I_D/I_G before (left) and after (right) the reaction. (B and C) XPS analysis of the reaction regarding the presence of F and N before (left) and after reaction (right).

Next step was the deprotection of the amine group through removal of phthalimide group by using hydrazine monohydrate ($N_2H_4 \cdot H_2O$)

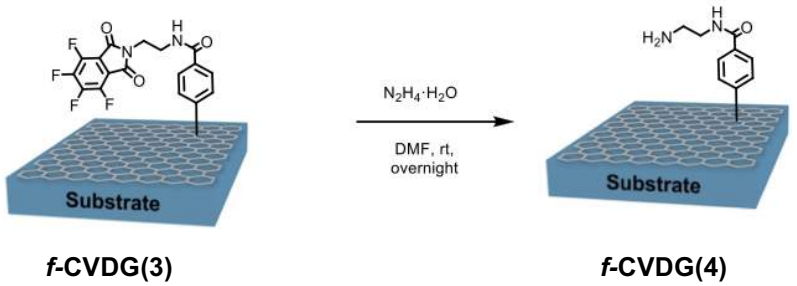

***f*-CVDG(3)** ***f*-CVDG(4)**

Figure 68. Scheme of amine deporotection CVD graphene electrode.

The deprotection of CVDG supported by XPS analysis where the presence of F atoms onto the graphene surface of *f*-CVDG(**4**) disappeared remaining the presence of N on the surface of CVDG.

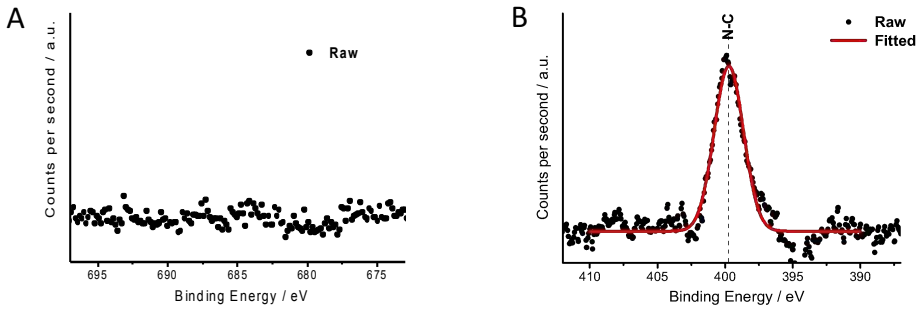

Figure 69. XPS analysis of the reaction regarding the absence of F (A) the presence of N(B).

The introduced moieties can potentially interact with desired bioactive molecules for the development of biomedical devices. In addition, this approach involves, for the first time, the introduction of protected amines with the possibility of it deprotection, being functional for multiple functionalization with orthogonal protecting groups.

2.4 Conventional aryne functionalization of graphene derivatives by decomposition of *o*-(trimethylsilyl)aryl triflates

Covalent modification of graphene *via* aryne reactions is a methodology already reported in different carbon nanomaterials, such as fullerene, carbon nanotubes and nanohorns.[92,93] In particular, aryne reactions were also reported in diverse graphene derivatives. However, it is an underexplored covalent modification for this carbon material, with a few scientific contributions. For instance, in 2010 the first functionalization of graphene with arynes was described, but they employed an inaccessible FLG obtained by arc-discharge.[95] Martín *et al.*[105] has also functionalized FLG with an uncommon C_{60}-aryne. Another graphene derivative as CVD graphene supported on copper was modified with benzyne with a unsatisfactory characterization. [131] Besides, to the best of our knowledge, other graphene derivatives as GO or rGO have never been reported.

Therefore, in this section the underexplored covalent modification of graphene derivatives with arynes by fluorine-induced decomposition of *o*-

(trimethylsilyl)aryl triflates will be performed, to develop a more selective, controllable and less aggressive modification method.

2.4.1 Aryne functionalization of FLG

First of all, the aryne modification was addressed in one of the most common graphene derivatives, exfoliated graphene, considering reported results.[93,104] FLG was obtained by Coleman method.[37] The first attempt was addressed by using ultrasounds and NMP as exfoliated solvent. The remaining graphite was separated from the exfoliated material by decantation, resulting a FLG suspension. Then, the FLG was functionalized with benzyne (**2**) by the fluoride induced decomposition of *o*-(trimethylsilyl)benzyl triflate (**1**) with tetra-*n*-butylammonium fluoride (TBAF, see section 1.8.1).

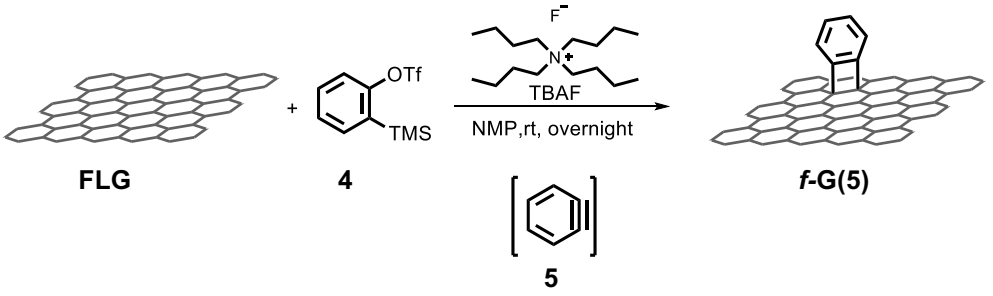

Figure 70. Scheme representation of the reaction of FLG with aryne precursor.

Raman spectroscopy showed a small increment in the D band for the *f*-G(**5**) respect to the pristine FLG, ($\Delta I_D/I_G$=0.04) (Figure 71).

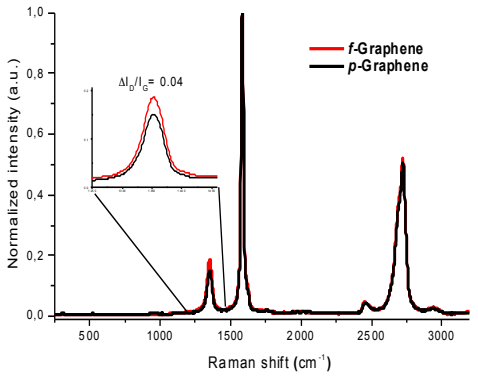

Figure 71. Raman spectra of *p*-Graphene and *f*-Graphene.

The morphology of graphene material was studied by TEM. A similar structure and dimensions were found between pristine and functionalized material.

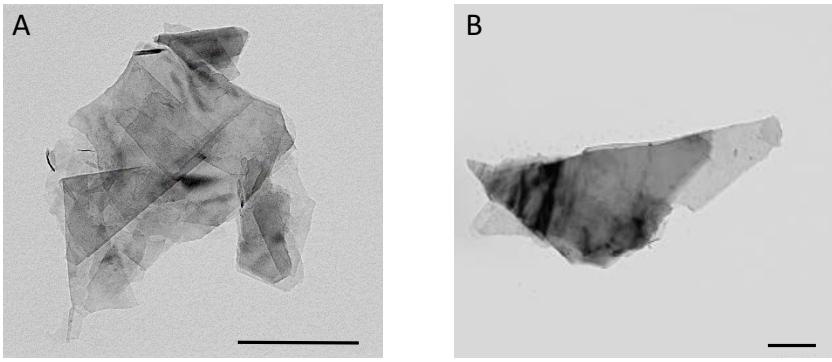

Figure 72. TEM images of of *p*-Graphene (A) and *f*-Graphene (B). Scale bar are 500nm.

New reaction conditions were explored to improve the functionalization approach. The control of solubility of the ion fluoride, through the election of the solvent, or the presence of additives as crown ethers,[171] allows to modulate the role of aryne generation. For instance, the employment of CsF in CH_3CN is very useful due to the partial solubility of the fluorinated salt. Thus, we decided to employ a mixture of solvents, ODCB that is a good exfoliating solvent of graphite, and the polar organic solvent CH_3CN that can partially solve CsF. In addition, we decided to add 18-crown-6 ether to improve the solubility of CsF in this mixture of solvents. (Figure 73).

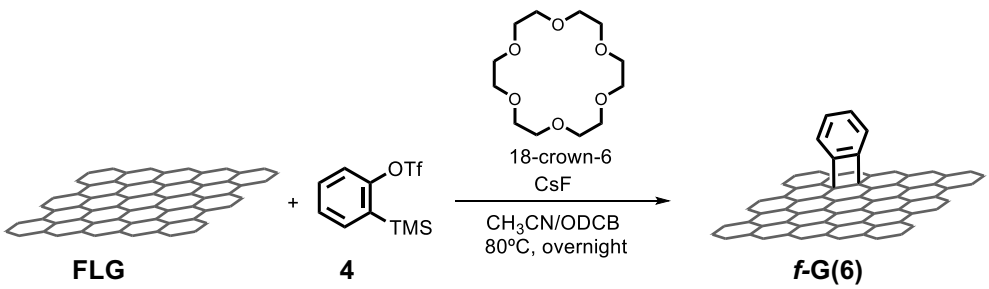

Figure 73. Scheme representation of covalent modification of graphene.

In addition, to discard false positives in the graphene modification, a control sample of the reaction was performed without the benzyne precursor **4** (*cs*-G(**6**)). The Raman spectra showed high differences between

the *p*-Graphene and the *f*-G(**6**). However, the *cs*-G(**6**) also revealed a significant increment of the D band which means that a modification occurred without the presence of benzyne (Figure 74). Probably, it is due to the presence of ODCB in the reaction media. Dresselhaus *et al*. reported experimental evidences and theoretical studies that suggest that ODCB can chemically and physically interact with walls of carbon nanotubes.[206]

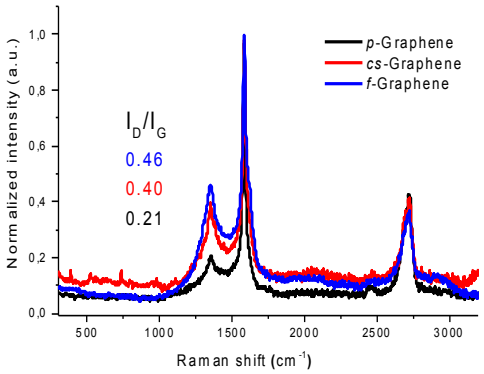

Figure 74. Raman spectra of *p*-Graphene (black), *cs*-Graphene (red) and *f*-Graphene (blue).

In the following attempt, we decided to use NMP instead of the halogenated solvent to avoid the possible undesired modifications. NMP was selected because of its high surface tension which make it as a good exfoliation solvent for graphite.[36]

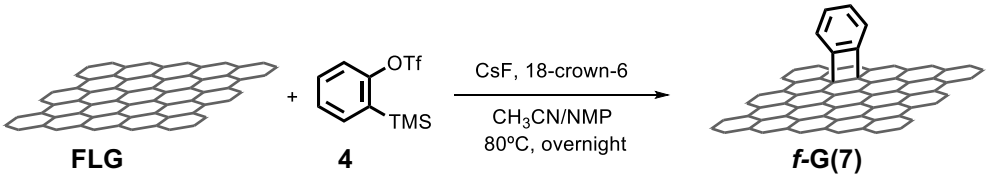

Figure 75. Scheme of the reaction with the use of acetonitrile and NMP as solvents.

The Raman spectra showed changes in the D band intensity ($\Delta I_D/I_G$= 0.08), being higher than the reactions described before. In this case, the control sample did not increase D band intensity.

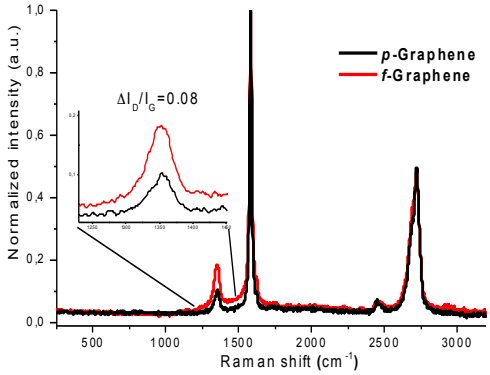

Figure 76. Raman spectra of *p*-Graphene (black) and *f*-Graphene (red).

In order to explore the potential of the new reaction conditions, the described graphene functionalization was performed with a structurally more complex aryne. [207]

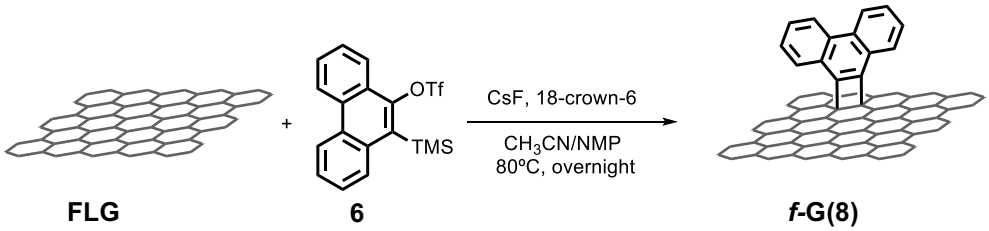

Figure 77. Scheme of functionalization of FLG graphene.

The covalent functionalization was confirmed again by Raman spectroscopy. On one hand, the control sample in absence of **6** did not modify the pristine graphene. On the other hand, a slight increase of the D band is detected for the functionalization with the generated aryne from **6**. In addition, TGA profiles showed only 1% variation between the control sample and the functionalized graphene. This increment represents a low degree of functionalization. These results encouraged to the search of new routes for the aryne functionalization onto graphene-based materials.

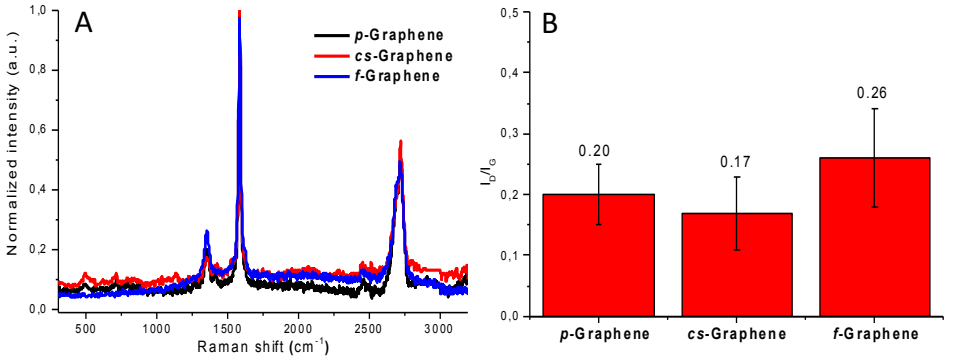

Figure 78. Raman spectra (A) and I_D/I_G ratio of *p*-Graphene, *cs*-G(**8**) and *f*-G(**8**) (B).

All the attempts of functionalization described above had the characteristic of low amount of final sample due to the exfoliation method which hindered a good characterization and the use of the material for further modifications, with bad dispersibility of the FLG during the reaction process. Therefore, we decided to use another graphene-based derivative with better dispersibility, such as rGO.

2.4.2 Aryne functionalization of rGO

The covalent functionalization of rGO with aryne precursors was performed using different reaction conditions with the following solvents: CH_3CN, CH_3CN/Toluene (1:4) and toluene, which correspond to *f*-rGO(**9**-**11**), respectively.

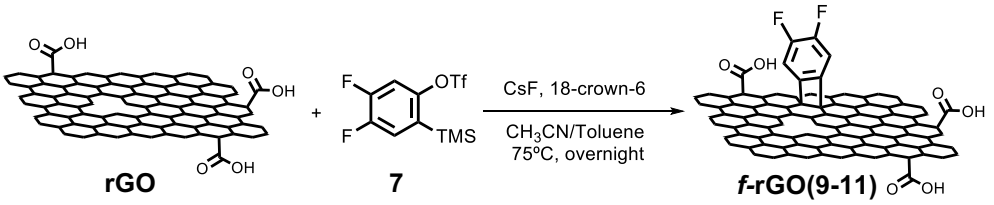

Figure 79. Schematic representation of chemical functionalization of rGO with the generated aryne from **7**.

In this case, Raman spectroscopy is not useful to confirm the covalent functionalization due to the highly defective structure of rGO, which is reflected in its high D band. However, the introduction of difluorophenylene allows the confirmation of functionalization by the detection of fluorine atoms in the chemical composition of the *f*-rGO by XPS

analysis. The Table 1 summarizes the composition of the different samples observing the presence of fluorine atoms in the surface of the material. In addition, the control sample *cs*-rGO(**10**), was performed in absence of **7**. All *f*-rGO showed a significant and similar atomic composition of fluorine atoms, being the *f*-rGO(**10**) the functionalized material with the most abundant fluorine atomic percentage. In addition, the reaction conditions of *f*-rGO(**9**-**10**) led to a loose of oxygen percentage in the final modified material; probably, because of a partial reduction. However, CsF is not totally inert all of these chemical modifications, because *cs*-rGO(**10**) showed a 5% of fluorine atoms in its atomic composition. Presumably, fluoride ions led to side reactions with rGO.

Table 1. Atomic composition percentage, functionalization degree[1*] (FD) and weight loss of rGO samples.

Sample	XPS analysis			TGA	
	C1s (%)	O1s (%)	F1s (%)	Weight Loss (%)	FD (μmol/g)
***r*GO**	63.3	36.7	-	10.6	-
***f*-rGO(9)**	52.8	15.1	32.1	14.4	257
***f*-rGO(10)**	36.7	15.1	33.6	12.6	135
***f*-rGO(11)**	42.5	34.5	23.0	16.3	385
***cs*-rGO(9)**	82	12.5	5.5	17.1	439

TGA results are in concordance with XPS analysis, where higher degree of functionalization is observed for the reaction with toluene (385 μmol/g) and acetonitrile (257 μmol/g) against the reaction with a mixture

[1*] In order to draw quantitative information from thermogravimetric plots, we performed the following calculation to obtain functionalization degree (FD); where *L* corresponds to the weight loss observed at 500 ºC (in %), after having subtracted the analogous loss from the pristine material. The molecular weight (*Mw*) is set for the expected desorbed moiety. The conversion factor (10^4) provides data in the desired unities (μmol/g).

$$\frac{L(\%)\cdot 10^4}{Mw(g/mol)} = FD\ (\mu mol/g) \qquad \text{Equation (1)}$$

CH_3CN/Toluene (1:4) (135 μmol/g). However, *cs*-rGO(**10**) showed a higher weight loss in TGA, due to the possible side-products with CsF. Finally, as conclusion we developed a methodology for covalent modification of rGO through anderexplore aryne cycloaddition reaction.

The morphology of functionalized reduced graphene materials was studied by TEM. A similar structure and dimensions to the pristine material after the described treatment was observed.

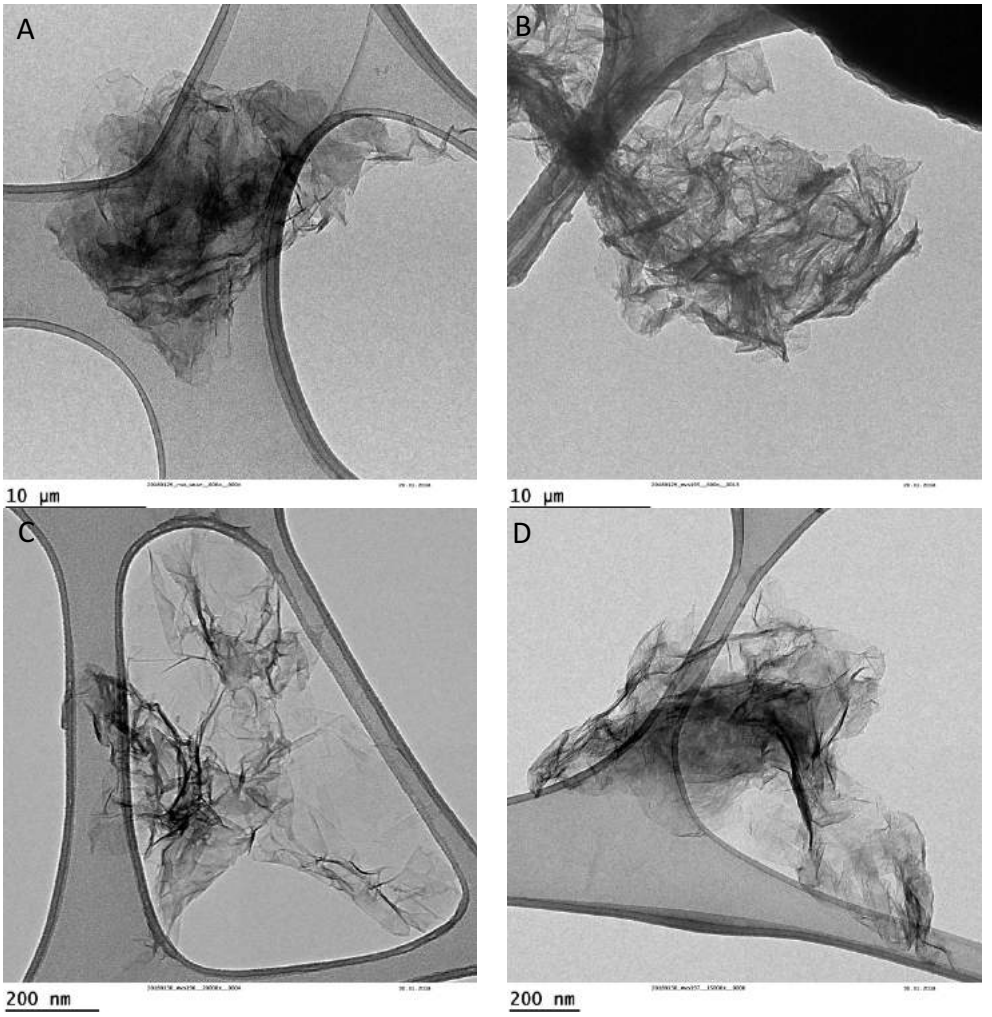

Figure 80. TEM images of (A) rGO, (B) *f*-rGO(**9**), (C) *f*-rGO(**10**) and (D) *f*-rGO(**11**).

2.4.3 Aryne functionalization on CVD graphene

As mention in section 2.3.1, chemical functionalization of graphene on substrates is a topic of paramount importance due to the direct surface modification of the material. Aryne functionalization on CVDG are an underexplored reaction, Magedov *et al.*[105] reported a benzyne functionalization using Cu as supporting substrate; however, there are no other examples in the literature with this graphene derivative. For that reason, different covalent modifications using arynes, combined with different strategies, were performed on graphene surface of CVDG on SiO_2, under different reaction conditions. As first approach, fluoride induced decomposition of triflate *o*-trimethylsililaryl precursor was developed, under stirring and the use of a non-soluble CsF in acetonitrile.

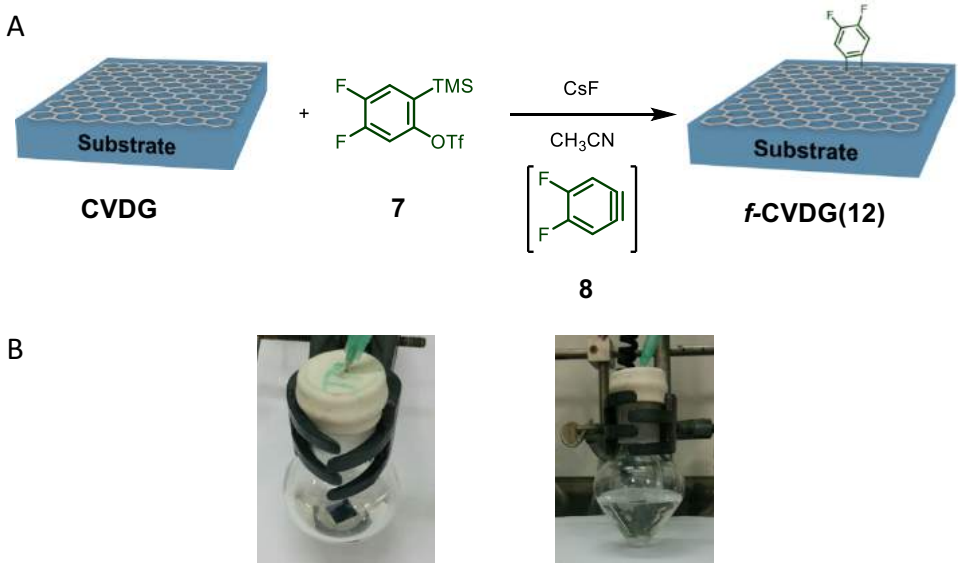

Figure 81. Scheme of the reaction of CVD-Graphene (A). Image of the specific procedure of the reaction (B).

Figure 81 shows how the reaction was performed in a pear-shaped flask, where the magnetic stirred was placed under the substrate, to avoid any interference with the graphene sample.

The functionalization was monitored by Raman spectroscopy. Graphene sample was mapped and characterized with more than one thousand points in order to have a representative area (>400μm²). The mapping observed after reaction showed high degree of detachment, where graphene was

practically removed from the substrate (Figure 82B). Only small portion of graphene was found by the Raman mapping with increase of the D band (Figure 82D).

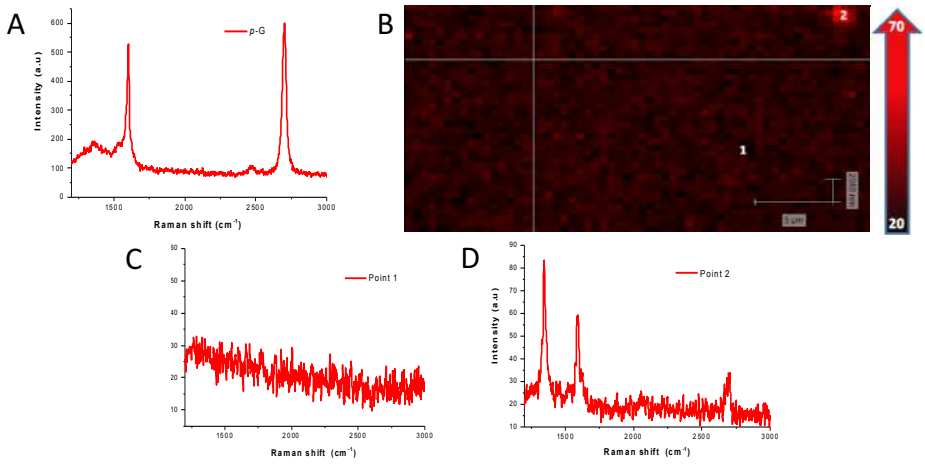

Figure 82. (A) Raman average spectrum of pristine graphene. (B) Mapping representation of the D band intensity (1355 cm^{-1}) of *f*-Graphene. (C) Example of a graphene detachment point without any characteristic band of graphene in the spectrum of *f*-Graphene. (D) Spectra of one of the few points where *f*-Graphene was observed.

Several control samples were performed without the presence of aryne precursor for the optimization of the process to study the influence of the reactant and solvent in the graphene derivative. Table 2 summarizes the approaches performed; from the use of different fluoride sources, different time or different solvents. In order to solve the detachment, we considered dispensing with stirring and replacing the partially solved fluorinated salt, such as CsF, by TBAF, which is totally soluble in organic solvents. Finally, we considered the entry 6 the most suitable condition to perform the covalent functionalization of aryne without risk of detachment.

Table 2. Conditions of the control sample reactions. [a]Detachment was calculated through optical microscopy.

ENTRY	Solvent (10mL)	Salt	Equiv of F^-	Time (h)	Stirring	Detachment (%)[a]
1	CH_3CN	CsF	1.5	24	Yes	99
2	CH_3CN	CsF	1.5	3	Yes	99
3	THF	TBAF	1.5	48	No	95
4	THF	TBAF	1.5	4	No	90
5	THF	TBAF	1.5	0.75	No	10
6	THF	TBAF	1.5	0.15	No	0

In a next step, the optimization of the CVDG modification with the aryne XX was addressed, considering the reaction conditions described above in the entry 6. In particular, the reaction parameters such as reaction time and concentration of the corresponding aryne precursor were investigated (Table 3).

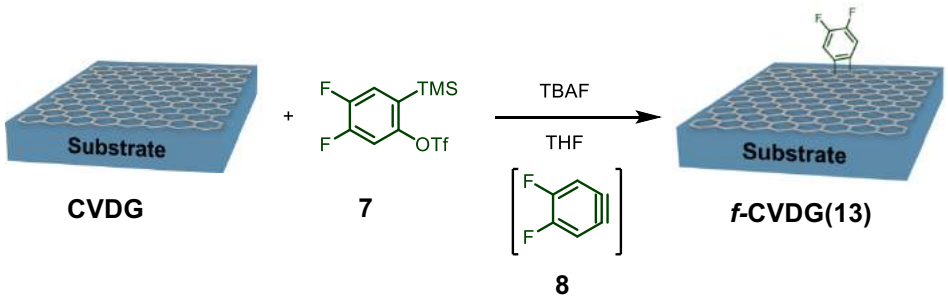

Figure 83. Scheme of the covalent functionalization of graphene with aryne precursor **7**.

Table 3. Different reaction conditions for the aryne reaction of CVDG. [a] Detachment was calculated through optical microscopy.

Entry	M (7)	Time / min	Equiv (7)	Detachment[a]	$\Delta(I_D/I_G)$
1	0.05	15	1.3	NO	0
2	0.05	30	1.5	NO	0
3	0.075	30	1.5	NO	0
4	0.125	40	1.5	YES (>90%)	0.6
5	0.15	45	1	NO	0.2

Table 3 shows the different approaches to perform the functionalization. The main problem was the detachment of the sample, that can be detected by optical microscopy and corroborated by Raman measurements. (Figure 84)

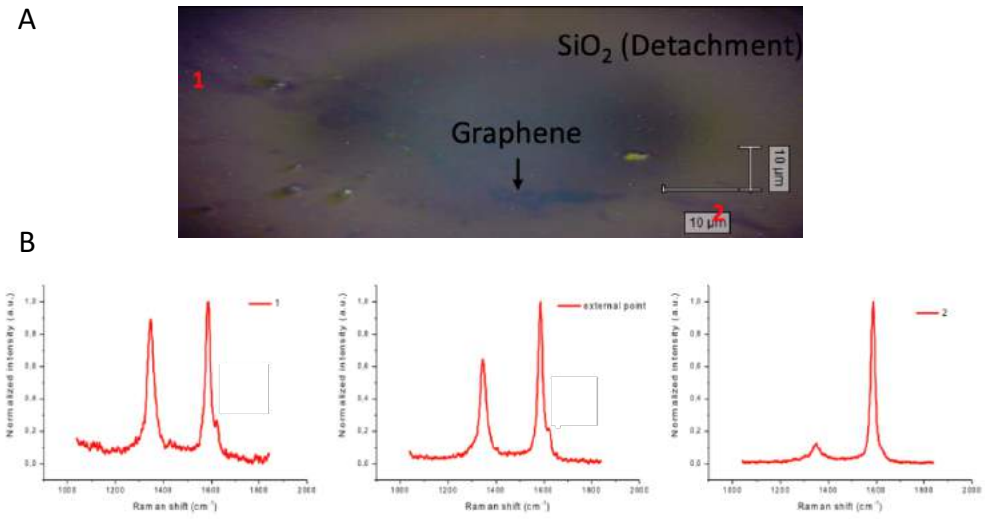

Figure 84. Example of functionalization and detachment by optical microscopy (A) and Raman measurement (B) of Entry 4 of the Table 3.

The optimal conditions are summarized in the entry 4 of Table 3. Raman mapping of the sample confirms the homogeneous increment of the D intensity in *f*-CVDG(**13**).

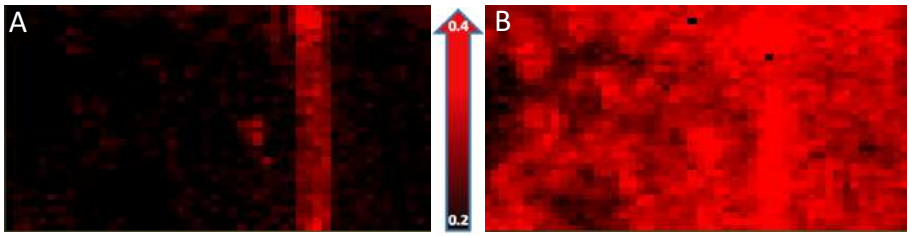

Figure 85. Representation of I_D/I_G before (A) and after (B) the reaction.

The functionalization with the difluoride aryne precursor was also confirmed by XPS analysis, due to the chemical modification of the functionalized graphene composition. The *f*-CVDG showed fluorine atoms on its surface atomic composition.

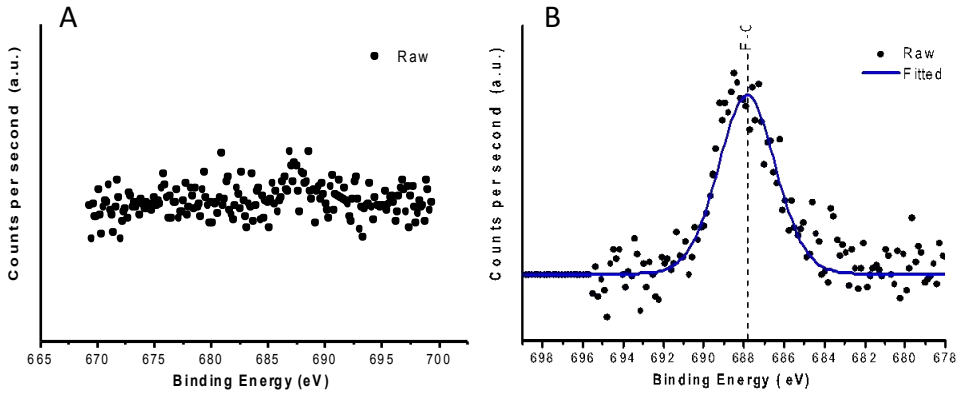

Figure 86. XPS analysis of the surface of *p*-CVDG and *f*-CVDG(**13**) for the detection of florine.

We were able to find the conditions to successfully perform the covalent functionalization of this CVDG in presence of arynes with the fluoride induced decomposition of triflate *o*-trimethylsililaryl precursor; however, we studied other routes to perform aryne reactions.

The decomposition of phenylene anhydrides or 1,2- dihalogentated benzene can generate benzyne. As mention in section 1.6, Yeon *et al* described generation of benzyne through the thermal decomposition of phthalic anhydride.[132] The aryne generation of *o*-dihalogenated and arylene anhydrides through photolysis was also described in the literature.[208–214]

Thermal decomposition of phthalic anhydride to generate the benzyne precursor was tested. After several attempts, we were not able to confirm the covalent functionalization of the substrate, sublimation of the organic moieties prevented the decomposition onto the surface of graphene.

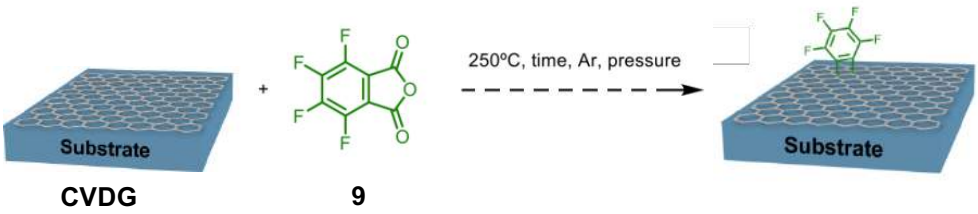

Figure 87. Schematic representation of the approach by thermal decomposition.

In order to find other alternative, the use of ultraviolet light for the decomposition of 1,2-diiodobenzene (**10**) was performed, we developed two approaches: on one hand the use of acetonitrile in order to dilute the aryne precursor, in the other hand, the substrate was directly dropped with the benzyne precursor.

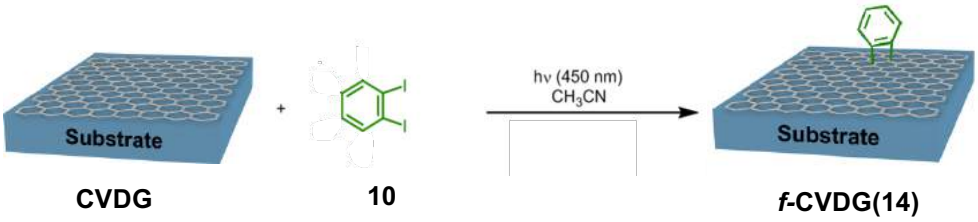

Figure 88. Schematic representation of the reaction between *p*-CVDG and 1,2-diiodobenzene (**10**), using CH_3CN.

After reaction represented in
Figure 88, Raman spectra showed high degree of detachment. However, the remained graphene on the substrate revealed small degree of functionalization in terms of I_D/I_G ratio.

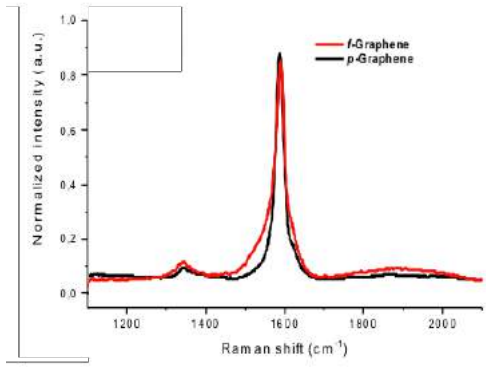

Figure 89. Raman spectra of *p*-CVDG and *f*-CVDG(**14**).

The reactions were performed six hours under UV irradiation (7mW/cm^2), the substrate was dropped until totally surface cover. The colour of the liquid changed from colourless to yellow.

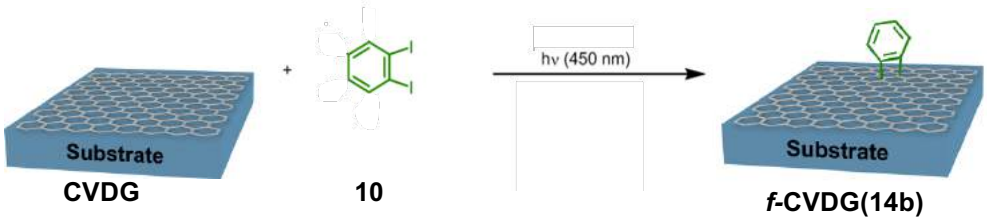

Figure 90. Schematic representation of the reaction between *p*-CVDG and 1,2-diiodobenzene (**10**).

Raman spectroscopy showed better results for this approach, functionalization was achieved without presence of solvent. The spectra of the Figure 91 is an average of a represented area of 1200 points.

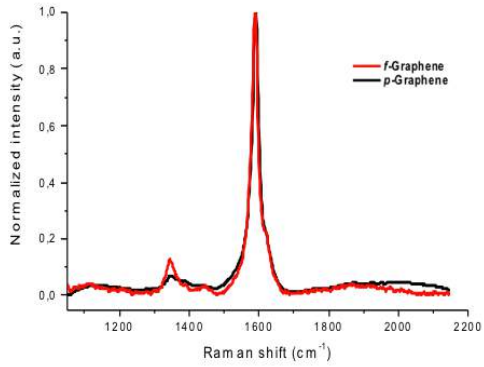

Figure 91. Raman spectra of *p*-CVDG and *f*-CVDG(**14b**).

Table 4. Conditions of *f*-CVD. [a] Detachment was calculated through optical microscopy

f-CVDG	Solvent	Time (h)	Power (mW/cm²)	Detachment (%)[a]	Δ(I_D/I_G)
14	CH_3CN	6	7	50	0.02
14b	-	6	7	0	0.07

In conclusion, the functionalization of CVDG on SiO_2 was performed under different aryne generation methods and reaction conditions. The functionalization was monitored by Raman spectroscopy. A moderate functionalization was development by fluoride induced decomposition of *o*-trimethylsililaryl triflate precursors and photodecomposition of *o*-dihalogenatedphenyl precursor. This procedure was also confirmed by X-ray photoelectron spectroscopy, due to the chemical modification of the functionalized CVDG composition.

2.4.3.1 Influence of the substrate in the graphene reactivity

CVDG is transferred to a large variety of substrates, depending on the application. In addition, graphene reactivity is strongly influenced by the underlying substrate. Strano *et al.* demonstrated that charged impurities or polar adsorbates on the surface of the substrate led to electron–hole charge fluctuations in the Fermi level of graphene, which increase its reactivity with diazonium salts.[215]

In order to study the reproducibility of the aryne reaction, this covalent modification was carried out with CVDG on diverse substrates. CVDG was transferred onto variety of substrates using a polymer-mediated transfer method. The tested substrates were: SiO_2, SiO_2 treated with HMDS, ITO and quartz. The corresponding covalent modification was performed using the abovementioned optimized conditions and graphene monitored by Raman spectroscopy.

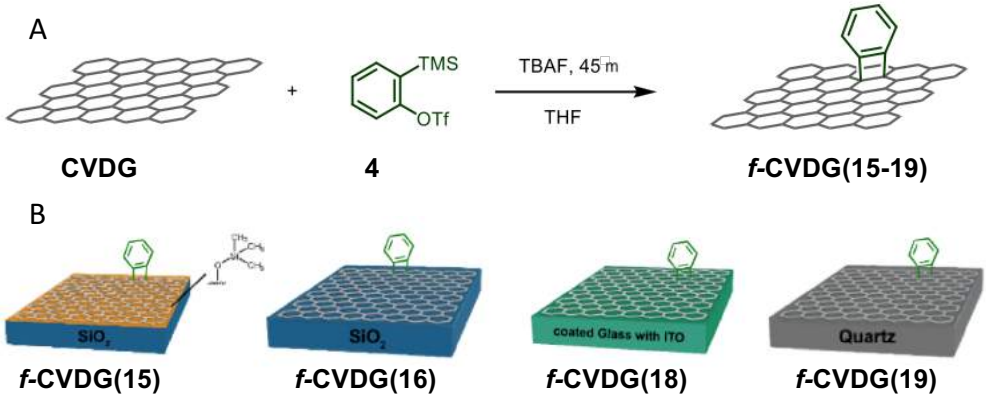

Figure 92. Scheme of the reaction (A) and different substrates used for the functionalization (B).

Typical substrates were tested for CVD graphene summarized in Table 5 and Table 6; However, the reaction was also performed on copper, Raman spectroscopy was difficult to explore due to the intense background signal from copper. For that reason, this widely used metal with CVDG could not be included in this study.

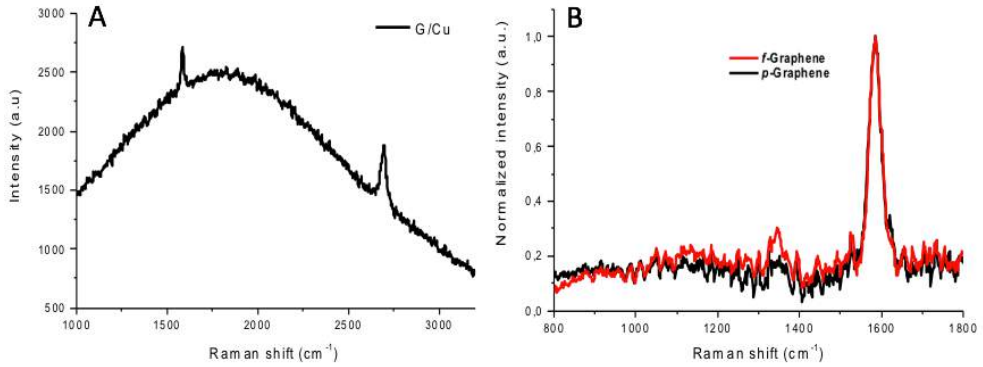

Figure 93. Raman spectrum of pristine graphene on Cu (A), *p*-Graphene and *f*-Graphene Raman spectra with baseline correction (B).

Table 5 shows the properties of the *p*-CVDG in different substrates. 2D Peak position near 2675 cm^{-1} with peak width under 30 cm^{-1} indicates better properties on graphene behaviour, acting as monolayer graphene.[71] For that reason, higher quality of graphene was found using ITO as supporting substrate. Table 6 collects the characteristic of the substrate after the functionalization, observing, a higher reactivity for hydrophilic substrates where the I_D/I_G ratios increased more after the functionalization. Probably, it

is attributed to higher electron-hole fluctuations in the Fermi level of graphene produced by underlying charged impurities on the surfaces.

Table 5. Study of pristine graphene for different substrates.

	Image	Optical image	I_D/I_G	2D Peak position	2D Peak width
SiO_2				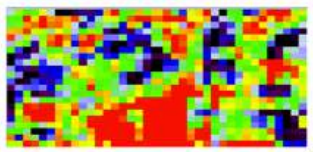	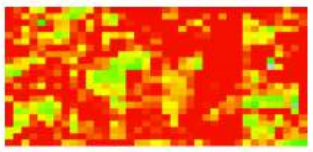
SiO_2 HDMS				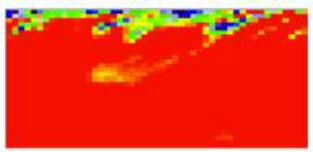	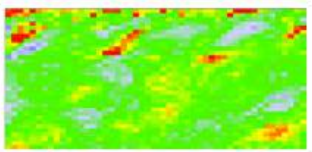
Quartz			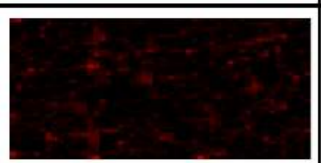		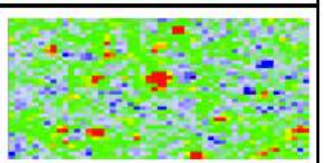
ITO			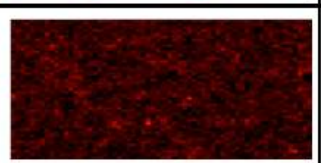	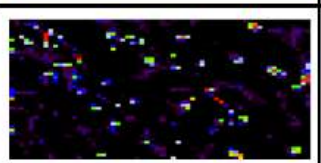	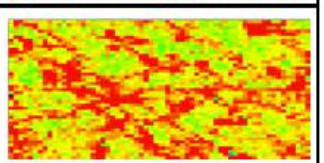
				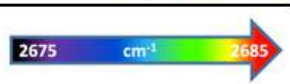	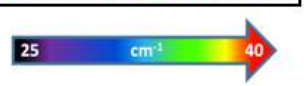

Table 6. Study of graphene after functionalization for different substrates.

	Optical image	I_D/I_G	I_D/I_G Spectrum	2D Peak position	2D Peak width
SiO_2			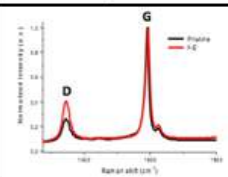	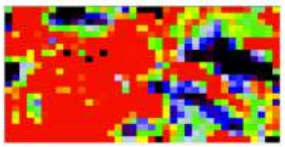	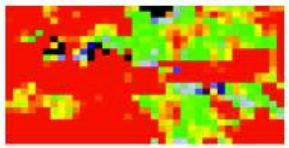
SiO_2 HDMS		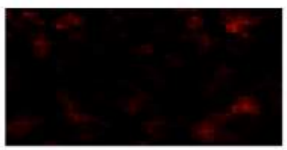	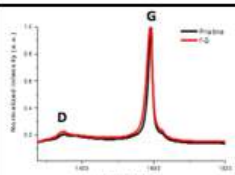	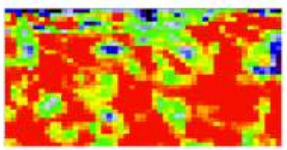	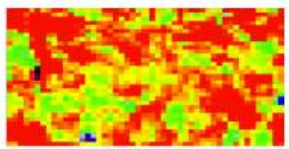
Quartz		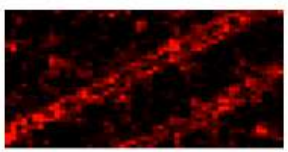	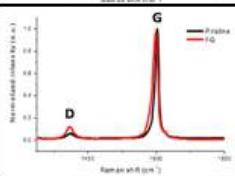		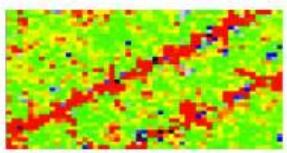
ITO		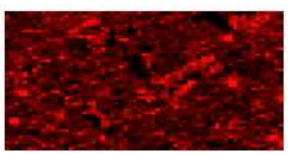	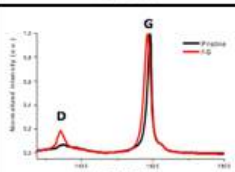	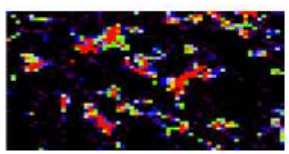	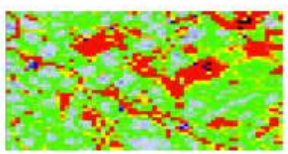

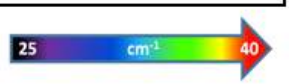

2.4.3.2 Preliminary results of the influence in the electronic properties of aryne functionalization of CVDG

The modification of graphene can tune the electronic behaviour of the material due to the transformation of sp^2 carbon atoms to sp^3. Cycloadditions becomes an interesting approach for the study of these properties due to the formation of a cyclic moiety with graphene.[201,216] For that reason, in collaboration with the group of Rosa Villa from the CNM-IMB, we carried out preliminary studies of the electrical properties of our functionalization.

The functionalization was performed in a graphene field effect transistor (GFET) device architecture composed by CVD graphene prepared for the measurement of the electrical properties represented in the Figure 94. The GFET consists in a graphene channel between two gold electrodes, one as source and the other as drain, with a gate contact to modulate the electronic response of the channel.

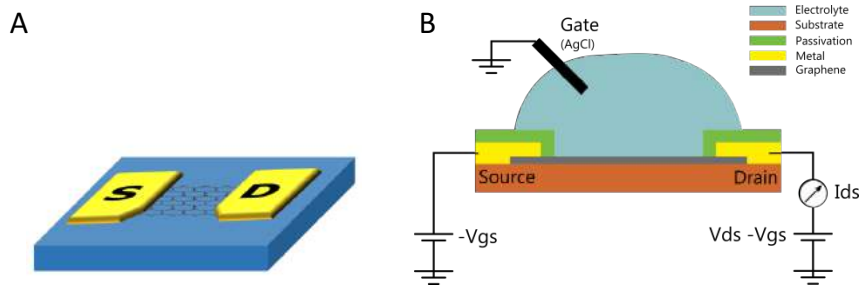

Figure 94. (A) Representation of the CVDG substrate on SiO_2 and two gold electrodes used for the functionalization. (B) Schematic representation of the electrical measurement.

The conditions used for the covalent functionalization are summarized in the Figure 95. A control sample without the presence of TBAF and **4** was performed in order to know the influence of solvents during the reaction and cleaning.

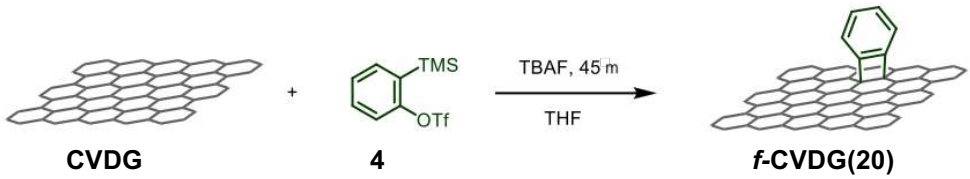

Figure 95. Schematic representation of the reaction.

The measurements of the electrical properties were carried out in the CNM-IMB in Barcelona. First results showed a significant shift after functionalization. However, the same tendency was observed in the control samples, indicating that the observed shift was induced by using solvent during the reaction (THF), probably, leading to a clean of the sample (CH_2Cl_2, H_2O, MeOH and AcOEt). The production of CVDG on different surfaces often need to be isolate from its growing substrate and then transferred to the target support with the aid of polymers. However, surface contamination is obtained, even after cleaning processes, due to the strong interaction between the corresponding polymer and chemical groups on graphene. Moreover, the conditions for the obtaining of *f*-CVDG(**20**) do not damage the sample or the electrical properties of the transistor, Figure 96 evidence how the signal-to-noise ratio is not highly altered; only a low decrease of intensity between source and drain (I_d) is obtained, probably due to the creation of sp^3 defects in the graphene structure.

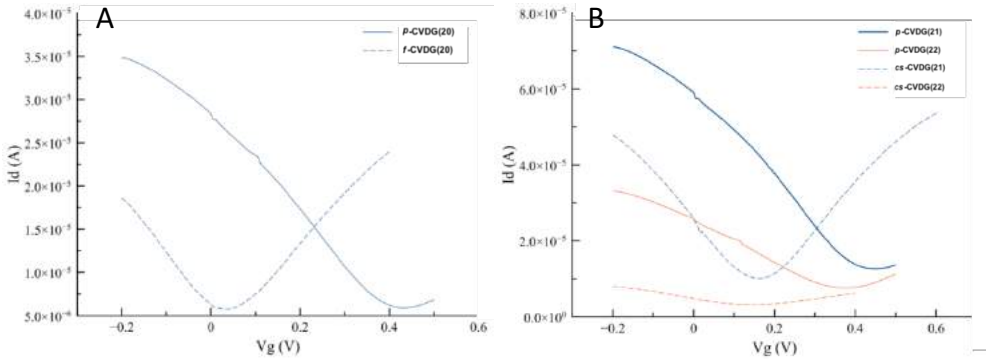

Figure 96. Current-Voltage graph of *f*-CVDG (A) and *cs*-CVDG (B).

In order to clarify if the morphology of the sample change after manipulation of the substrates, AFM study was carried out. Slightly differences can be observed between *p*-CVDG where granular shapes are more pronounced than after the functionalization.

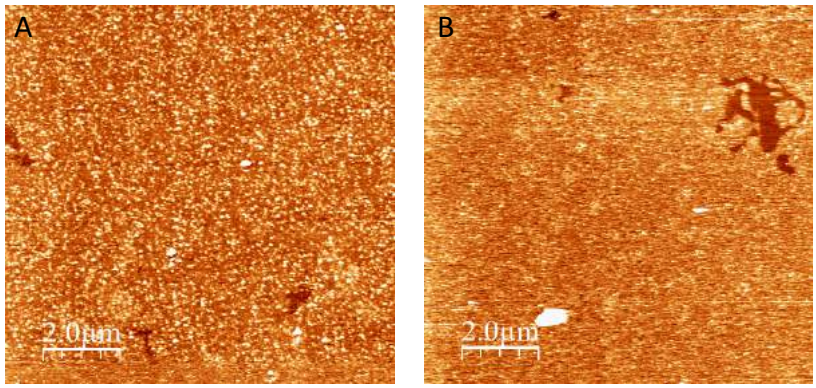

Figure 97. AFM images of *p*-CVDG (A) and *f*-CVDG.

In conclusion, we developed preliminary results of electronic properties of CVDG functionalized with arynes. However, the results show that a clean protocol after preparation of the sample is demanded, as well as deeper study of the influence of the solvents in CVDG production. Then, the influence of aryne reaction on electronic properties of graphene will be addressed in further studies.

2.5 Microwave-induced functionalization of graphene under solvent-free conditions

In the sections described above, we have experimentally demonstrated the difficulties of the chemical modification of graphene, its control and the subsequent application after the functionalization.

In 2009 Yeon *et al.* reported a simple procedure to perform fast pyrolytic reactions with aromatic molecules by using graphite and MWCNTs as MW absorbing matrices.[132] For example, they carried out the MW reaction of phthalic anhydride with graphite and a product mixture of different aromatic compounds in a low yield was detected. It is worth to mention that the synthesis of all aromatic products could be explained by the generation of benzyne by the thermal decomposition of phthalic anhydride.

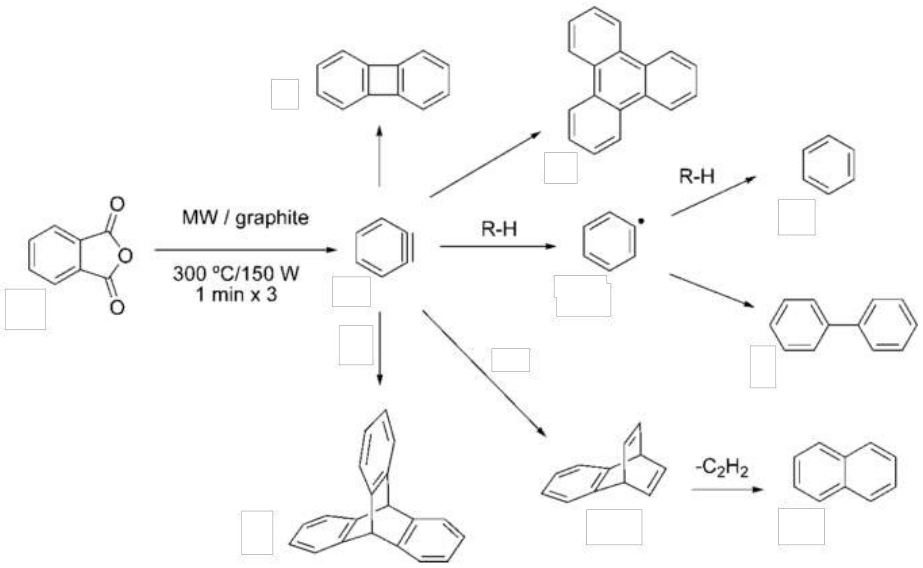

Figure 98. Microwave-induced generation of benzyne using graphite as matrix. Adapted from Yeon *et al.*[132]

We considered the use of MW irradiation as a great value to perform a novel non-conventional covalent modification of graphene. In particular, we were focused on the advantage of a simple and fast MW-induced functionalization of graphene under solvent-free conditions. The graphene material was employed as a MW matrix and, at the same time, as reagent in the underexplored reactions of arynes.[205,95] In particular, we generated different arynes by thermal decomposition of the corresponding arylene anhydrides at high temperatures.[217]

2.5.1 Benzyne generation by thermal decomposition of phthalic anhydride at high temperatures

Initially, we have studied the reaction conditions for the generation of benzyne (**5**) by the thermal decomposition of phthalic anhydride (**11**) in a solvent-free process. **11** decomposes loosing CO_2 and CO in pyrolytic processes to yield benzyne (**5**).[218] To reach elevated temperatures, we decided to irradiate graphite in the reaction media with MW, considering similar reaction conditions reported by Yeon *et al.*[132] as starting point. In order to confirm the generation of benzyne (**5**), its "capture" was carried out by adding anthracene (**12**), as thermally stable diene into the solid mixture, because can yield the easily characterized aromatic compound triptycene (**12**), derived from a [4+2] cycloaddition.[219] The benzyne precursor **5**,

anthracene (**12**) and graphite as MW matrix, were thoroughly mixed by using a mortar. Then, the homogeneous mixture was rapidly heated up by MW irradiation (Figure 99). The NMR analysis of the reaction mixture led to the detection of **13** as the major product and with the presence of **11** and **12**, (Figure 99). Probably, the aromatic compound **13** is derived from a [4+2] cycloaddition of benzyne (**5**) with anthracene (**12**) as diene. This result successfully proves the generation of benzyne (**5**) from phthalic anhydride (**11**) by thermal decomposition under the described conditions.

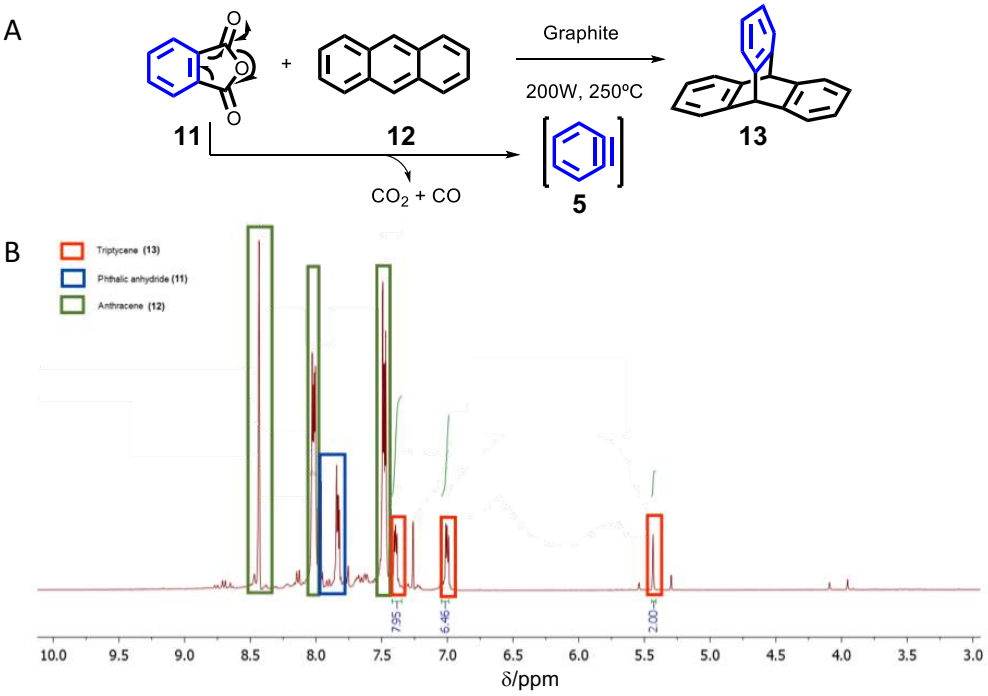

Figure 99. (A) Synthesis of triptycene by MW irradiation under solvent-free conditions with graphene as MW absorbing matrix. (B) ^{1}HNMR spectrum (300 MHz, $CDCl_3$) of organic layer of the reaction mixture, mainly composed by anthracene (**12**), phthalic anhydride (**11**) and triptycene (**13**).

This result allows us to perform a controllable method for the functionalization of graphene with arynes. Then, we decided to use the described reaction conditions to functionalize FLG.

2.5.2 Preparation of pristine graphene

The pristine graphene material used in this section was obtained through exfoliation of graphite following a Coleman's procedure (similar approach as section 2.2). Powder graphite was added to NMP and ultrasonicated

using a sonic tip for 4 h.[220] Then, the resulted expanded graphite was filtered and resonicated in a smaller volume of NMP in a conventional ultrasonic bath for 1 h. The stable dispersion was filtered, resulting in a powder graphene derivative (Figure 100)

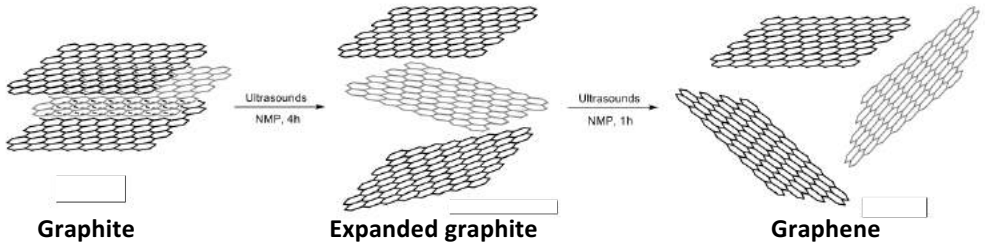

Figure 100. Coleman's method for the preparation of FLG.

Raman spectroscopy showed that the exfoliated carbon material is quite different from bulk graphite (Figure 100). In addition, the deconvolution of its 2D band was decomposed into four Lorentzian-shaped peaks (Figure 101). So, we can conclude that the produced graphene consisted of few layers.[21,221]

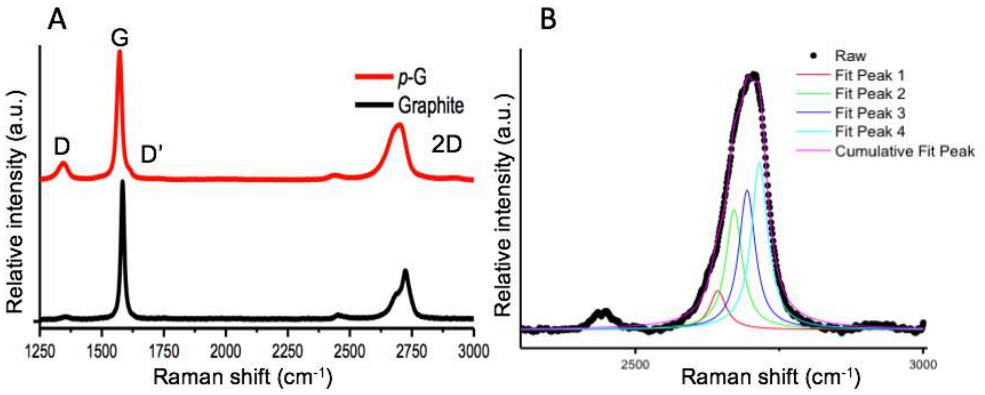

Figure 101. (A) Raman spectra of graphite (black) and FLG (red). (B) Raman deconvolution of 2D band for FLG.

2.5.3 First method

We decided to investigate a controllable chemical functionalization of GBMs with benzyne, generated by the thermal decomposition of the commercially available phthalic anhydride (**5**).[222]

The number of publications in the area of MW, growth in the last years,[223] because conventional heating has as disadvantage: a non-homogeneous warmth. However, microwave irradiation can simultaneously increase the temperature of the whole Vessel. (Figure 102).

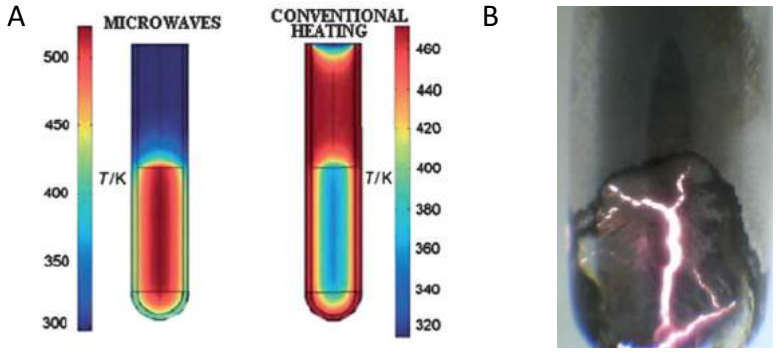

Figure 102. (A) Temperature profiles of MW and conventional heating. Adapted from Kappe *et al*.[224] (right) Image of the quartz Vessel during the reaction process for the functionalization of FLG.

The reaction was performed with the phthalic anhydride (**11**) and exfoliated FLG thoroughly mixed by using a mortar. Then, the homogeneous mixture was rapidly heated up under MW irradiation and solvent-free conditions. The parameters that we can control to run the experiment are varied: temperature, power, holding time and cooling, the use of cycles, pretreatment of the sample, pressure and number of equivalents. After some attempts we decided to use a method summarized in Figure 103: The temperature was fixed at 250 ºC for one minute with a maximum power of 200 W that could be variable for the stability of the temperature. The procedure was repeated three times with a vigorous outsider cooling of the Vessel with air.

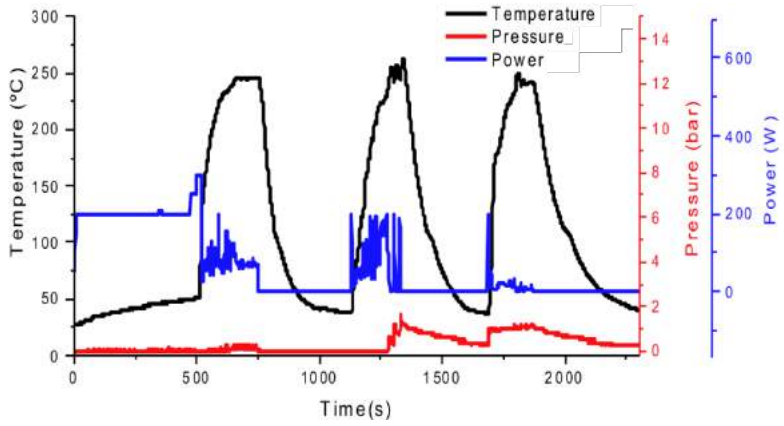

Figure 103. Variation of MW irradiation power (blue), temperature (black) and pressure in the Vessel against the reaction time.

Raman spectroscopy showed an increment of the intensity ratio between D and G bands for the functionalized graphene *f*-G(**27**) (I_D/I_G = 0.57) respect to the pristine material. This increment is related to the generation of sp^3 carbon atoms replacing the sp^2 carbon atoms in the covalent modification. Although variation of I_D/I_G is a semiquantitative parameter, this high enhancement of the D band can be interpolated as a high modification of the aromatic structure of graphene. The characterization by TGA also confirmed a weight loss of 5% until 500 ºC. Probably, this weight loss is due to the phenylene groups attached onto the graphene surface. It is worth to mention that the sample was previously washed, conscientiously, with several solvents of different nature to avoid any impurity that could alter the weight loss in TGA (Figure 104) The corresponding FD for *f*-G(**27**) was 658 μmol of phenylene group per g of graphene material.

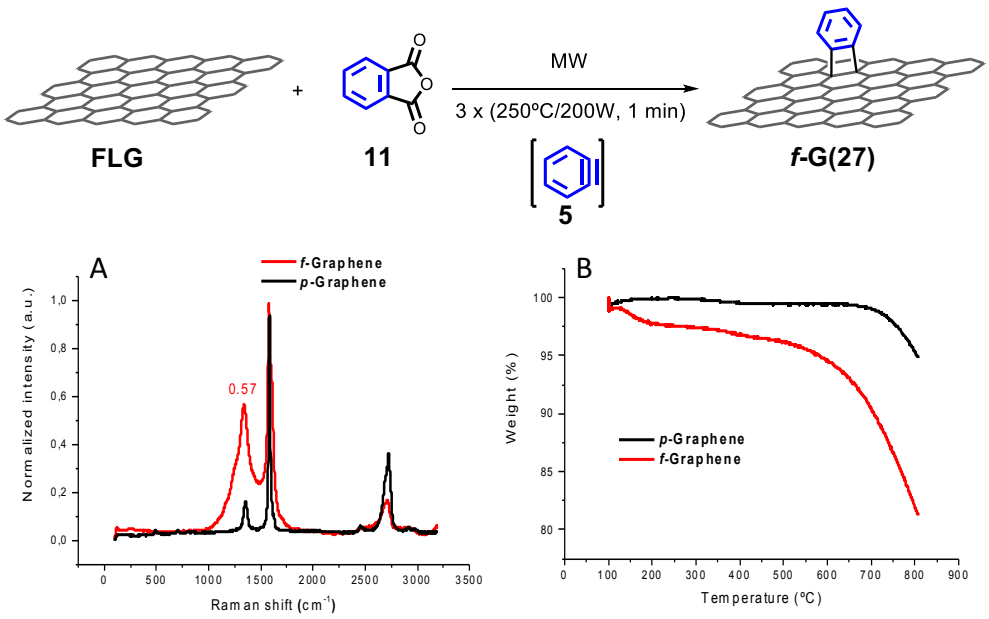

Figure 104. Reaction of the first method with the corresponding Raman (A) and TGA profiles (B).

Our next step was the control of the functionalization degree, because in the obtained Raman spectrum, we observed a high functionalization. A large number of defects of graphene can alter their properties.[225] For that reason, we performed a new approach using a lower irradiation power in the functionalization method, at 200 ºC as maximum temperature and one cycle. However, the result was a too low surface modification corresponding to a $\Delta(I_D/I_G)$ of 0.04 (Figure 105).

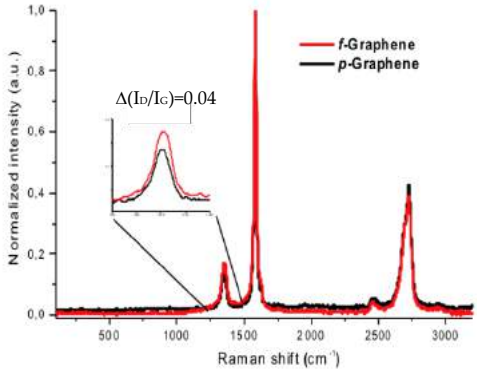

Figure 105. Raman spectra of the low modification of graphene with **11**.

2.5.3.1 Number of cycles and equivalents

The reduction of temperature and power produced small variations in our functionalization method. Then, we decided to investigate the number of applied cycles and the equivalents of benzyne precursor as key points for a controllable functionalization.

Several experiments were attempted with phthalic anhydride (**11**) and FLG. On one hand, a deep study of the influence of the cycles in the functionalization was carried out. The TGA profiles of the functionalized graphene samples at different cycles showed FDs of 184, 276, 276 μmol/g for 1, 2 and 3 cycles, respectively, which are in line with the applied cycles. However, the Raman spectroscopy showed I_D/I_G ratios that are not related to the applied cycles.

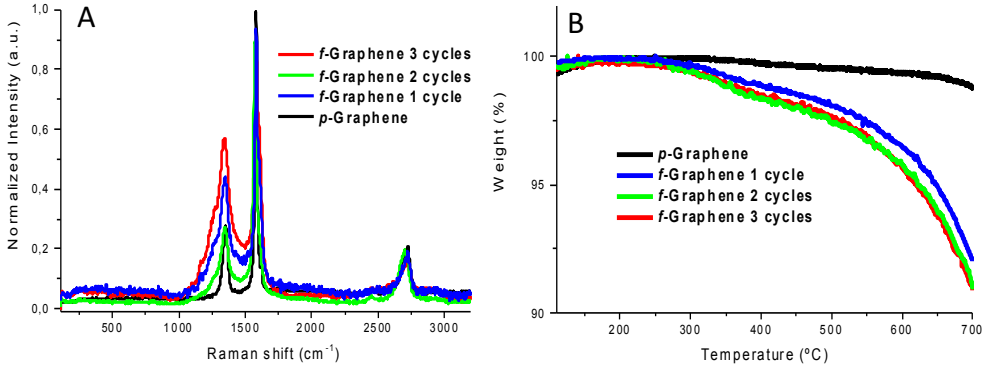

Figure 106. Raman spectra and TGA profiles depending on the applied number of cycles in the functionalization method of FLG.

On the other hand, a complete study of the number of equivalents for the optimization of the method was also done, from low equivalents of aryne precursors (1 equivalent of the benzyne precursor **11** with respect to 1 atomic equivalent of C atoms) to high quantities (3 equivalents of the benzyne precursor **11**, Figure 107) The analysis of the Raman spectroscopy data showed that 1 and 3 equivalents are in good balance for the graphene functionalization, regarding the I_D/I_G ratio.

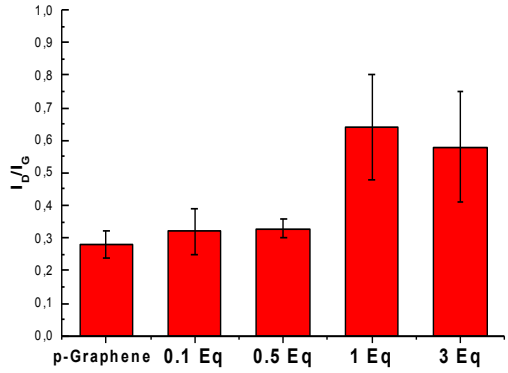

Figure 107. I_D/I_G Raman intensity of *f*-Gs depending on the number of cycles.

In conclusion, this methodology is useful for a high functionalization but not for a controllable route for the chemical modification of graphene.

2.5.4 Second method

After considering the above-mentioned parameters, we were not able to achieve our objective yet: the total control of a fast-covalent functionalization under MW irradiation and solvent-free condition. Then, our efforts were focussed on the total control of the MW irradiation power, creating a second method functionalization. This new method is defined by the application in each cycle of 200 W of MW power until reaching 250 ºC, in about 5 seconds (Figure 108), in each cycle. The following cycle started after a vigorous external cooling of the Vessel until reaching 175 ºC.

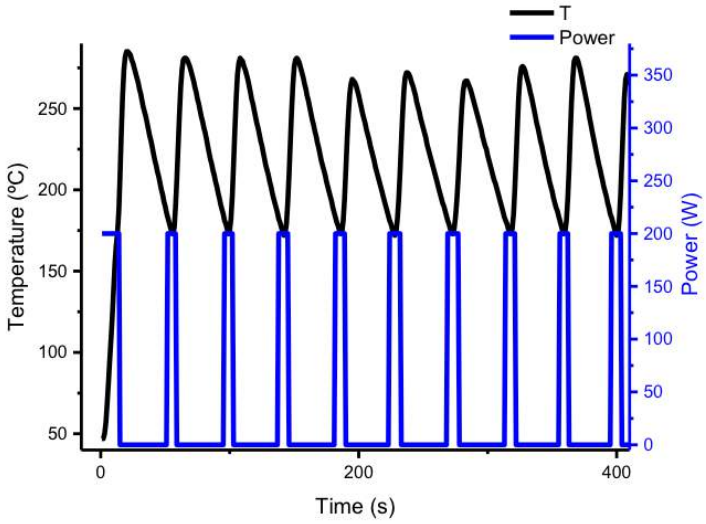

Figure 108. Temperature (blue line) and power evolution of microwave irradiation (black line) against the time.

A new confirmation of the capture of generated benzyne was carried out under these new reaction conditions, by adding anthracene (**12**) as diene. In this case, graphene was employed as MW absorbing matrix (in detail in the experimental part of the chapter 3, section 3.7). The NMR analysis of the reaction mixture led to the detection of **13** as the major product in approximately 33% corrected conversion, and 60 and 27% of recovered **11** and **12**, respectively. The detection of triptycene (**13**) as major product again verifies the generation of benzyne by thermal decomposition of **11** and the validation of the method. (Figure 109)

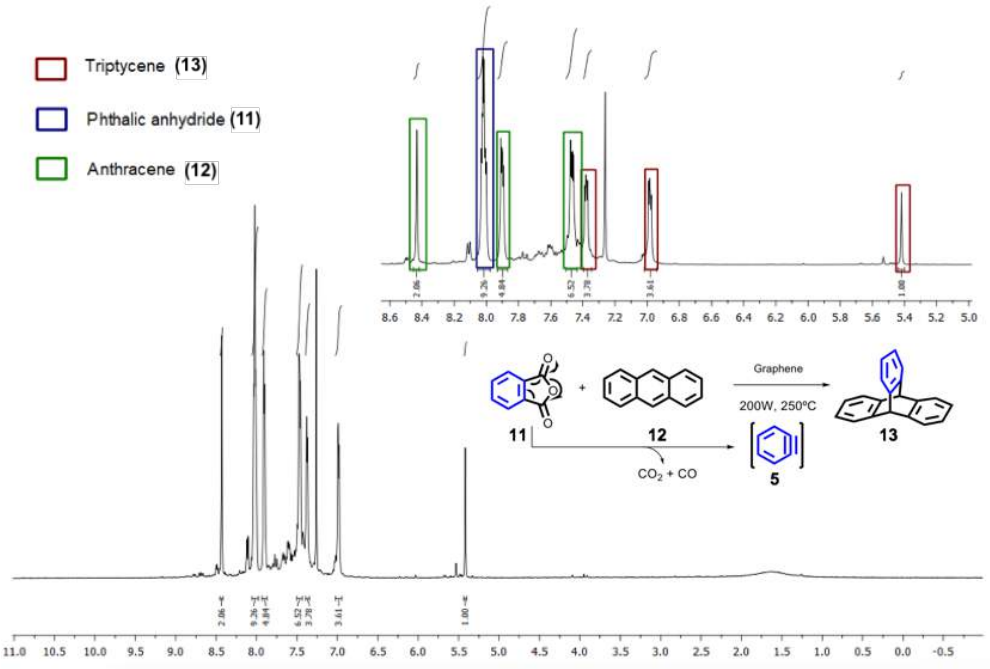

Figure 109. ^{1}HNMR spectrum (300 MHz, $CDCl_3$) of organic layer of the reaction.

2.5.4.1 Number of cycles

With this methodology, each cycle at 200 W is set to 5 seconds with an intermediate cooling between them. Again, a study at different cycles (1,3,5,10 and 40) was performed to elucidate the controllable functionalization.

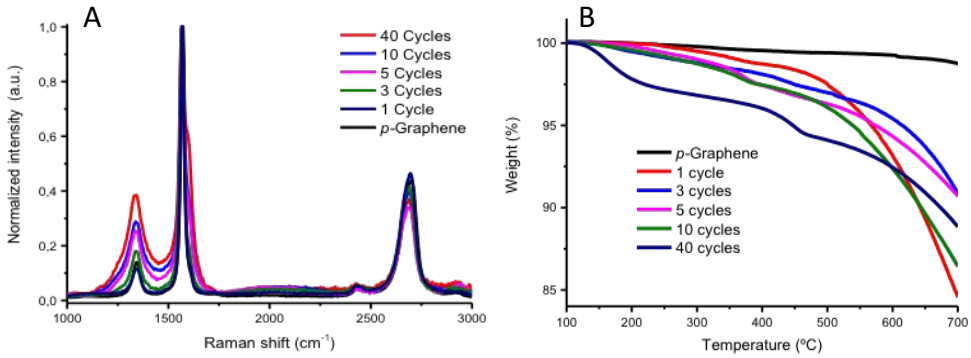

Figure 110. Raman spectroscopy (A) and TGA profiles (B) of *f*-G(**29**) with different number of applied cycles.

The combination between the FD by TGA and I_D/I_G by Raman spectroscopy summarized in the Figure 111 clearly confirms the chemical modification of graphene with benzyne (**5**).

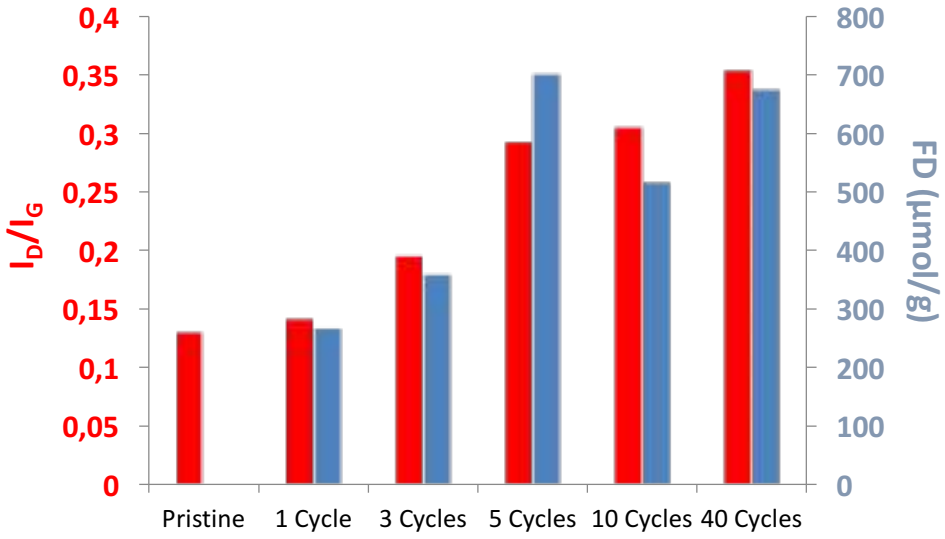

Figure 111. I_D/I_G ratio (red) and FD (blue) for *f*-Graphene with **11** at different cycles.

TGA results showed significant variations in the FD depending on the number of cycles, while a slight increment in the I_D/I_G ratio by Raman was observed. Both experimental results were in line until 5 cycles, where the corresponding functionalized graphene presented a FD of 122 µmol/g with a I_D/I_G ratio of 0.29, in addition of a slight increment of its D' band (Figure 112).

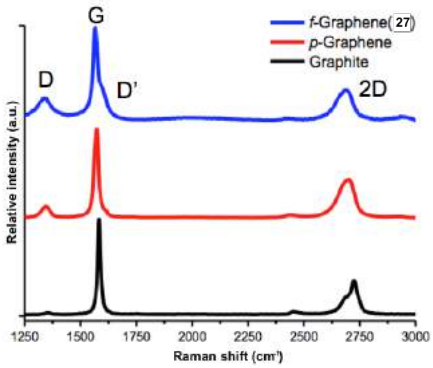

Figure 112. Raman spectra of graphite (black), *p*-G (red) and *f*-G (blue).

However, after 5 cycles, the FD by TGA decreased while the defects are still mildly increasing by Raman. It is worth mentioning that this chemical process was performed at high temperatures. Probably, the small introduced functional groups are being decomposing[92,93] or retro-cycloaddition of benzyne[99,100,90] is occurring under these reaction conditions. In fact, theoretical studies support this possibility as they have reported energy barriers of 1.9 eV for the retro-cycloaddition reaction of the corresponding adduct of benzyne with graphene, which can be overcome at moderated high temperatures.[100]

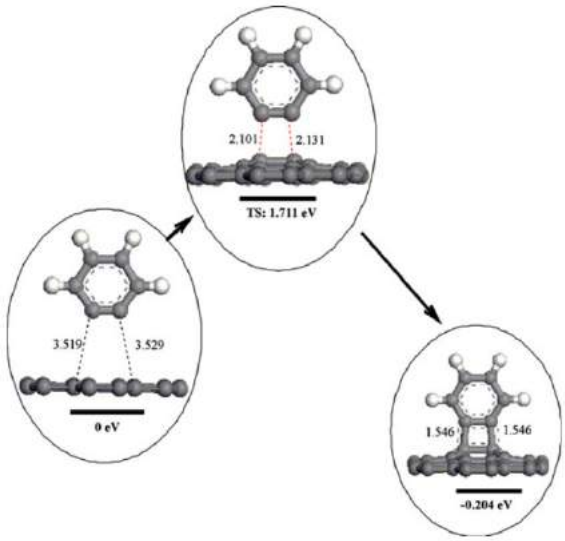

Figure 113. Theoretical representation of the energies barriers for the functionalization of graphene with a single C_6H_4. Adapted from Zhao *et al.*[100]

Accordingly, functionalized graphene materials with more than 5 cycles showed smaller FD with a high I_D/I_G ratio. In addition, defects can be introduced in the graphene lattice after large number of cycles, independently of the organic functionalization with benzyne. This last assessment is supported by TGA profiles of functionalized graphene with benzyne, where a thermal decomposition is observed after around 200 ºC (Figure 110). Therefore, the 5 cycles modification was established as standard method because it generates an adequate functionalization degree with a concordant I_D/I_G ratio. However, less functionalization can be done applying from 1 to 5 cycles.

In conclusion, the TGA and Raman spectroscopy data confirmed the modulable functionalization with a strict control of the MW irradiation power in the reaction, for cycles between 1 and 5, being capable to obtain from low functionalized FLG (1 cycle) to a high functionalized graphene (more than 5 cycles).

2.5.5 Functionalization of more complex arynes

The described graphene functionalization was performed with structurally more complex arynes (Figure 114) *via* thermal decomposition of the corresponding anhydrides **11,13-18** by established conditions described in Figure 114. *via* thermal decomposition of the corresponding arylene anhydrides **11, 13-18** by the established conditions described in section 2.5.4. In particular, phenylene groups with heteroatoms such as a fluoride-substituted phenylene (*f*-G(**30**)) and aromatic moieties with a large number of fused-benzene rings (*f*-G(**31-34**)) have been covalently linked to the graphene structure. In the latter case, aromatic groups were introduced with the same number of benzene rings but with different topologies (*f*-G(**32-33**)). The new modified graphene derivatives were characterized by Raman spectroscopy, TGA, TEM, as well as XPS techniques.

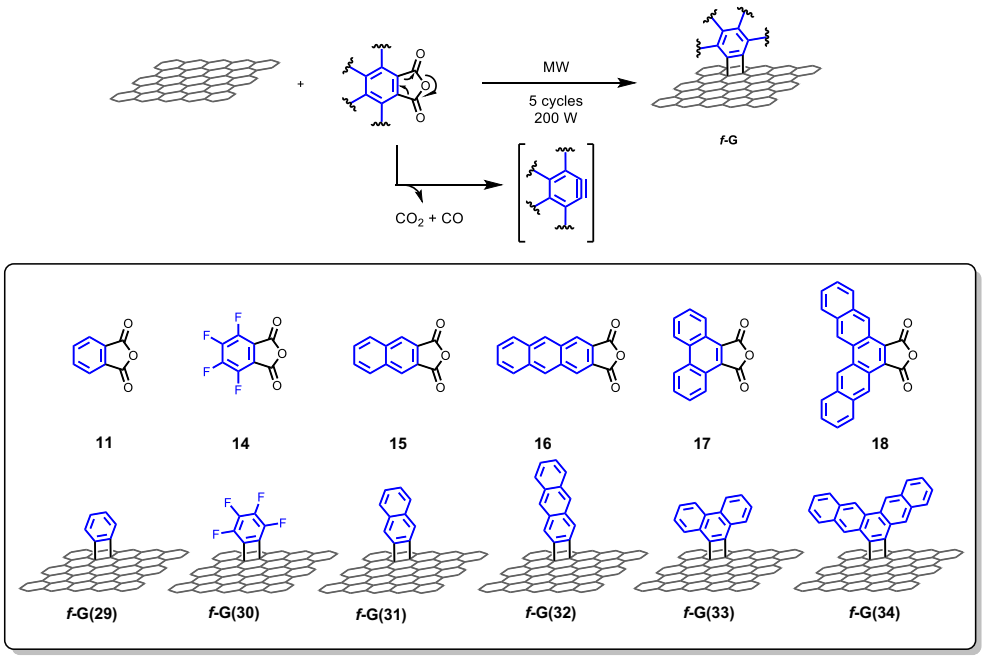

Figure 114. Functionalization of exfoliated FLG with arynes by thermal decomposition from the aryl anhydrides **11,14-18** to obtain the *f*-G(**29-34**), under MW irradiation and solvent-free conditions using the second methodology.

The TGA and Raman spectroscopy data are significant and in line with the obtained previous results. Remarkably, *f*-G(**29**) and *f*-G(**32**) showed the highest FDs.

Table 7. Average I_D/I_G ratio, functionalization degree by TGA and production yield for modified graphene derivatives. [a] (mg f-G/mg FLG)•100; [b] (mg f-G/mg Graphite)•100

Aryne precursor	*f*-G	$\Delta I_D/I_G$	FD (μmol/g)	Functionalization Yield (%)[a]	Production Yield (%)[b]
11	**29**	0.16	699	114	3
14	**30**	0.18	380	178	5
15	**31**	0.14	366	190	5
16	**32**	0.17	751	100	3
17	**33**	0.52	239	134	4
18	**34**	0.26	301	188	5

In addition, XPS analysis was used to provide evidences of the functionalization of graphene derivatives by identifying and quantifying the functional groups anchored to the surface. The atomic percentage, binding energies and peak assignments for different cores are summarized in Table 8 and Table 9, respectively. In particular, fluorine atoms from the aryne precursor **14** (Figure 114) were used as diagnostic signal for the functionalization of FLG.

Table 8. Core level of graphene derivatives determined from the XPS survey spectra.

Graphene material	Core	BE (eV)	Atomic %
p-Graphene	C1s	284.71	98.1
	O1s	532.56	1.9
cs-Graphene	C1s	284.37	93.8
	O1s	531.46	6.2
f-G(**29**)	C1s	284.39	87.4
	O1s	531.80	12.6
f-G(**30**)	C1s	284.31	79.7
	O1s	532.76	2.8
	F1s	687.01	17.5
f-G(**31**)	C1s	531.92	73.5
	O1s	284.37	26.5
f-G(**32**)	C1s	531.80	67.8
	O1s	284.40	32.2
f-G(**33**)	C1s	531.56	80.3
	O1s	284.31	19.7
f-G(**34**)	C1s	531.54	89.0
	O1s	284.59	10.0

The *f*-G(**30**) has shown a 17% of F atoms due to the introduced tetrafluorophenylene moieties. The presence of oxygen in the modified graphene derivative is probably due to oxygenated groups, generated during the exfoliation and the irradiation process (see the composition of FLG and *cs*-G in Table 9, respectively). The deconvolution of C1s and F1s core levels of *f*-G(**30**) (Figure 115), showed a peak to 286.11 and 687.15 eV, respectively, corresponding to C-F bond.[226] The presence of fluorine and the energy of these peaks suggests the presence of tetrafluorophenylene moieties in the graphene structure, confirming the chemical modification.

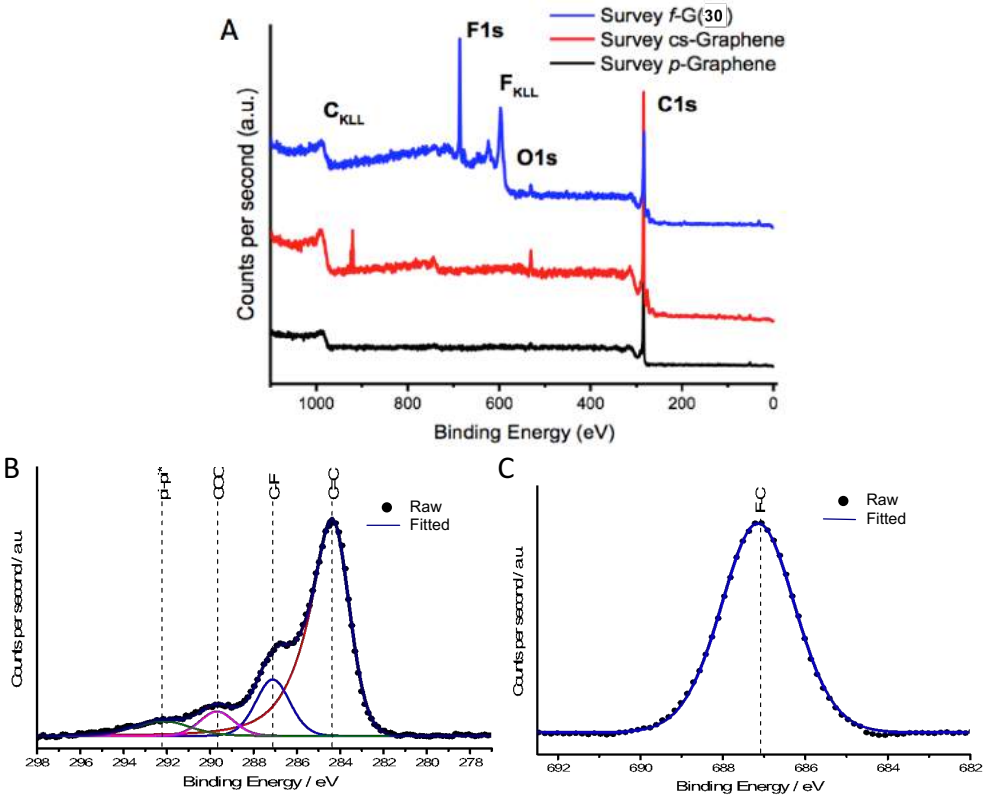

Figure 115. XPS survey spectra (A) C1s (B) and F1s core level(C) for *f*-G(**30**).

Table 9. Core levels and deconvoluted components for graphene derivatives.

Sample		*p*-Graphene	*cs*-Graphene	*f*-G(**29**)	*f*-G(**30**)	*f*-G(**31**)	*f*-G(**32**)	*f*-G(**33**)	*f*-G(**34**)
C1s /eV	sp^2 C	284.37	284.37	284.37	284.37	284.37	284.37	284.37	284.37
	C-F	-	-	-	286.11	-	-	-	-
	C-O	286.31	287.05	285.66	-	287.44	286.55	286.61	-
	C=O	287.71	288.22	-	-	-	288.44	288.6	288.07
	COO	-	-	-	289.69	289.85	-	-	290.15
	π-π*	290.72	290.68	291.48	292.23	292.33	-	-	292.24
O1s / eV	O-C	533.14	531.78	533.11	533.59	532.11	532.83	532.48	532.32
	O=C	531.19	529.99	531.93	531.92	530.8	531.50	530.83	531.39
F1s / eV	F-C	-	-	-	687.15	-	-	-	-

The morphology of functionalized graphene materials was studied by transmission electron microscopy (TEM). All graphene derivatives kept a similar structure and dimensions to the pristine material after the described treatment at high temperatures. Besides, it was not possible to observe organic layers on the graphene surface from these images, thus supporting our previous claim about the molecular functionalization. (Figure 116)

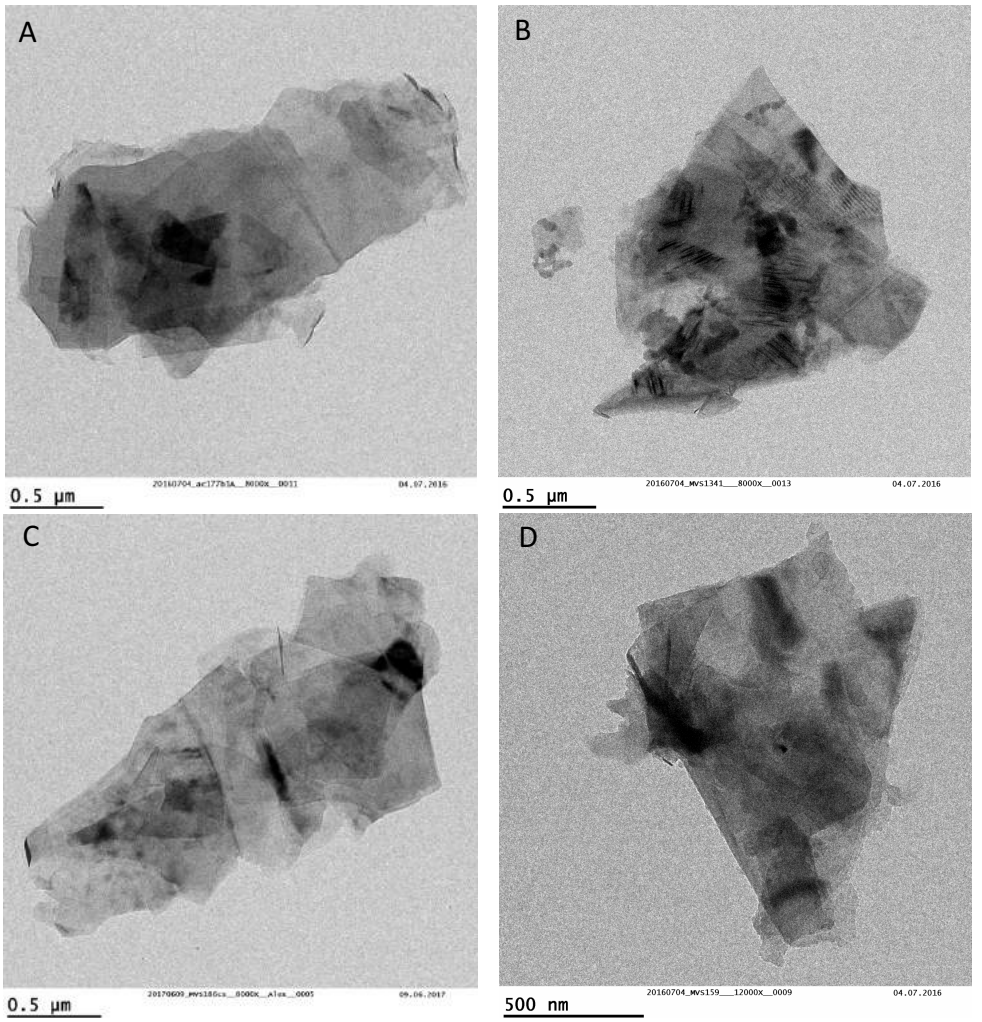

Figure 116. TEM images of *p*-Graphene (A), *f*-G(**29**) (B), *cs*-Graphene (C) and f-G(**30**) (D).

Emission and absorption spectra were measured; however, the spectra were of very low quality, without the observation of the typical bands of the corresponding aromatic units, but only a broad absorption barely visible

above the noise. This result is probably due to a possible quenching effect by graphene.[227]

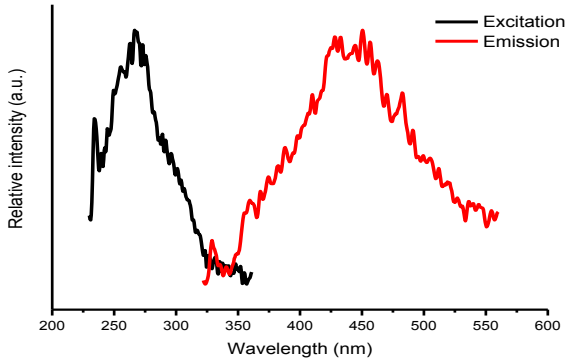

Figure 117. Excitation and emission spectra of *f*-G(**34**) in EtOH.

2.5.6 Properties

The functionalization of graphene is expected to improve the dispersibility of graphene material in organic solvents, because the introduced functional groups can avoid re-aggregation and subsequent precipitation.[36,116,95] In order to explore the dispersion stability of functionalized FLG materials, different solvents were tested. The *f*-Gs exhibited significantly improved solubility in EtOH and DMF, after a previous sonication for 5 min. In particular, the *f*-Gs showed an improved dispersibility in EtOH (Figure 118). Particularly, the *f*-G(**29**) showed a high stability in EtOH dispersion after 15 days due to the introduced polar functional groups such as tetraphenyl moieties.

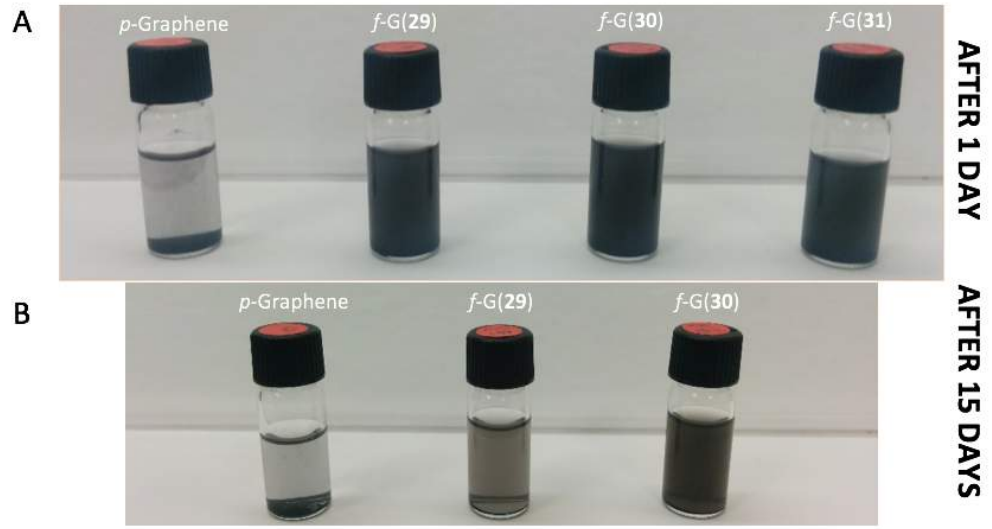

Figure 118. (A) Suspensions of *p*-Graphene and *f*-G(**29**-**31**) in EtOH (0.2 mg/mL) after 1 day. (B) Suspensions of *p*-Graphene, *f*-G(**29**) and *f*-G(**30**) (from the left to the right) in EtOH (0.2 mg/mL) after 15 days.

2.5.7 Transfer to Carbon Nanotubes

After the successful development of a fast, efficiently and mild modification procedure for graphene with easily accessible aryne precursors, we consider transferring the described functionalization to other carbon materials as carbon nanotubes as a tool of great value. Double-walled carbon nanotubes (DWCNTs) have two concentric carbon nanotubes having higher mechanical strength and better thermal and chemical stability than SWCNTs. In addition, the double-walled structure allows to selectively functionalized the outer wall maintaining an intact inner-tube.[228]

The covalent functionalization of DWCNTswith arynes was performed using the first method (Figure 119) with the final purpose of obtaining a maximum degree of functionalization as graphene.

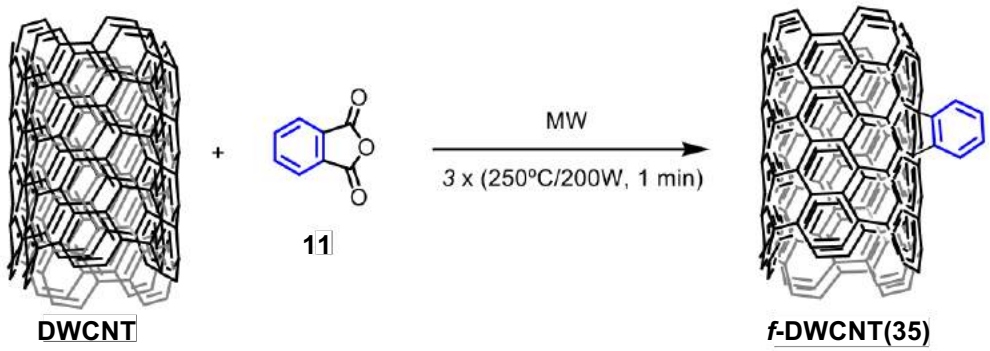

Figure 119. DWCNTs functionalization with under first method conditions.

The *f*-DWCNTs was done with different equivalents to check reactivity from 0.1 atomic equivalents to 3 equivalents. As we expected, the Raman spectroscopy data showed a higher reactivity for DWCNTs than FLG with small amount of benzyne precursor, in terms of $\Delta I_D/I_G$. Probably, it is because of the higher deformation and curvature of CNTs than the planar graphene structure.[204,229]

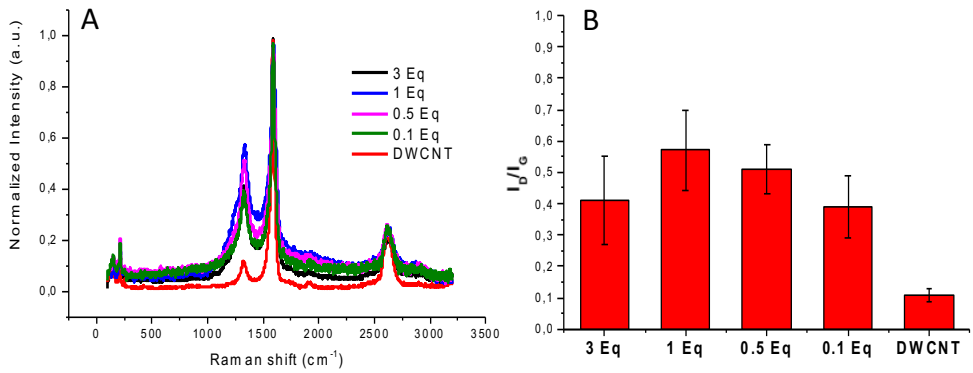

Figure 120. (A) Raman spectroscopy of DWCNTs with different number of equivalents. (B) I_D/I_G Raman average of the described Raman spectra.

As graphene modifications, heteroatoms were introduced on the DWCNT by the covalent attachment of the corresponding aryne, generated from the aryne precursor **14**. The functionalization was confirmed through Raman spectroscopy with $\Delta I_D/I_G$ of 0.28. In addition, the modification was also confirmed by the detection of fluorine atoms in the atomic composition of *f*-DWCNT(**36**) by XPS analysis.

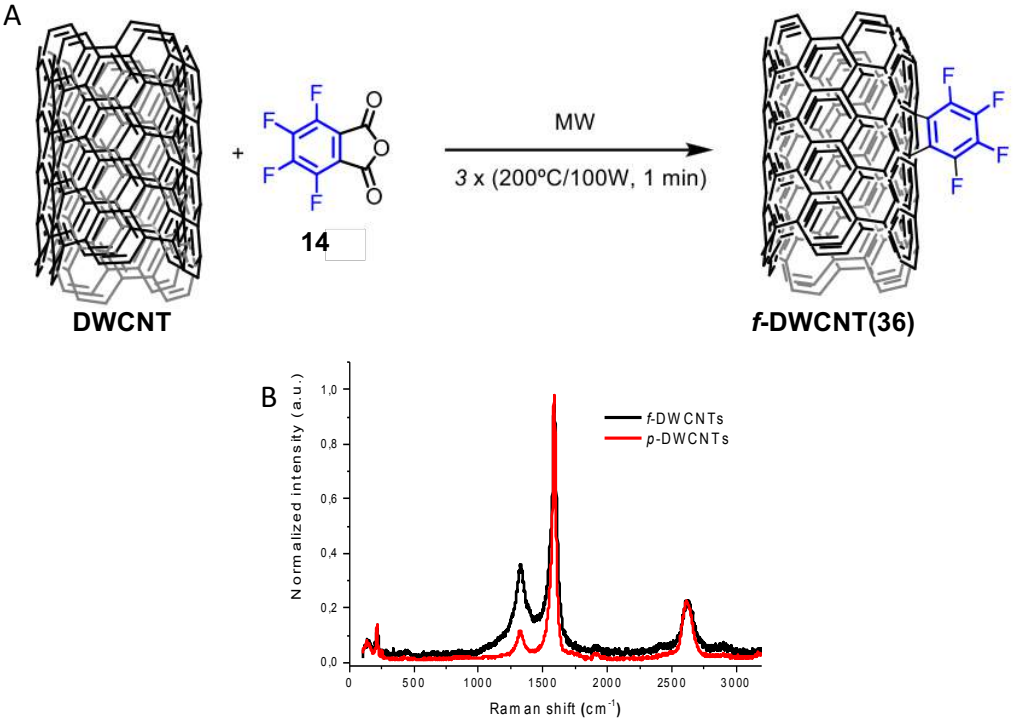

Figure 121. (A)Scheme of the reaction of *f*-DWCNTs with the introduction of fluorine atoms in the carbon material. (B) Characterization by Raman spectroscopy.

The XPS analysis of *f*-DWCNT(**36**) showed an increment of 11% of fluorine atoms of atomic composition on the surface of the material, confirming the chemical modification (Table 10).

Table 10. Atomic ratios of DWCNTs derivatives determined from the XPS survey spectra.

DWCNTs	Core	BE (eV)	Atomic %
35	C1s	285.01	96.5
	O1s	532.96	3.5
36	C1s	285.33	85.5
	O1s	533.18	3.9
	F1s	688.28	10.6

The functionalized DWCNTs were also characterized by TEM was performed (Figure 122). Considerable changes were not observed in the morphology of the CNTs.

As it happened with FLG, the described functionalization led to a higher dispersibility of *f*-DWCNTs in EtOH at 1mg/mL concentration, in comparison to the pristine material.

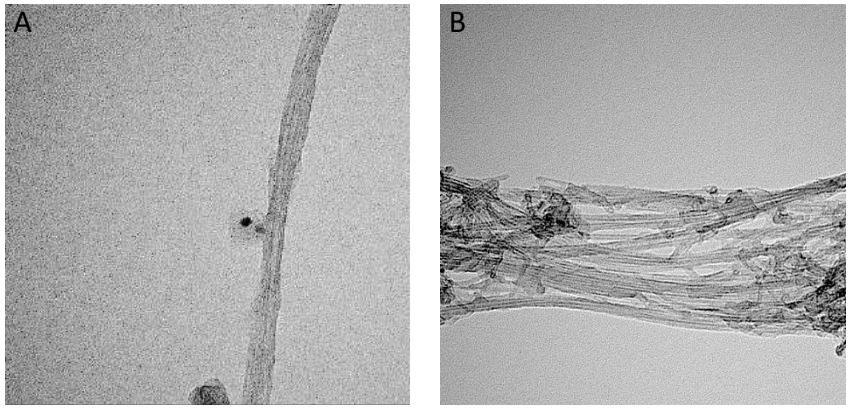

Figure 122. TEM images of *p*-DWCNTs (A) and *f*-DWCNT(**35**) (B).

In summary, we were able to transfer our methodology to other carbon material as DWCNTs, to confirm the multivalent application of this novel covalent modification. However, this procedure was also attempted on fullerene C_{60} without the desired formation of the cycloaddition. Possibly, for the development of this methodology is necessary another matrix with better MW absorption capacity.

2.5.8 Aromatic anhydride ball milling exfoliation and microwave functionalization of graphene.

It has been demonstrated that the use of mechanical force can modify and produce by exfoliation carbon nanostructures, especially with molecular adsorption on the graphene surface for the compensation of Van der Waals forces.[230,231] Taking advantage of the aromatic structure of arylene anhydrides, we decided to use these aryne precursors as exfoliating agents in presence of mechanical force using ball milling exfoliation method. This approach offers a new alternative for the production of better quality graphene and direct functionalization avoiding time and reagents compared to the above-mentioned method in the previous sections. In particular, the NMP exfoliation of graphite would be avoided and a more

homogeneus mixture with a better interaction between the carbon material and the corresponding reagent would be performed. In addition, arylene anhydrides would play two roles: as exfoliating agent and reagent.

The production of graphene layers using aromatic compounds as exfoliation agent is a well-known approach in the literature.[232–234] For that reason, in collaboration with the group of Dr. Ester Vázquez from the University of Castilla-La Mancha, powder graphite and phthalic anhydride (**11**) were ball-milled at 100 rpm during 30 minutes using air atmosphere as shown in Figure 123.

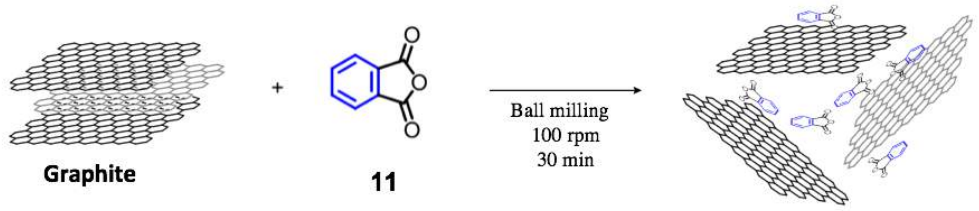

Figure 123. Scheme of graphite exfoliation with **11** through ball milling.

The resulting mixture was washed and filtered with several solvents in order to obtain the powder exfoliated graphite for characterization purposes. Besides, the procedure was repeated without the presence of phthalic anhydride in order to know the influence of the aromatic compound as control sample (*cs*). Raman spectroscopy (Figure 124) showed characteristic features. The presence of the aromatic moieties had a direct influence on the 2D shape of the exfoliated material which consists on few layers graphene; in addition, the number of defects originated in presence of the **11** notably increased, probably, because of the increment of edge defects respect to the basal plane.

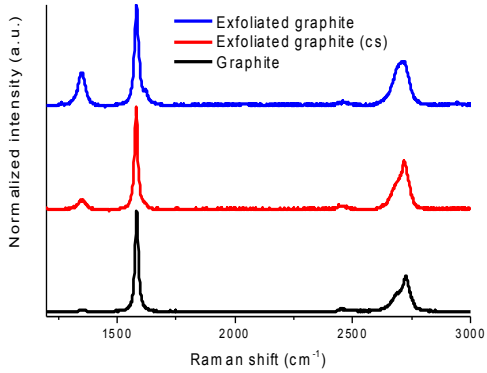

Figure 124. Raman spectra of exfoliated graphite in presence of **11** (blue), control sample without **11** (red) and raw graphite (black).

However, the activation or initiation of a chemical reaction can be done through all kinds of energies from effective sources like light emission, thermal heating or microwave irradiation to less effective but possible like mechanical energy.[235] Thus, in order to detect if the increase in the D band observed during the ball milling process was not due to the reaction of benzyne from **11**, we decided to perform an attempt (Figure 125) to check if we can generate benzyne in presence of anthracene (**12**).

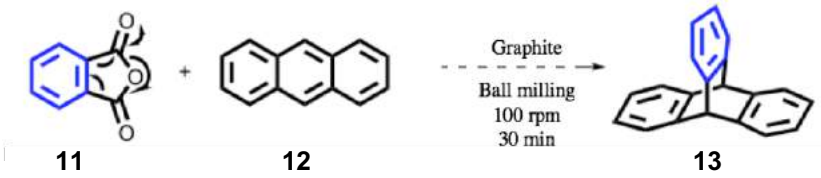

Figure 125. Scheme of the attempt of [4+2] cycloaddition through ball milling exfoliation.

The resulting sample after ball milling process was filtered collecting the residues, but **13** derived from a [4+2] cycloaddition between benzyne and **12**, was not detected in the organic layer by ^{1}HNMR and MS (EI). Therefore, we can suppose that the generation of benzyne from **11** was not possible under the described mechanical process. Thus, the increment of D band in Raman spectra was produced by the exfoliation process.

In the next steps, the functionalization of the exfoliated graphene was carried out. Our purpose, shown in the Figure 126, was to perform a more effective exfoliation and functionalization. In addition, in order to see the

influence of the aromatic rings during the ball milling process, we employed the arylene anhydrides **11**, **15** and **16**.

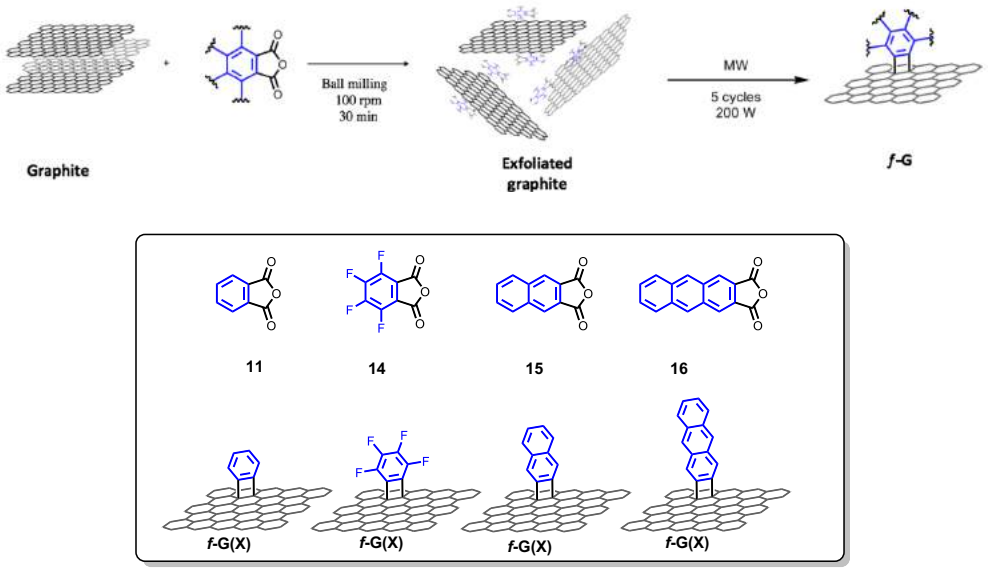

Figure 126. Schematic representation of ball milling exfoliation and subsequent MW functionalization expected with arylene anhydrides **11, 14-16**.

Powder graphite was mixed with the arylene anhydrides **11**, **15** and **16**. After ball milling and a subsequent thoroughly wash with different solvents, Raman spectroscopy was performed to the resulting materials. The 2D band of exfoliated graphene materials showed a characteristic feature of few-layer graphene with non significant differences between samples. Therefore, we can consider **11**, **15** and **16** as potential good exfoliating agents. In addition to the graphene bands, for the samples treated with **16** and **15** other signals can be observed, which are from the corresponding arylene anhydrides. This result suggests a better absorption of **15** and **16** on the graphene surface, in comparison with **11**, because of the larger number of fused benzene rings.

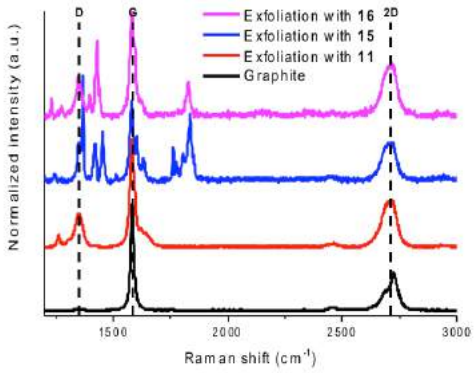

Figure 127. Raman spectra of powder mixture of arylene anhydrides **11**, **15**-**16** with graphite after ball milling exfoliation.

After ball milling, the powder mixture was collected and transfer onto a Quartz vessel to perform a MW reaction with the methodology developed on section 2.5.4. The results of this reaction were summarized in Table 11.

Table 11. Average I_D/I_G ratio and functionalization degree by TGA [a] $\Delta I_D/I_G$ between exfoliated graphite and ***f*-G**.

Aryne precursor	***f*-G**	**$\Delta I_D/I_G$[a]**	**FD (μmol/g)**
11	**37**	0.21	380
14	**38**	0.66	480
15	**39**	0.30	451
16	**40**	0.13	638

The increase of D band was clearly observed for all samples. Related to the FD, it is in accordance with the Raman data for *f*-G(**37**), *f*-G(**38**) and *f*-G(**39**). However, *f*-G(**40**) showed a lower increment of D band intensity with a considerable FD of 638 μmol/g. This incoherent result can be explained considering the large number of benzene rings of **16** that can led to a strong adsorption on graphene. This non-covalent interaction could hinder an optimal removal after MW treatment. Nevertheless, the functionalization step was convenient for the aryne precursors **11**, **14** and **15**.

As summary, we developed initial studies for a rapid method that allows exfoliation and functionalization of graphene sheets with the aryne precursors **11**, **14** and **15**. In addition, the employment of the arylene anhydrides **11**, **14**, **15** and **16** as potential exfoliating agents in ball milling processes was obtained.

These results open a new alternative for a rapid, cheap and efficient approach with the possibility to produce large quantities of material in a short period of time, where arylene anhydrides were used as exfoliated agents and reagents; but further studies are needed.

2.6 Conclusions

In conclusion, during this PhD, we were able to perform the covalent modification of graphene derivatives *via* a well-known electrochemical approach, we have successfully developed a protocol for the modification of already functionalized graphene electrodes for the unspecific detection of oligonucleotides and the modification of CVDG electrodes with protected amines. On the other hand, we have also investigated the underexplored covalent functionalization of graphene-based materials with arynes, in different graphene derivatives, such as FLG, rGO and CVDG, and reaction conditions.

In order to find a solution to the problems of the conventional modifications of graphene, we have developed novel, fast, scalable and simple entries to a covalently modified graphene. These new approaches show further advantages than classical functionalization reactions, since allows avoiding unstable graphene suspensions at low concentrations. In fact, the described solvent-free conditions pave the way for green protocols and large-scale functionalization processes of graphene derivatives. Besides, to the best of our knowledge, it is the first chemical modification where GBMs behave like unique MW absorbing matrix and reagent at the same time in covalent modification. With the advantage of the two methods a successful transfer to other carbon nanomaterial as DWCNTs was performed.

In addition, this approach allows the synthesis of modified graphene derivatives with good suspension stability, which makes them processable materials; for instance, as good candidates for devices made by deposition coating processes.

3. EXPERIMENTAL PART

3.1 Experimental details

Materials and techniques

All the chemicals and solvents were purchased from different commercial companies and they were used as received without further purification.

All reactions were carried out under Argon using oven-dried glassware. TLC was performed on Merck silica gel 60 F254; chromatograms were visualized with UV light (254 and 360 nm). Flash column chromatography was performed on Merck silica gel 60 (ASTM 230-400 mesh).

Graphite as purchased from Bay Carbon, Inc. (SP-1 graphite powder), (Michiga, United States). DWCNTs were purchased from Nanocyl SA (Sambreville, Belgium). CVD Graphene was received from Graphenea S.A. (Donostia, Spain)

NMR

^{1}H and ^{13}C NMR spectra were recorded at 300 and 75 MHz or 400 and 101 MHz (Varian Mercury 300 or Varian Inova-400 instruments), respectively.

Raman spectroscopy

Raman spectra were recorded with an Invia Renishaw microspectrometer (50) equipped with He–Ne laser at 532 nm and 633 nm. For graphene samples, the powders were dispersed in EtOH, drop-cast onto a silicon wafer and the solvent evaporated; at least 20 spectra per sample were recorded on different areas of the sample to assess the uniformity of the materials. DWCNTs were crashed onto a glass cover without further preparation and measured at least 20 spectra.

TGA

Thermogravimetry analyses (TGA) measurements were run on a TA Instruments Discovery system under N_2 purge using 0.5-1.5 mg of sample, Experiment consist on a equilibration at 100 ºC for 20 min and a ramp with a heating rate of 10 $°C \cdot min^{-1}$ up to 800.

XPS

XPS data was performed in a SPECS Sage HR 100 spectrometer with a non-monochromatic X ray source of Magnesium with a Kα line of 1253.6 eV energy and 250 W. The samples were placed perpendicular to the analyser axis and calibrated using the $3d^{5/2}$ line of Ag with a full width at half maximum (FWHM) of 1.1 eV. An electron flood gun was used to compensate for charging during XPS data acquisition. The selected resolution was 30 and 15 eV of Pass Energy and 0.5 and 0.15 eV/step for the survey and high-resolution spectra, respectively. Measurements were made in an ultra-high vacuum (UHV) chamber at a pressure below $8 \cdot 10^{-8}$ mbar. Fitting of the XPS data were done using CasaXPS 2.3.16 PR 1.6 software. For this data, the Shirley-type background subtraction was used, and all curves were defined as 30% Lorentzian, 70% Gaussian. Atomic ratios were computed from experimental intensity ratios and normalized by atomic sensitivity factors.

TEM

A concentrated dispersion of the sample was drop-cast on a copper grid (200 mesh, copper, carbon only and lacey carbon 200 mesh, copper, carbon only), after evaporation of the solvent under vacuum, the samples were analysed with a Philips EM 208 microscope operating at 100 kV.

Microwave assisted reactions

Microwave-assisted reactions were carried out in CEM Discover reactor, with infrared pyrometer, pressure-controlled system, stirring and air cooler option. Functionalization of Graphene and DWCNTs was done in a Quartz vessel of 10 mL to avoid breaks in the tube.

Electrochemical measurements

All electrochemical measurements were performed on a Autolab 302 N electrochemical workstation (Metrohm, The Netherlands) at room temperature, using a conventional three-electrode system composed by a modified glassy carbon electrode (GCE; CH Instrument, CH 104) as a working electrode, a platinum wire as an auxiliary electrode and a Ag/AgCl (CH Instrument, CH 111) as a reference electrode. Previously, the buffer solution was purged with high purity Nitrogen, all the experiments were performed under inert atmosphere. All presented results are averaged upon

five independent measurements.

SEM

SEM measurements were carried out with a SEM-LEICA STEREOSCAN 430i microscope. Images were acquired collecting secondary electrons.

AFM

AFM images were obtained with a Nanoscope IIIa, VEECO Instruments. As a general procedure to perform AFM analyses, tapping mode with a HQ:NSC19/ALBS probe (80 kHz; 0.6 N/m) (MikroMasch). The obtained AFM-images were analyzed in Gwyddion 2.41.

3.2 General methods

3.2.1 General method for the preparation of FLG

3.2.1.1 Method 1

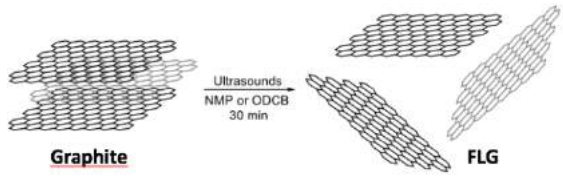

Graphite (25 mg) was added to the corresponding solvent (200 mL) in a round-bottom flask. The, the suspension was sonicated for 30 minutes at the sonicator bath. The resulted mixture of expanded graphite and FLG was decanted after 16 hours. To know the concentration, an aliquot (10 mL) was filtered and washed with CH_2Cl_2 (3 x 20 mL), H_2O (3 x 20 mL), MeOH (3 x 20 mL), AcOEt (3 x 20 mL) and few drops of Et_2O. Concentrations were about than 0.01 mg/mL.

The corresponding dispersions were directly used for chemical reactions with a previous 1-minute sonication in order to refresh the mixture.

3.2.1.2 Method 2

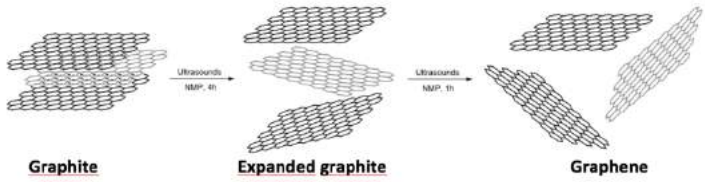

Powder graphite (4g) was mixed in a solution (40 mL) of NMP and ultrasonicated in a sonic tip for 4 h (1 second of relaxing time; 23% of power), the resulted expanded graphite was washed with 2-propanol and filtered. The powder was dispersed (800 mL) in NMP and resonicated in a conventional ultrasonic bath for 1 h, the stable dispersion was decanted, filtered and washed several times with methanol given black powder considered as few layer graphene.

3.2.2 General electrochemical procedure

Glassy carbon electrode was polished with sand paper and then with (1.0 μm and 0.3 μm) alumina powder. After rinsing thoroughly with deionized water, it was sonicated in deionized water to remove any alumina residues, and was then cycled 3 times in 0.10 M phosphate buffer solution (PBS) between 0.9 and −0.3 V at 0.10 V s^{-1} to perform the electrochemical polishing.

The surface state reproducibility was controlled for each electrode measuring one cyclic voltammogram in 1 mM potassium ferricyanide. Electrodes present a difference between redox peak potentials higher than 0.08 V were discarded.

3.2.2.1 Modification of GCE with GO

GCE was modified dropping 10 μL of a dispersion of GO (0.25 mg/mL). Optionally 0.05% of Nafion® in the solution was added. The sample was dried at room temperature for 2 hours. Electrochemical reduction was performed in buffer solution (PBS, pH 7.40), previously purged with high purity Nitrogen. Then, the electrode was immersed into an electrochemical cell containing. The electrochemical experiment performed was cyclic voltammetry. It was conducted at a scan rate of 50 mV/s between 0 to -1.5V, observing a reduction peak at -1.04 V.

3.2.2.2 Modification of GCE with rGO

GCE was modified dropping 10 μL of a dispersion of rGO (1mg/mL).

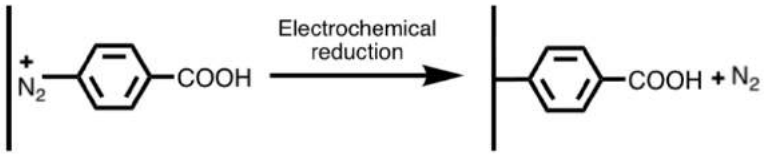

CBD electroreduction was performed under the presence of CBD 5 mM and HCl 0.1 M, through cyclic voltammetry, conducted at a scan rate of 20 mV/s between 0.8 to -0.6V. The activation solution (0.2 M EDC and 50 mM NHS in PBS buffer) was then cast on the surface (30 μL) to activate the carboxyl group for 30 minutes under humidity atmosphere. After rinsing with deionized water, 5-Guanine oligonucleotide (100 μM- 10 μM), previously

treated 5 minutes at 90 ºC and 10 minutes at 0 ºC, was dropped (30 µL) to the modified the electrode for 30 and 60 minutes and washed with deionized water. The electrochemical measurements were performed in phosphate buffer 0.05M (pH 7.4) and NaCl 0.2M.

3.2.3 General method for functionalization of CVDG

1 cm^2 CVDG was submerged onto solution reaction with conditions described in different sections of part 2 avoiding light presence and under inert atmosphere. After reaction, CVDG was washed several times in THF (5 x 20 mL), CH_2Cl_2 (5 x 20 mL), H_2O (5 x 20 mL), MeOH (5 x 20 mL), AcOEt (5 x 20 mL) and dried with N_2.

3.2.4 General method for conventional functionalization of FLG with arynes

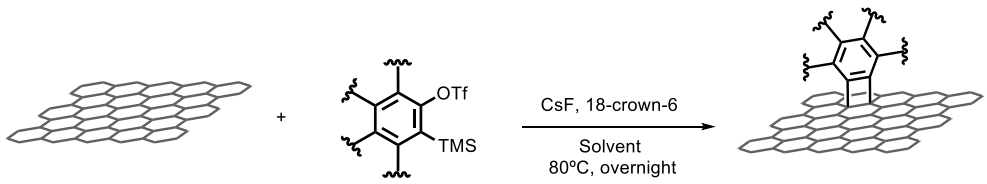

Pristine graphene was prepared following the procedure mentioned above. The dispersion of graphene (1.0 atomic equiv, assuming the sample to be of pure carbon) was mixed aryne precursor (4.0 equiv), cesium fluoride (12 equiv) and 18-crown-6 (3.6 equiv). The mixture was heat overnight at 80 ºC. Then, several washes and filtrations in a Millipore system of the resulting *f*-G were performed with: CH_2Cl_2 (3 x 20 mL), H_2O (3 x 20 mL), MeOH (3 x 20 mL), AcOEt (3 x 20 mL) and few drops of Et_2O.

3.2.5 General method for conventional functionalization of rGO with difluorophenylene arynes

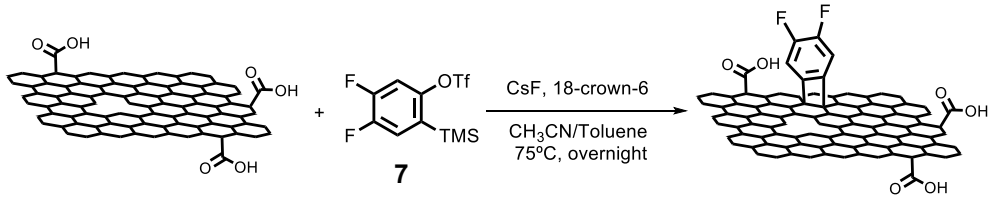

rGO (10mg) was dispersed in solvent (20 mL). The dispersion of rGO (1.0 atomic equiv, assuming the sample to be of pure carbon) was mixed with **7** (4.0 equiv), cesium fluoride (12 equiv) and 18-crown-6 (3.6 equiv). The mixture was heat overnight at 75 ºC. Then, several washes and filtrations in a Millipore system of the resulting *f*-rGO were performed with: CH_2Cl_2 (3 x 20 mL), H_2O (3 x 20 mL), MeOH (3 x 20 mL), AcOEt (3 x 20 mL) and few drops of Et_2O.

3.2.6 General method for functionalization of FLG with arynes: Method 1

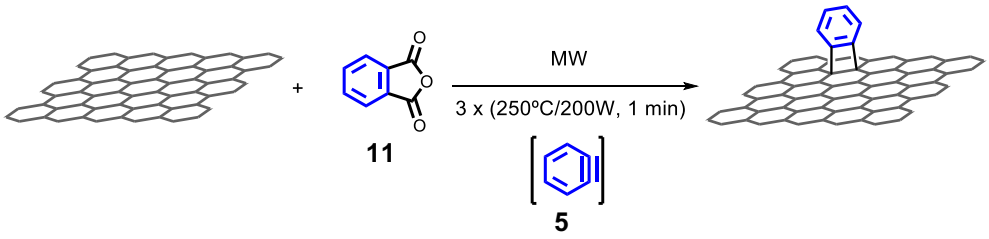

FLG (1.0 atomic equiv, assuming the sample to be of pure carbon) phthalic anhydride (**11**, 3.0 equiv) were added to a mortar. The grind of the sample was done until observe a homogeneous mixture. The powder was transfer onto a quartz Vessel. The reaction was performed with a fixed temperature (250 ºC W) with a maximum power of 200W regulated by the microwave, after one minute the vessel was cooled to 50 ºC and repeat it 3 cycles. Then, several washes and filtrations in a Millipore system of the resulting *f*-G were performed with: CH_2Cl_2 (3 x 20 mL), H_2O (3 x 20 mL), MeOH (3 x 20 mL), AcOEt (3 x 20 mL) and few drops of Et_2O.

3.2.7 General method for functionalization of FLG with arynes: Method 2

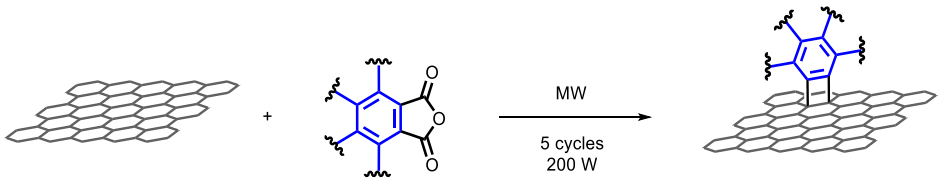

The reactions were carried out under N_2, functionalized graphene (*f*-G) were prepared following the next procedure. FLG (1.0 atomic equiv, assuming the sample to be of pure carbon) phthalic anhydride (**11**, 3.0 equiv) were added to a mortar. The grind of the sample was done until observe a homogeneous mixture. The powder was transfer onto a quartz Vessel. Then, 5 cycles of MW irradiation were applied. In each cycle, the reaction was performed with a fixed power of 200 W until a rise of the temperature of 250 ºC in about 5 seconds. The reaction mixture was cooling down by applying outsider cooling, until the temperature decreased to 175 ºC. Then, several washes and filtrations in a Millipore system of the resulting *f*-G were performed with: CH_2Cl_2 (3 x 20 mL), H_2O (3 x 20 mL), MeOH (3 x 20 mL), AcOEt (3 x 20 mL) and few drops of Et_2O.

3.2.8 General method for functionalization of DWCNTs with arynes: Method 1

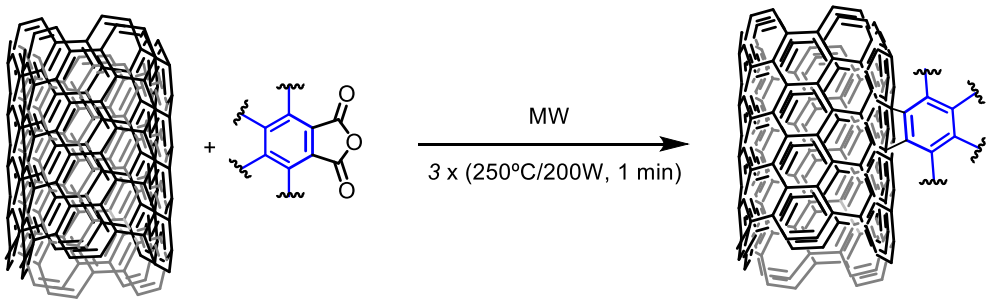

The reactions were carried out under N_2. DWCNT (1.0 atomic equiv, assuming the sample to be of pure carbon) and phthalic anhydride (3.0 equiv) were added to a mortar. The grind of the sample was done until observe a homogeneous mixture. The powder was transfer onto a quartz Vessel. The reaction was performed with a fixed temperature (250 ºC W) with a maximum power of 200W regulated by the microwave, after one minute the vessel was cooled to 50 ºC and repeat it 3 cycles. Then, several washes and filtrations in a Millipore system of the resulting *f*-DWCNT were performed with: CH_2Cl_2 (3 x 20 mL), H_2O (3 x 20 mL), MeOH (3 x 20 mL), AcOEt (3 x 20 mL) and few drops of Et_2O.

3.2.9 General method for ball milling exfoliation and microwave functionalization of graphene

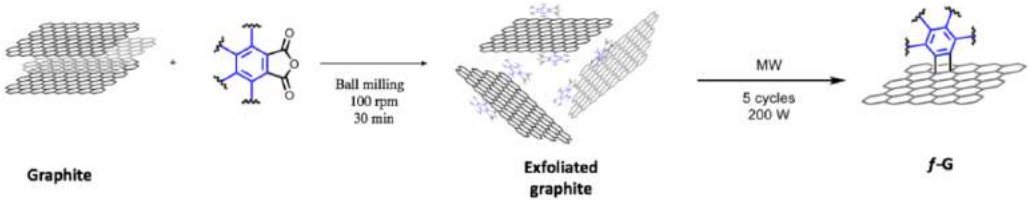

The reactions to obtain functionalized graphene (*f*-G) with a previous treatment in a ball-milling process were prepared following the next procedure. First of all, powder graphite and the corresponding arylene anhydride were added to a mortar (1:3 weight proportion). The grind of the sample was done until observe a homogeneous mixture. The powder was ball-milled in a 50mL stainless Steel jar with 10 stainless Steel balls of 1cm diameter each under 100 rpm for 30 minutes. The resulting solid mixture was transferred onto a quartz Vessel. Then, 5 cycles of MW irradiation were applied under N_2. In each cycle, the reaction was performed with a fixed power of 200 W until a rise of the temperature of 250 ºC in about 5 seconds. The reaction mixture was cooling down by applying outsider cooling, until the temperature decreased to 175 ºC. Then, several washes and filtrations in a Millipore system of the resulting *f*-G were performed with: CH_2Cl_2 (3 x 20 mL), H_2O (3 x 20 mL), MeOH (3 x 20 mL), AcOEt (3 x 20 mL) and few drops of Et_2O.

3.3 Synthesis of diazonium salt and aryne precursors

*3.3.1 Synthesis of **3***

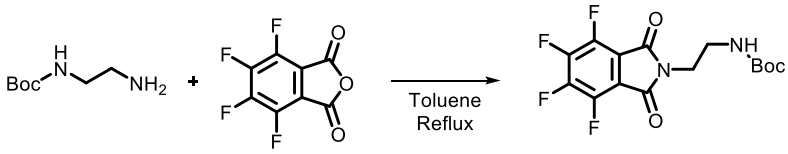

23 **9** **24**

A mixture of **23** (2.09 g 13.1 mmol) and tetrafluorophthalic anhydride **(9**, 2.88 g, 13.1 mmol) in toluene (50 mL) was refluxed under Ar overnight. The crude product was purified by column chromatography (SiO_2, Hexane/CH_2Cl_2/AcOEt 5:1:4) to afford **24** (2.36 g, 50% yield).

^{1}H NMR (298 K, 300 MHz, $CDCl_3$) δ: 4.78 (s, 1H), 3.83 (m, 2H), 3.44 (dd, 2H) 1.36 (s, 9H) ppm

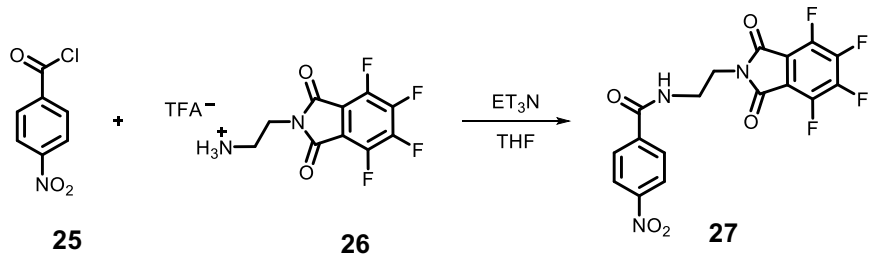

25 **26** **27**

Benzoyl chloride **25** (492 mg, 2.66 mmol) was added in a solution of Et_3N (1.1 mL, 7.98 mmol) in THF (30 mL). The corresponding amonium salt **26** (1 g, 2.66 mmol) was added. The resulting mixture was stirred at room temperature overnight. The volume of the solution was reduced under reduced pressure. Then the residue was solved in CH_2Cl_2 (100 mL). The solution was worked up with $NaHCO_3$ (100 mL). The aqueous layer was extracted with CH_2Cl_2 (2x100 mL). The organic layers were dried with $MgSO_4$ anhydrous, filtered and concentrated under reduced pressure. The crude was purified by column chromatography (SiO_2, CH_2Cl_2/AcOEt 1:9) to afford **26** (891 mg, 99% yield).

^{1}H NMR (298 K, 300 MHz, $CDCl_3$) δ: 8.23 (m, 2 H), 7.82 (m, 2H), 4.78 (s, 1H), 3.95 (dd, 2H), 3.72 (dd, 2H) ppm

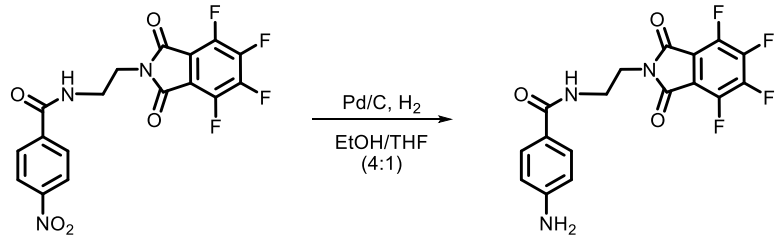

27 **3**

The corresponding nitrophenyl **27** (890 mg, 2.63 mmol) was mixed in THF (50mL) and EtOH (200 mL). The catalyst Pd/C was added (10%, catalytic amount). Then, the solution was deoxygenated under vacuum and H_2 was added (3 cycles). The reaction was stirred under H_2 atmosphere overnight. The suspension was filtered and filtered over celite. The filtered solution was concentrated under reduced pressure. The mixture was purified by column chromatography (SiO_2, CH_2Cl_2/AcOEt 6:4) to afford **3** (576 mg, 70% yield).

^{1}H NMR (298 K, 300 MHz, $CDCl_3$) δ: 7.55 (m, 2 H), 6.64 (m, 2H), 5.12 (s, 1H), 3.86 (dd, 2H), 3.66 (dd, 2H) ppm

3.3.2 Synthesis of o-(trimethylsilyl)aryl triflates aryne precursors

Aryne precursors **4**, **6**[236] and **19**[222] were prepared following published procedures.

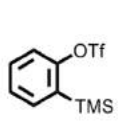

4

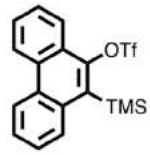

6

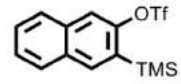

19

*3.3.3 Synthesis of dimethyl phenanthrene-9,10-dicarboxylate (**21**)*

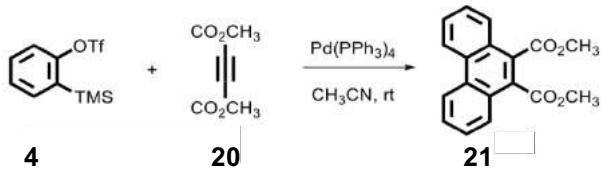

4 **20** **21**

To a deoxygenated solution of triflate **4** (408 mg, 1.37 mmol), dimethyl acetylenedicarboxylate (**20**, 196 μL, 1.92 mmol) and $Pd(PPh_3)_4$ (158 mg, 0.137 mmol) in anhydrous CH_3CN (27 mL) was added CsF (521 mg, 3.43 mmol), and the resulting mixture was stirred at room temperature for 16 h. Then, H_2O (20 mL) and Et_2O (20 mL) were added, the layers were separated and the aqueous layer extracted with Et_2O (2 x 20 mL). The combined organic layers were dried over anhydrous Na_2SO_4, filtered, and concentrated under reduced pressure. The crude product was purified by column chromatography (SiO_2, Hexane/CH_2Cl_2 9:1) to afford dimethyl phenanthrene-9,10-dicarboxylate (**21,** 338 mg, 84% yield) as a white solid.

^1H NMR (298 K, 300 MHz, $CDCl_3$) δ: 8.64 (dd, *J* = 7.9, 1.6 Hz, 2H), 8.15 (dd, *J* = 7.9, 1.8 Hz, 2H), 7.76–7.56 (m, 4H), 4.04 (s, 6H) ppm.

*3.3.4 Synthesis of dimethyl pentaphene-6,7-dicarboxylate (**22**)*

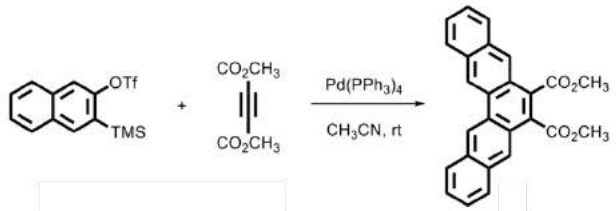

19 **20** **22**

To a deoxygenated solution of triflate **19** (661 mg, 1.9 mmol), dimethyl acetylenedicarboxylate (**20**, 271.5 μL, 2.66 mmol) and $Pd(PPh_3)_4$ (219 mg, 0.19 mmol) in anhydrous CH_3CN (38 mL) was added CsF (722 mg, 4.75 mmol), and the resulting mixture was stirred at room temperature for 16 h. Then, H_2O (30 mL) and Et_2O (30 mL) were added, the layers were separated, and the aqueous layer extracted with Et_2O (2 x 30 mL). The combined organic layers were dried over anhydrous Na_2SO_4, filtered, and concentrated under reduced pressure. The crude product was purified by column chromatography (SiO_2, Hexane/CH_2Cl_2 9:1) to afford dimethyl pentaphene-6,7-dicarboxylate (**22,** 449 mg, 60% yield) as a yellow solid.

^{1}H NMR (298 K, 300 MHz, $CDCl_3$) δ: 9.18 (s, 2H), 8.52 (s, 2H), 8.10 (d, *J* = 8.1 Hz, 2H), 7.99 (d, *J* = 7.6 Hz, 2H), 7.68–7.48 (m, 4H), 4.11 (s, 6H) ppm.

^{13}C NMR (298 K, 75 MHz, $CDCl_3$) δ: 168.4 (2C), 132.9 (2C), 132.4 (2C), 130.8 (2C), 128.9 (2C), 128.6 (2CH), 128.3 (2CH), 127.3 (2CH), 126.9 (2CH), 126.6 (2CH), 125.4 (2C), 122.3 (2CH), 52.8 (2CH3) ppm.

MS (EI), *m*/*z* (%): 394 (100). HRMS (EI) for $C_{26}H_{18}O_4$, calculated: 394.1205, found: 394.1211.

*3.3.5 Synthesis of phenanthro[9,10-c]furan-1,3-dione (**17**)*

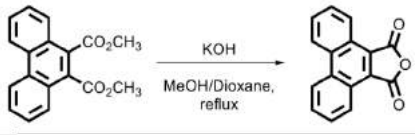

21 **17**

In a round bottom flask, a suspension of dimethyl phenanthrene-9,10-dicarboxylate (**21**, 338 mg, 1.15 mmol) in EtOH/dioxane (1:1, 230 mL) was prepared. Then, a solution of KOH (3.79 g, 68 mmol) in EtOH (38 mL) was added, and the mixture refluxed for 2h. After that, aqueous HCl (10%, 20 mL) and Et_2O (30 mL) were added, the layers were separated and the aqueous layer extracted with CH_2Cl_2 (3 x 30 mL). The combined organic layers were dried over anhydrous Na_2SO_4, filtered, and concentrated under reduced pressure. The crude product was purified by column chromatography (SiO_2, CH_2Cl_2/AcOEt 49:1) to afford anhydride **17** (291 mg, 98% yield) as a pale-yellow solid.

^{1}H NMR (298 K, 300 MHz, $CDCl_3$) δ: 9.03 (dd, *J* = 8.2, 1.3 Hz, 2H), 8.80 (d, *J* = 8.1 Hz, 2H), 8.00–7.79 (m, 4H) ppm.[236]

*3.3.6 Synthesis of pentapheno[6,7-c]furan-6,8-dione (**18**)*

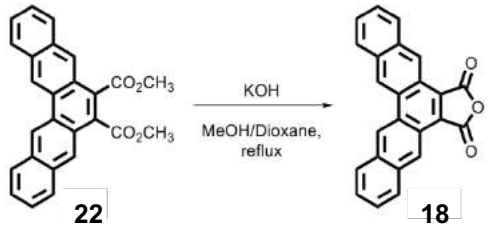

In a round bottom flask, a suspension of dimethyl pentaphene-6,7-dicarboxylate (**22**, 449 mg, 1.14 mmol) in EtOH/dioxane (1:1, 228 mL) was prepared. Then, a solution of KOH (3.77 g, 67 mmol) in EtOH (37 mL) was added, and the mixture refluxed for 2h. After that, aqueous HCl (10%, 20 mL) and Et_2O (30 mL) were added, the layers were separated, and the aqueous layer extracted with CH_2Cl_2 (5 x 30 mL). The combined organic layers were dried over anhydrous Na_2SO_4, filtered, and concentrated under reduced pressure. The crude product was subsequently washed with H_2O (2 x 4 mL), Et_2O (3 x 4 mL) and pentane (2 x 4 mL) to afford anhydride **18** (297 mg, 75% yield) as an orange solid.

^{1}H NMR (388 K, 400 MHz, DMSO-D_6) δ: 9.68 (s, 2H), 9.36 (s, 2H), 8.43 – 8.25 (m, 4H), 7.89 – 7.69 (m, 4H) ppm.

^{13}C NMR (388 K, 101 MHz, DMSO-D_6) δ: 162.96 (2C), 133.13 (2C), 131.55 (2C), 129.91 (2C), 129.57 (2C), 128.22 (2CH), 128.04 (2CH), 127.94 (2CH), 126.98 (2CH), 125.67 (2CH), 123.31 (2CH), 121.36 (2C) ppm.

MS (EI), *m*/*z* (%): 348 (100), 276 (87). HRMS (EI) for $C_{24}H_{12}O_3$, calculated: 348.0786, found: 348.0786.

3.4 Specific experimental procedures

Preparation of GO

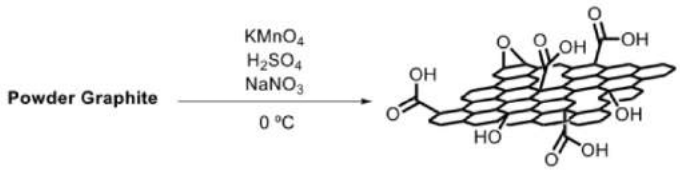

Powder graphite (3.0 g) 2ith $NaNO_3$ (1.5 g) was cooled at 0 ºC, slowly $KMnO_4$ (9.0 g) was added to keep the reaction bellow 20 ºC. The mixture was warmed to 35 ºC under vigorous stirring. The, H_2O (138 mL) was carefully added; external heating was applied at 98 ºC for 15 minutes. After cooling the reaction, additional H_2O was added (420 mL) and H_2O_2 (3.0 mL, 30%). The black suspension was filtered on a Teflon membrane (Millipore, GTTP, 0.45 μm) and centrifugated at 4000 rpm. The mixture was washed and centrifugated with H_2O (2 x 200 mL), HCL 30 % (2 x 200 mL) and C_2H_6O (2 x 200 mL).

Preparation of rGO

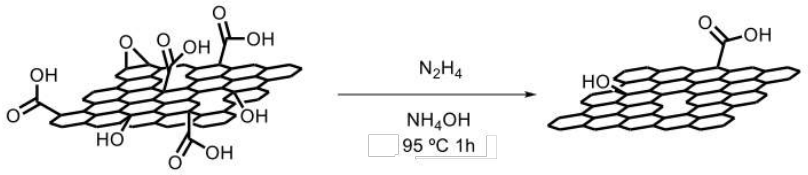

GO (210 mg) was dispersed in water (420 mL by sonication. Then, a NH_4OH solution (950 μL, pH=10) and hydrazine monohydrate (147 mg) were added. The mixture was stirred at 95 ºC for 1 h. Then, the suspension was dialyzed (300000 Da cut-off) in distilled water for 2 d. Subsequently, the black suspension was filtered on a Teflon membrane (Millipore, GTTP, 0.1 μm) and washed by filtration with DMF (3 x 100 mL) and MeOH (3 x 100 mL).

Functionalization *f*-CVDG(1)

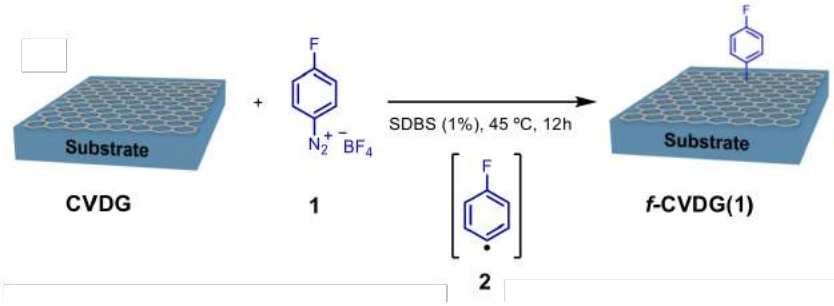

The general procedure 3.2.3 was followed, the substrate was fully immersed in a solution of **1** (105 mg) and SDBS in water (10 mL) at 45 ºC with absence of light. After reaction the substrate was washed: THF (5 x 20 mL), CH_2Cl_2 (5 x 20 mL), H_2O (5 x 20 mL), MeOH (5 x 20 mL), AcOEt (5 x 20 mL) and dried with N_2. The sample was totally detached.

Functionalization *f*-CVDG(2)

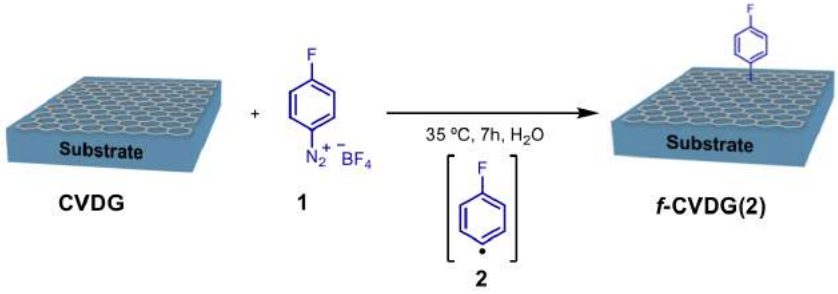

The general procedure 3.2.3 was followed, the substrate was fully immersed in a solution of **1** (3.4 mg) in water (100 mL) at 35 ºC with absence of light for 7 hours. After reaction the substrate was washed: THF (5 x 20 mL), CH_2Cl_2 (5 x 20 mL), H_2O (5 x 20 mL), MeOH (5 x 20 mL), AcOEt (5 x 20 mL) and dried with N_2. $\Delta I_D/I_G$=0.6, Detachment: 5%.

Functionalization *f*-CVDG(3)

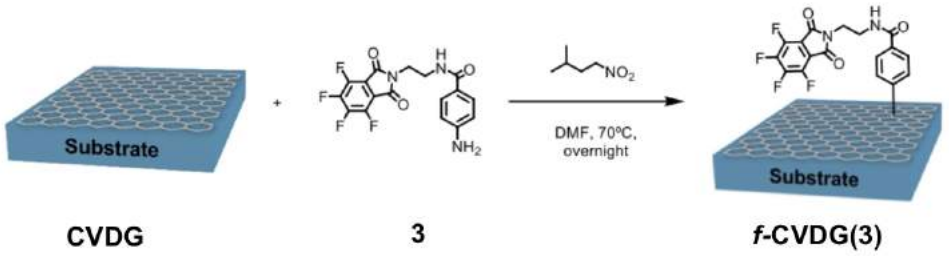

The general procedure 3.2.3 was followed, the substrate was fully immersed in a solution of **3** (15 mg) and isopentyl nitrite (27 μL) in DMF (10 mL) at 70 ºC for 2 hours. After reaction the substrate was washed: DMF (20 mL overnight) THF (5 x 20 mL), CH_2Cl_2 (5 x 20 mL), H_2O (5 x 20 mL), MeOH (5 x 20 mL), AcOEt (5 x 20 mL) and dried with N_2.

Functionalization *f*-CVDG(4)

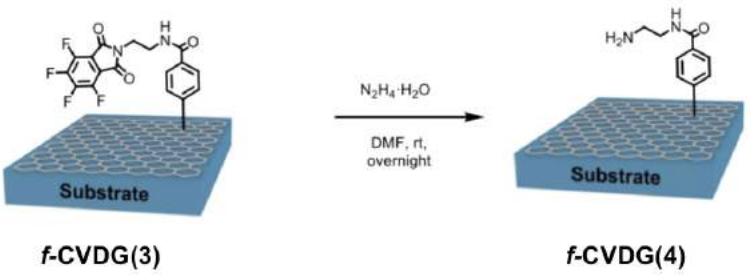

The general procedure 3.2.3 was followed, the *f*-CVDG(**4**) was fully immersed in a solution of N_2H_4 (50 μL) in isopentyl nitrite (0.5 mL) in DMF (10 mL) at room temperature overnight. After reaction the substrate was washed: DMF (5 x 20 mL) THF (5 x 20 mL), CH_2Cl_2 (5 x 20 mL), H_2O (5 x 20 mL), MeOH (5 x 20 mL), AcOEt (5 x 20 mL) and dried with N_2.

Functionalization *f*-G(5)

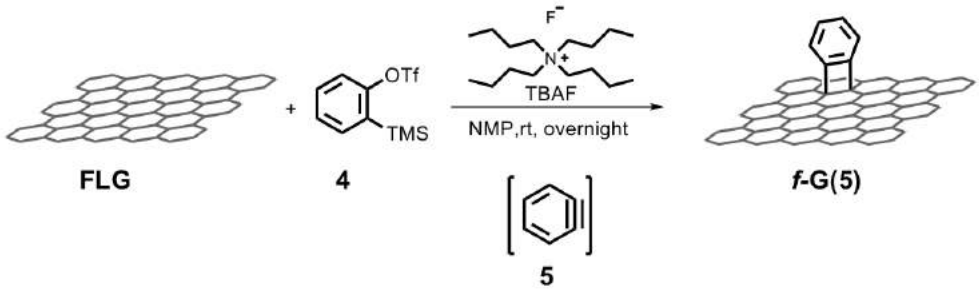

The general procedure 3.2.4 was followed, to a dispersion (208 mL) of previous exfoliated graphene (general procedure 3.2.1.1 with 2.5 mg obtained) was added **4** (247 mg) and CsF (380 mg). After overnight at rt the sample was washed and filtered several times: CH_2Cl_2 (3 x 20 mL), H_2O (3 x 20 mL), MeOH (3 x 20 mL), AcOEt (3 x 20 mL) and few drops of Et_2O. Obtained mass: 0.7 mg, $\Delta I_D/I_G$=0.04, FD: 592 μmol/g (TGA).

Functionalization *f*-G(6)

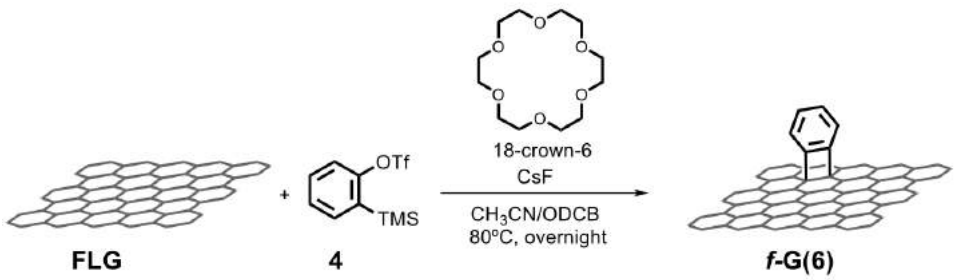

The general procedure 3.2.4 was followed, to a dispersion (275 mL) of previous exfoliated graphene in ODCB (general procedure 3.2.1.1 with 3.32 mg obtained) was added CH_3CN (50 mL), **4** (329 mg), CsF (504 mg) and 18-crown-6 (263 mg). After overnight at 80 ºC the sample was washed and filtered several times: CH_2Cl_2 (3 x 20 mL), H_2O (3 x 20 mL), MeOH (3 x 20 mL), AcOEt (3 x 20 mL) and few drops of Et_2O. Obtained mass: 1.5 mg, $\Delta I_D/I_G$=0.25, FD: 620 μmol/g (TGA).

Functionalization *f*-G(7)

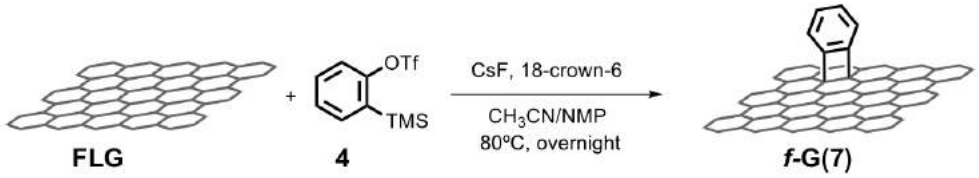

The general procedure 3.2.4 was followed, to a dispersion (550 mL) of previous exfoliated graphene in NMP (general procedure 3.2.1.1 with 7.7 mg obtained) was added CH_3CN (75 mL), **4** (762 mg), CsF (1170 mg) and 18-crown-6 (689 mg). After overnight at 80 ºC the sample was washed and filtered several times: CH_2Cl_2 (3 x 20 mL), H_2O (3 x 20 mL), MeOH (3 x 20 mL), AcOEt (3 x 20 mL) and few drops of Et_2O. Obtained mass: 5.5 mg, $\Delta I_D/I_G$=0.08, FD: 394 μmol/g (TGA)

Functionalization *f*-G(8)

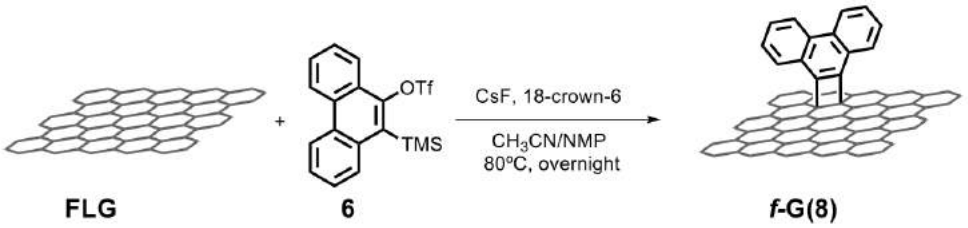

The general procedure 3.2.4 was followed, to a dispersion (300 mL) of previous exfoliated graphene in NMP (general procedure 3.2.1.1 with 2.5 mg obtained) was added CH_3CN (50 mL), **6** (330 mg), CsF (380 mg) and 18-crown-6 (198 mg). After overnight at 80 ºC the sample was washed and filtered several times: CH_2Cl_2 (3 x 20 mL), H_2O (3 x 20 mL), MeOH (3 x 20 mL), AcOEt (3 x 20 mL) and few drops of Et_2O. Obtained mass: 1.1 mg, $\Delta I_D/I_G$=0.06, FD: 113 μmol/g (TGA).

Functionalization *f*-rGO(9-11)

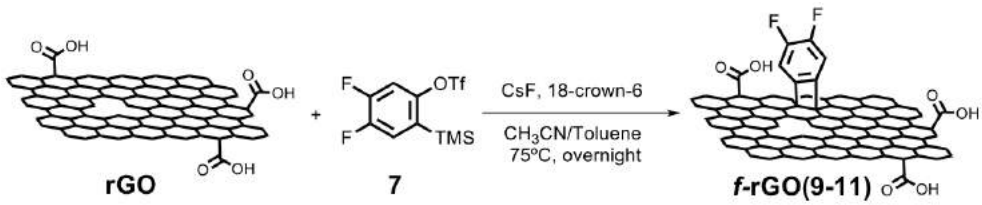

The general procedure 3.2.5 was followed, 10 mg of rGO were dispersed for 90 minutes in solvent (*f*-rGO(**9**): 20 mL of CH_3CN, *f*-rGO(**10**): 15 mL of CH_3CN and 5 mL of toluene, *f*-rGO(**11**): 20 mL of toluene). The dispersion of rGO was mixed with **7** (1112 mg), CsF (1520 mg) and in case of *f*-rGO(**10**) and *f*-rGO(**11**) 18-crown-6 (788 mg). After overnight at 80 ºC the sample was washed and filtered several times: CH_2Cl_2 (3 x 20 mL), H_2O (3 x 20 mL), MeOH (3 x 20 mL), AcOEt (3 x 20 mL) and few drops of Et_2O. *f*-rGO(**9**): Obtained mass: 8.1 mg, FD: 257 µmol/g (TGA), XPS surface atomic percentages: 52.8 % C1s, 15.1 % O1s, 32.1 % F1s. *cs*-rGO(**10**): FD: 439 µmol/g (TGA), XPS surface atomic percentages: 82 % C1s, 12.5 % O1s, 5.5 % F1s. . *f*-rGO(**10**): Obtained mass: 7.5 mg, FD: 135 µmol/g (TGA), XPS surface atomic percentages: 36.7 % C1s, 15.1 % O1s, 33.6 % F1s. *f*-rGO(**11**): Obtained mass: 8.7 mg, FD: 385 µmol/g (TGA), XPS surface atomic percentages: 42.5 % C1s, 34.5 % O1s, 23.9 % F1s.

Functionalization *f*-CVDG(12)

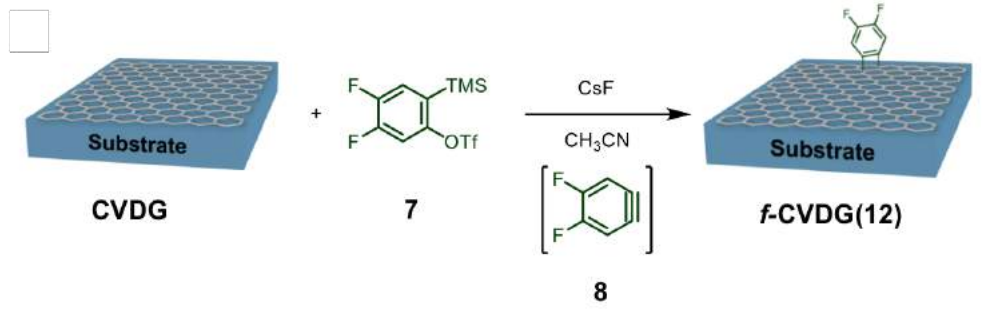

The general procedure 3.2.3 was followed, the substrate was fully immersed in a solution of **7** (154 mg) in CH_3CN (10 mL) and CsF (535 mg) at rt overnight. After reaction the substrate was washed: THF (5 x 20 mL), CH_2Cl_2 (5 x 20 mL), H_2O (5 x 20 mL), MeOH (5 x 20 mL), AcOEt (5 x 20 mL)

and dried with N_2. Detachment: 99%.

Functionalization *f*-CVDG(13)

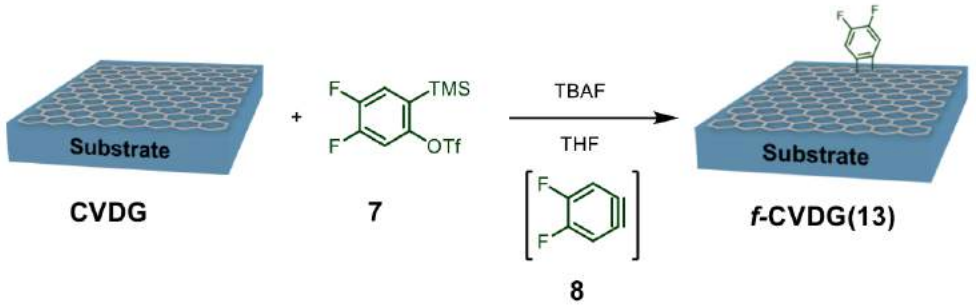

The general procedure 3.2.3 was followed, the substrate was fully immersed in a solution of **7** (250 mg) in THF (5 mL) and TBAF (294 mg) at rt for 2h. After reaction the substrate was washed: THF (5 x 20 mL), CH_2Cl_2 (5 x 20 mL), H_2O (5 x 20 mL), MeOH (5 x 20 mL), AcOEt (5 x 20 mL) and dried with N_2. $\Delta I_D/I_G$=0.32.

Functionalization *f*-CVDG(14)

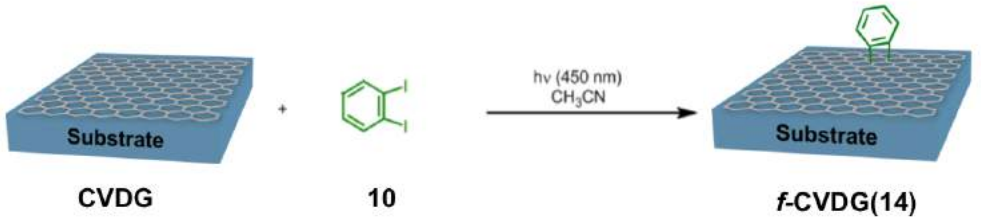

The substrate was fully immersed in a solution of **10** (2475 mg) in CH_3CN (15 mL) and exposed to UV lamp with 7 mW/cm^2 power at rt for 6 h (original ν 250 nm). After reaction the substrate was washed: THF (5 x 20 mL), CH_2Cl_2 (5 x 20 mL), H_2O (5 x 20 mL), MeOH (5 x 20 mL), AcOEt (5 x 20 mL) and dried with N_2. Detachment: 50%, $\Delta I_D/I_G$=0.32

Functionalization *f*-CVDG(14b)

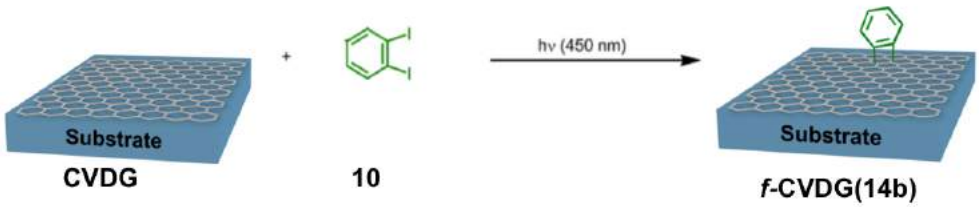

The substrate was fully dropped with **10** and exposed to UV lamp with 7 mW/cm^2 power at rt for 6 h (original ν 250 nm). After reaction the substrate was washed: THF (5 x 20 mL), CH_2Cl_2 (5 x 20 mL), H_2O (5 x 20 mL), MeOH (5 x 20 mL), AcOEt (5 x 20 mL) and dried with N_2. $\Delta I_D/I_G$=0.07.

Functionalization *f*-CVDG(15-19)

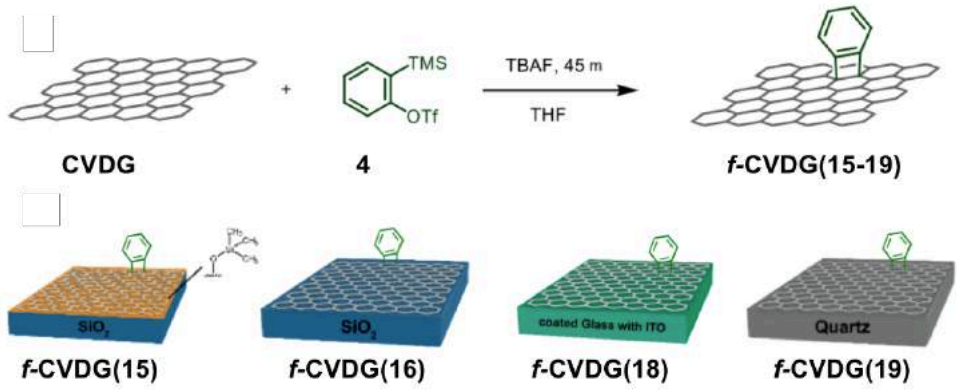

The general procedure 3.2.3 was followed, the substrate was fully immersed in a solution of **4** (233 mg) in THF (4.7 mL) and TBAF (294 mg) at rt for 45 minutes. After reaction the substrate was washed: THF (5 x 20 mL), CH_2Cl_2 (5 x 20 mL), H_2O (5 x 20 mL), MeOH (5 x 20 mL), AcOEt (5 x 20 mL) and dried with N_2. *f*-CVDG(**15**): $\Delta I_D/I_G$=0.02, *f*-CVDG(**16**): $\Delta I_D/I_G$=0.09, *f*-CVDG(**17**) (Cupper substrate): $\Delta I_D/I_G$=0.03, *f*-CVDG(**18**): $\Delta I_D/I_G$=0.12, *f*-CVDG(**19**): $\Delta I_D/I_G$=0.06.

Functionalization *f*-CVDG(20)

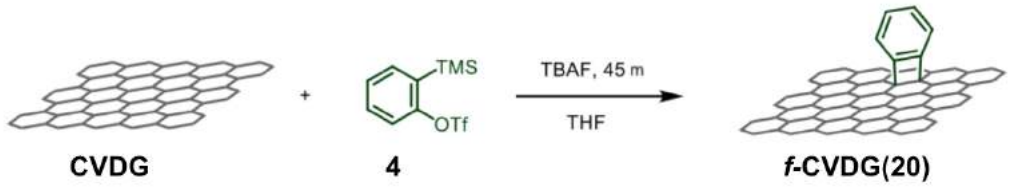

The general procedure 3.2.3 was followed, the substrate was fully immersed in a solution of **4** (233 mg) in THF (4.7 mL) and TBAF (294 mg) at rt for 45 minutes. After reaction the substrate was washed: THF (5 x 20 mL), CH_2Cl_2 (5 x 20 mL), H_2O (5 x 20 mL), MeOH (5 x 20 mL), AcOEt (5 x 20 mL) and dried with N_2. *f*-CVDG(**15**): $\Delta I_D/I_G$=0.01,

Synthesis of triptycene (13) using graphite as matrix

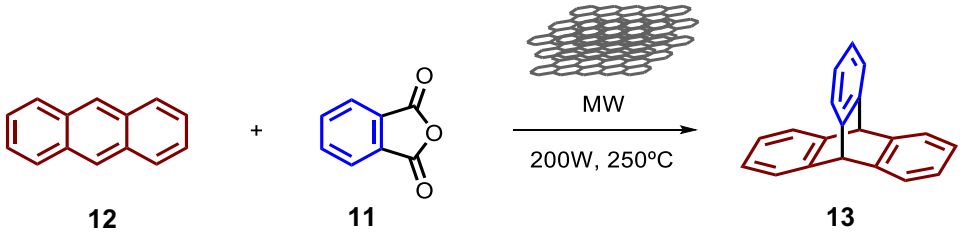

In a mortar, anthracene (**12**, 104 mg, 0.58 mmol) phthalic anhydride (**11**, 86 mg, 0.58 mmol) and FLG (7.0 mg) were added. The grind of the sample was done until observe a homogeneous mixture. The powder was transfer onto a quartz Vessel. The reaction was performed using method 1 of microwave reaction, with a fixed temperature of 250 ºC and a maximum power of 200 W, 3 times. Then, the resulting solid mixture was washed with CH_2Cl_2 and filtrated in a Millipore system. The organic layer was dried under reduced pressure.

^{1}H NMR (388 K, 400 MHz, $CDCl_3$) δ: 7.39 (m, *J* = 5.3, 3.2 Hz, 6H) 7.0 (dd, *J* = 5.4, 3.1 Hz, 6H) 5.43 (s, 2H) ppm.

Synthesis of triptycene (13) using few FLG as matrix

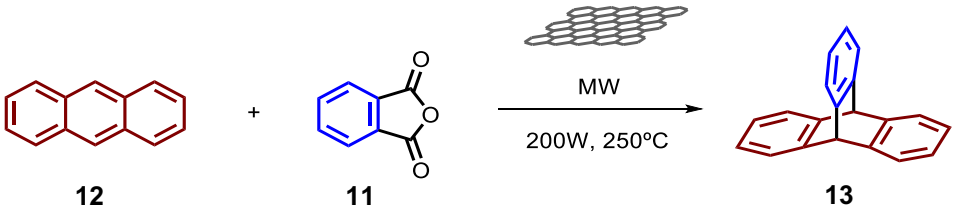

In a mortar, anthracene (**12**, 104 mg, 0.58 mmol) phthalic anhydride (**11**, 86 mg, 0.58 mmol) and FLG (7.0 mg) were added. The grind of the sample was done until observe a homogeneous mixture. The powder was transfer onto a quartz Vessel. The reaction was performed using method 2 with a fixed power (200 W) until a rise of the temperature of 250 ºC (10 cycles). Then, the resulting solid mixture was washed with CH_2Cl_2 and filtrated in a Millipore system. The organic layer was dried under reduced pressure. By the analysis of the ^{1}HNMR, triptycene (**13**) was obtained in 13% conversion.

4. REFERENCES

(1) Anders, E.; Grevesse, N. Abundances of the Elements: Meteoric and Solar. *Geochim. Cosmochim.\ Acta* **1989**, *53*, 197–214.

(2) McDonough, W. F.; Sun, S. s. The Composition of the Earth. *Chem. Geol.* **1995**, *120* (3-4), 223–253.

(3) Pierson, H. O. Handbook of Carbon, Graphite, Diamond and Fullerenes. *Handb. Carbon, Graph. Diam. Fullerenes* **1993**, 25–69.

(4) Georgakilas, V.; Perman, J. A.; Tucek, J.; Zboril, R. Broad Family of Carbon Nanoallotropes: Classification, Chemistry, and Applications of Fullerenes, Carbon Dots, Nanotubes, Graphene, Nanodiamonds, and Combined Superstructures. *Chem. Rev.* **2015**, *115* (11), 4744–4822.

(5) Kroto, H. W.; Heath, J. R.; O'Brien, S. C.; Curl, R. F.; Smalley, R. E. C 60: Buckminsterfullerene. *Nature* **1985**, *318*, 162–163.

(6) He, Y.; Chen, H.; Hou, J.; Li, Y. Indene-C 60 Bisadduct : A New Acceptor for High-Performance Polymer Solar Cells. *J. Am. Chem. Soc.* **2010**, *132* (19), 1377–1382.

(7) Iijima, S. Helical Microtubes of Graphitic Carbon. *Lett. to Nat.* **1991**, *354*, 737–740.

(8) Thostenson, E. T.; Ren, Z.; Chou, T.-W. Advances in the Science and Technology of Carbon Nanotubes and Their Composites: A Review. *Compos. Sci. Technol.* **2001**, *61* (13), 1899–1912.

(9) K.S. Novoselov1, A.K. Geim1, S.V. Morozov2, D. Jiang1, Y. Zhang1, S.V. Dubonos2, I.V.Grigorieva1, a. a. F. Electric Field Effect in Atomically Thin Carbon Films.

(10) Lee, C.; Wei, X.; Kysar, J. W.; Hone, J. Measurement of the Elastic Properties and Intrinsic Strength of Monolayer Graphene. *Science (80-.).* **2008**, *321* (5887), 385–388.

(11) Morozov, S. V.; Novoselov, K. S.; Katsnelson, M. I.; Schedin, F.; Elias, D. C.; Jaszczak, J. A.; Geim, A. K. Giant Intrinsic Carrier Mobilities in Graphene and Its Bilayer. *Phys. Rev. Lett.* **2008**, *100* (1), 11–14.

(12) Neto, A. H. C.; Guinea, F.; Peres, N. M. R.; Novoselov, K. S.; Geim, A. K. The Electronic Properties of Graphene. **2007**, *81* (March).

(13) Nair, R. R.; Blake, P.; Grigorenko, A. N.; Novoselov, K. S.; Booth, T. J.; Stauber, T.; Peres, N. M. R.; Geim, A. K. Fine Structure Constant Defines Visual Transparency of Graphene. *Science (80-.).* **2008**, *320* (5881), 1308–1308.

(14) Wang, X.; Zhi, L.; Müllen, K. Transparent, Conductive Graphene Electrodes for Dye-Sensitized Solar Cells. *Nano Lett.* **2008**, *8* (1), 323–327.

(15) Matyba, P., Yamaguchi, H., Eda, G., Chhowalla, M., Edman, L. y Robinson, N. D. Graphene and Mobile Ions: The Key to All Plastic, Solution Processed Light Emitting Devices. *ACS Nano* **2010**, *4* (2), 637–642.

(16) Bae, S.; Kim, H.; Lee, Y.; Xu, X.; Park, J.-S.; Zheng, Y.; Balakrishnan, J.; Lei, T.; Kim, H. R.; Song, Y. Il; et al. Roll-to-Roll Production of 30-Inch Graphene Films for Transparent Electrodes. *Nat. Nanotechnol.* **2010**, *5* (August), 574–578.

(17) Balandin, A. A.; Ghosh, S.; Bao, W.; Calizo, I.; Teweldebrhan, D.; Miao, F.; Lau, C. N. Superior Thermal Conductivity of Single-Layer Graphene. *Nano Lett.* **2008**, *8* (3), 902–907.

(18) Ferrari, A. C.; Bonaccorso, F.; Falko, V.; Novoselov, K. S.; Roche, S.; Bøggild, P.; Borini, S.; Koppens, F.; Palermo, V.; Pugno, N.; et al. Science and Technology Roadmap for Graphene, Related Two-Dimensional Crystals, and Hybrid Systems. *Nanoscale* **2014**.

(19) Dresselhaus, M. S.; Jorio, A.; Saito, R. Characterizing Graphene, Graphite, and Carbon Nanotubes by Raman Spectroscopy. *Annu. Rev. Condens. Matter Phys.* **2010**, *1* (1), 89–108.

(20) Sato, K.; Saito, R.; Oyama, Y.; Jiang, J.; Cançado, L. G.; Pimenta, M. A.; Jorio, A.; Samsonidze, G. G.; Dresselhaus, G.; Dresselhaus, M. S. D-Band Raman Intensity of Graphitic Materials as a Function of Laser Energy and Crystallite Size. *Chem. Phys. Lett.* **2006**, *427* (1-3), 117–121.

(21) Ferrari, a. C.; Meyer, J. C.; Scardaci, V.; Casiraghi, C.; Lazzeri, M.; Mauri, F.; Piscanec, S.; Jiang, D.; Novoselov, K. S.; Roth, S.; et al. Raman Spectrum of Graphene and Graphene Layers. *Phys. Rev. Lett.* **2006**, *97* (18), 187401.

(22) Beams, R.; Gustavo Cançado, L.; Novotny, L. Raman Characterization of Defects and Dopants in Graphene. *J. Phys. Condens. Matter* **2015**, *27* (8), 083002.

(23) Maultzsch, J.; Telg, H.; Reich, S.; Thomsen, C. Radial Breathing Mode of Single-Walled Carbon Nanotubes: Optical Transition Energies and Chiral-

Index Assignment. *Phys. Rev. B - Condens. Matter Mater. Phys.* **2005**, *72* (20), 1–16.

(24) Pang, L. S. K.; Saxby, J. D.; Chatfield, S. P. Thermogravimetric Analysis of Carbon Nanotubes and Nanoparticles. *J. Phys. Chem.* **1993**, *97* (27), 6941–6942.

(25) Tressaud, A.; Moguet, F.; Flandrois, S.; Chambon, M.; Guimon, C.; Nanse, G.; Papirer, E.; Gupta, V.; Bahl, O. P. On the Nature of C-F Bonds in Various Fluorinated Carbon Materials: XPS and TEM Investigations. *J. Phys. Chem. Solids* **1996**, *57* (6-8), 745–751.

(26) Cuenot, S.; Frétigny, C.; Demoustier-Champagne, S.; Nysten, B. Surface Tension Effect on the Mechanical Properties of Nanomaterials Measured by Atomic Force Microscopy. *Phys. Rev. B* **2004**, *69* (16), 165410.

(27) Choi, W.; Lahiri, I.; Seelaboyina, R.; Kang, Y. S. Synthesis of Graphene and Its Applications: A Review. *Crit. Rev. Solid State Mater. Sci.* **2010**, *35* (1), 52–71.

(28) Zhu, Y.; Ji, H.; Cheng, H.-M.; Ruoff, R. S. Mass Production and Industrial Applications of Graphene Materials. *Natl. Sci. Rev.* **2017**, No. December, 1–12.

(29) Segal, M. Selling Graphene by the Ton. *Nat. Nanotechnol.* **2009**, *4* (10), 612–614.

(30) Noorden, B. R. Van. The Trials of New Carbon. **2011**.

(31) Alonso, J. M.; Díaz-Álvarez, A. E.; Criado, A.; Pérez, D.; Peña, D.; Guitián, E. Cloverphene: A Clover-Shaped Cata-Condensed Nanographene with Sixteen Fused Benzene Rings. *Angew. Chemie - Int. Ed.* **2012**, *51* (1), 173–177.

(32) Cheung, K. Y.; Chan, C. K.; Liu, Z.; Miao, Q. A Twisted Nanographene Consisting of 96 Carbon Atoms. *Angew. Chemie - Int. Ed.* **2017**, *56* (31), 9003–9007.

(33) Bonaccorso, F.; Lombardo, A.; Hasan, T.; Sun, Z.; Colombo, L.; Ferrari, A. C. Production and Processing of Graphene and 2d Crystals. *Mater. Today* **2012**, *15* (12), 564–589.

(34) Casiraghi, C.; Hartschuh, A.; Lidorikis, E.; Qian, H.; Harutyunyan, H.; Gokus, T.; Novoselov, K. S.; Ferrari, A. C. Rayleigh Imaging of Graphene and Graphene Layers. *Nano Lett.* **2007**, *7* (9), 2711–2717.

(35) Nicolosi, V.; Chhowalla, M.; Kanatzidis, M. G.; Strano, M. S.; Coleman, J. N. Liquid Exfoliation of Layered Materials. *Science (80-.).* **2013**, *340* (6139), 1226419–1226419.

(36) Ciesielski, A.; Samorì, P. Graphene via Sonication Assisted Liquid-Phase Exfoliation. *Chem. Soc. Rev.* **2014**, *43* (1), 381–398.

(37) Hernandez, Y.; Nicolosi, V.; Lotya, M.; Blighe, F. M.; Sun, Z.; De, S.; McGovern, I. T.; Holland, B.; Byrne, M.; Gun'Ko, Y. K.; et al. High-Yield Production of Graphene by Liquid-Phase Exfoliation of Graphite. *Nat. Nanotechnol.* **2008**, *3* (9), 563–568.

(38) Pokhrel, N.; Vabbina, P. K.; Pala, N. Sonochemistry: Science and Engineering. *Ultrason. Sonochem.* **2016**, *29*, 104–128.

(39) Bonaccorso, F.; Lombardo, A.; Hasan, T.; Sun, Z.; Colombo, L.; Ferrari, A. C. Production, Processing and Placement of Graphene and Two Dimensional Crystals. **2012**, 1–28.

(40) Bourlinos, A. B.; Georgakilas, V.; Zboril, R.; Sterioti, T. A.; Stubos, A. K. Liquid-Phase Exfoliation of Graphite Towards Solubilized Graphenes. *Small* **2009**, *5* (16), 1841–1845.

(41) Lotya, M.; King, P. J.; Khan, U.; De, S.; Coleman, J. N. High-Concentration, Surfactant- Stabilized Graphene Dispersions. *ACS Nano* **2010**, *4* (6), 3155–3162.

(42) Yi, M.; Shen, Z.; Ma, S.; Zhang, X. A Mixed-Solvent Strategy for Facile and Green Preparation of Graphene by Liquid-Phase Exfoliation of Graphite. *J. Nanoparticle Res.* **2012**, *14* (8).

(43) Torrisi, F.; Hasan, T.; Wu, W.; Sun, Z.; Lombardo, A.; Kulmala, T. S.; Hsieh, G. W.; Jung, S.; Bonaccorso, F.; Paul, P. J.; et al. Inkjet-Printed Graphene Electronics. *ACS Nano* **2012**, *6* (4), 2992–3006.

(44) Lotya, M.; Hernandez, Y.; King, P. J.; Smith, R. J.; Nicolosi, V.; Karlsson, L. S.; Blighe, M.; De, S.; Wang, Z.; Mcgovern, I. T.; et al. Liquid Phase Production of Graphene by Exfoliation of Graphite in Surfactant / Water Solutions Liquid Phase Production of Graphene by Exfoliation of Graphite in Surfactant / Water Solutions. **2009**, No. 11, 3611–3620.

(45) Kern, W.; Schnable, G. L. Low-Pressure Chemical Vapor Deposition for Very Large-Scale Integration Processing - A Review. *IEEE Trans Electron Devices* **1979**, *26*, 647.

(46) Coraux, J.; N'Diaye, A. T.; Busse, C.; Michely, T. Structural Coherency of Graphene on Ir(111). *Nano Lett.* **2008**, *8* (2), 565–570.

(47) Li, X.; Cai, W.; An, J.; Kim, S.; Nah, J.; Yang, D.; Piner, R.; Velamakanni, A.; Jung, I.; Tutuc, E.; et al. Large-Area Synthesis of High-Quality and Uniform Graphene Films on Copper Foils. *Science (80-.).* **2009**, *324* (5932), 1312–1314.

(48) Mattevi, C.; Kim, H.; Chhowalla, M. A Review of Chemical Vapour Deposition of Graphene on Copper. *J. Mater. Chem.* **2011**, *21* (10), 3324–3334.

(49) Li, X.; Magnuson, C. W.; Venugopal, A.; An, J.; Suk, J. W.; Han, B.; Borysiak, M.; Cai, W.; Velamakanni, A.; Zhu, Y.; et al. Graphene Films with Large Domain Size by a Two-Step Chemical Vapor Deposition Process. *Nano Lett.* **2010**, *10* (11), 4328–4334.

(50) Lin, M.-Y.; Guo, W.-C.; Wu, M.-H.; Wang, P.-Y.; Liu, T.-H.; Pao, C.-W.; Chang, C.-C.; Lee, S.-C.; Lin, S.-Y. Low-Temperature Grown Graphene Films by Using Molecular Beam Epitaxy. *Appl. Phys. Lett.* **2012**, *101* (22), 221911.

(51) Duhee Yoon, Young-Woo Son, H. C. Negative Thermal Expansion Coefficient of Graphene Measured by Raman Spectroscopy. *Nano Lett.* **2011**, *11*, 3227–3231.

(52) Li, X.; Cai, W.; Colombo, L.; Ruoff, R. S. Evolution of Graphene Growth on Ni and Cu by Carbon Isotope Labeling. *Nano Lett.* **2009**, *9* (12), 4268–4272.

(53) Peng, H.; Schröter, N. B. M.; Yin, J.; Wang, H.; Chung, T. F.; Yang, H.; Ekahana, S.; Liu, Z.; Jiang, J.; Yang, L.; et al. Substrate Doping Effect and Unusually Large Angle van Hove Singularity Evolution in Twisted Bi- and Multilayer Graphene. *Adv. Mater.* **2017**, *29* (27), 1–7.

(54) Criado, A.; Melchionna, M.; Marchesan, S.; Prato, M. The Covalent Functionalization of Graphene on Substrates Angewandte. **2015**, 10734–10750.

(55) Suk, J. W.; Kitt, A.; Magnuson, C. W.; Hao, Y.; Ahmed, S.; An, J.; Swan, A. K.; Goldberg, B. B.; Ruoff, R. S. Transfer of CVD-Grown Monolayer Graphene onto Arbitrary Substrates. *ACS Nano* **2011**, *5* (9), 6916–6924.

(56) Boscá, A.; Pedrós, J.; Martínez, J.; Palacios, T.; Calle, F. Automatic Graphene Transfer System for Improved Material Quality and Efficiency. *Sci. Rep.* **2016**, *6* (October 2015), 21676.

(57) Lee, S.; Lee, S. K.; Kang, C. G.; Cho, C.; Lee, Y. G.; Jung, U.; Lee, B. H. Graphene Transfer in Vacuum Yielding a High Quality Graphene. *Carbon N. Y.* **2015**, *93* (May), 286–294.

(58) Hallam, T.; Berner, N. C.; Yim, C.; Duesberg, G. S. Strain, Bubbles, Dirt, and Folds: A Study of Graphene Polymer-Assisted Transfer. *Adv. Mater. Interfaces* **2014**, *1* (6), 1–7.

(59) Mishra, N.; Boeckl, J.; Motta, N.; Iacopi, F. Graphene Growth on Silicon Carbide: A Review. *Phys. Status Solidi* **2016**, *213* (9), 2277–2289.

(60) Novoselov, K. S.; Fal'ko, V. I.; Colombo, L.; Gellert, P. R.; Schwab, M. G.; Kim, K. A Roadmap for Graphene. *Nature* **2012**, *490* (7419), 192–200.

(61) Hummers, W. S.; Offeman, R. E. Preparation of Graphitic Oxide. *J. Am. Chem. Soc.* **1958**, *80* (6), 1339.

(62) Pumera, M. Graphene in Biosensing. *Mater. Today* **2011**, *14* (7-8), 308–315.

(63) Gao, W. The Chemistry of Graphene Oxide. *Graphene Oxide Reduct. Recipes, Spectrosc. Appl.* **2015**, 61–95.

(64) Davies, T. J.; Hyde, M. E.; Compton, R. G. Nanotrench Arrays Reveal Insight into Graphite Electrochemistry. *Angew. Chemie - Int. Ed.* **2005**, *44* (32), 5121–5126.

(65) Rozada, R.; Paredes, J. I.; Villar-rodil, S.; Martínez-alonso, A.; Tascón, J. M. D. Towards Full Repair of Defects in Reduced Graphene Oxide Films by Two-Step Graphitization. **2013**, *6* (3), 216–233.

(66) Tkachev, S. V.; Buslaeva, E. Y.; Naumkin, A. V.; Kotova, S. L.; Laure, I. V.; Gubin, S. P. Reduced Graphene Oxide. *Inorg. Mater.* **2012**, *48* (8), 796–802.

(67) Lee, B. S.; Lee, Y.; Hwang, J. Y.; Choi, Y. C. Structural Properties of Reduced Graphene Oxides Prepared Using Various Reducing Agents. *Carbon Lett.* **2015**, *16* (4), 255–259.

(68) Chen, D.; Feng, H.; Li, J. Graphene Oxide : Preparation , Functionalization , and Electrochemical Applications. *Chem. Rev.* **2004**, *112*, 6027–6053.

(69) Wick, P.; Louw-Gaume, A. E.; Kucki, M.; Krug, H. F.; Kostarelos, K.; Fadeel, B.; Dawson, K. a.; Salvati, A.; Vázquez, E.; Ballerini, L.; et al. Classification Framework for Graphene-Based Materials. *Angew. Chemie Int. Ed.* **2014**, *53*, 2–7.

(70) Dhakate, S. R.; Chauhan, N.; Sharma, S.; Tawale, J.; Singh, S.; Sahare, P. D.; Mathur, R. B. An Approach to Produce Single and Double Layer Graphene from Re-Exfoliation of Expanded Graphite. *Carbon N. Y.* **2011**, *49* (6), 1946–1954.

(71) Ferrari, A. C.; Basko, D. M. Raman Spectroscopy as a Versatile Tool for Studying the Properties of Graphene. *Nat. Nanotechnol.* **2013**, *8* (4), 235–246.

(72) Obraztsov, P. A.; Rybin, M. G.; Tyurnina, A. V.; Garnov, S. V.; Obraztsova, E. D.; Obraztsov, A. N.; Svirko, Y. P. Broadband Light-Induced Absorbance Change in Multilayer Graphene. *Nano Lett.* **2011**, *11* (4), 1540–1545.

(73) Gao, W.; Alemany, L. B.; Ci, L.; Ajayan, P. M. New Insights into the Structure and Reduction of Graphite Oxide. *Nat. Chem.* **2009**, *1* (5), 403–408.

(74) Dreyer, D. R.; Park, S.; Bielawski, C. W.; Ruoff, R. S. The Chemistry of Graphene Oxide. *Chem. Soc. Rev.* **2010**, *39* (1), 228–240.

(75) Wang, J.; Wang, Y.; He, D.; Liu, Z.; Wu, H.; Wang, H.; Zhao, Y.; Zhang, H.; Yang, B.; Xu, H.; et al. Direct Synthesis of Hydrophobic Graphene-Based Nanosheets via Chemical Modification of Exfoliated Graphene Oxide. *J. Nanosci. Nanotechnol.* **2012**, *12* (8), 6460–6466.

(76) Paredes, J. I.; Villar-Rodil, S.; Solís-Fernández, P.; Martínez-Alonso, A.; Tascón, J. M. D. Atomic Force and Scanning Tunneling Microscopy Imaging of Graphene Nanosheets Derived from Graphite Oxide. *Langmuir* **2009**, *25* (10), 5957–5968.

(77) Georgakilas, V.; Otyepka, M.; Bourlinos, A. B.; Chandra, V.; Kim, N.; Kemp, K. C.; Hobza, P.; Zboril, R.; Kim, K. S. Functionalization of Graphene: Covalent and Non-Covalent Approaches, Derivatives and Applications. *Chem. Rev.* **2012**, *112* (11), 6156–6214.

(78) Loh, K. P.; Bao, Q.; Ang, P. K.; Yang, J. The Chemistry of Graphene. *J. Mater. Chem.* **2010**, *20* (12), 2277.

(79) Paulus, G. L. C.; Wang, Q. H.; Strano, M. S. Covalent Electron Transfer Chemistry of Graphene with Diazonium Salts. *Acc. Chem. Res.* **2013**, *46* (1), 160–170.

(80) Dyke, C. A.; Stewart, M. P.; Maya, F.; Tour, J. M. Diazonium-Based Functionalization of Carbon Nanotubes: XPS and GC-MS Analysis and Mechanistic Implications. *Synlett* **2004**, No. 1, 155–160.

(81) Niyogi, S.; Bekyarova, E.; Itkis, M. E.; Zhang, H.; Shepperd, K.; Hicks, J.; Sprinkle, M.; Berger, C.; Lau, C. N.; Deheer, W. A.; et al. Spectroscopy of Covalently Functionalized Graphene. *Nano Lett.* **2010**, *10* (10), 4061–4066.

(82) Sharma, R.; Baik, J. H.; Perera, C. J.; Strano, M. S. Anomalously Large Reactivity of Single Graphene Layers and Edges toward Electron Transfer Chemistries. *Nano Lett.* **2010**, *10* (2), 398–405.

(83) D. Bouša a, M. Pumera b, D. Sedmidubský a, J. Šturala c, J. Luxa a, V. M. a and Z. S. a. Fine Tuning of Graphene Properties Using Modification with Aryl Halogens. *Nanoscale* **2013**, 1–3.

(84) Cinti, S.; Arduini, F. Graphene-Based Screen-Printed Electrochemical (bio)sensors and Their Applications: Efforts and Criticisms. *Biosensors and Bioelectronics*. 2017.

(85) Pumera, M.; Ambrosi, A.; Bonanni, A.; Chng, E. L. K.; Poh, H. L. Graphene for Electrochemical Sensing and Biosensing. *TrAC - Trends Anal. Chem.* **2010**, *29* (9), 954–965.

(86) Yang, M.; Wang, C.; Wei, Q.; Du, B.; Li, H.; Qian, Z. Functionalized Graphene for Biosensing Applications. *Biosens. Nanomater.* **2011**, No. i, 221–235.

(87) Georgakilas, V.; Bourlinos, A. B.; Zboril, R.; Steriotis, T. a; Dallas, P.; Stubos, A. K.; Trapalis, C. Organic Functionalisation of Graphenes. *Chem. Commun. (Camb).* **2010**, *46* (10), 1766–1768.

(88) Quintana, M.; Spyrou, K.; Grzelczak, M.; Browne, W. R.; Rudolf, P.; Prato, M. Functionalization of Graphene via 1,3- Dipolar Cycloaddition. *ACS Nano* **2010**, *4* (6), 3527–3533.

(89) Quintana, M.; Spyrou, K.; Grzelczak, M.; Browne, W. R.; Rudolf, P.; Prato, M. Functionalization of Graphene via 1,3- Dipolar Cycloaddition. *ACS Nano* **2010**, *4* (6), 3527–3533.

(90) Sarkar, S.; Bekyarova, E.; Niyogi, S.; Haddon, R. C. Diels-Alder Chemistry of Graphite and Graphene: Graphene as Diene and Dienophile. *J. Am. Chem. Soc.* **2011**, *133* (10), 3324–3327.

(91) Hoke, S. H.; Molstad, J.; Dilettato, D.; Jay, M. J.; Carlson, D.; Kahr, B.; Cooks, R. G. Reaction of Fullerenes and Benzyne. *J. Org. Chem.* **1992**, *57* (9), 5069–5071.

(92) Criado, A.; Vizuete, M.; Gómez-Escalonilla, M. J.; García-Rodriguez, S.; Fierro, J. L. G.; Cobas, A.; Peña, D.; Guitián, E.; Langa, F. Efficient Cycloaddition of Arynes to Carbon Nanotubes under Microwave Irradiation. *Carbon N. Y.* **2013**, *63*, 140–148.

(93) Criado, A.; Gómez-Escalonilla, M. J.; Fierro, J. L. G.; Urbina, A.; Peña, D.; Guitián, E.; Langa, F. Cycloaddition of Benzyne to SWCNT: Towards CNT-Based Paddle Wheels. *Chem. Commun. (Camb).* **2010**, *46* (37), 7028–7030.

(94) Chronopoulos, D.; Karousis, N.; Ichihashi, T.; Yudasaka, M.; Iijima, S.; Tagmatarchis, N. Benzyne Cycloaddition onto Carbon Nanohorns. *Nanoscale* **2013**, *5* (14), 6388–6394.

(95) Zhong, X.; Jin, J.; Li, S.; Niu, Z.; Hu, W.; Li, R.; Ma, J. Aryne Cycloaddition: Highly Efficient Chemical Modification of Graphene. *Chem. Commun. (Camb).* **2010**, *46* (39), 7340–7342.

(96) Yang, T.; Zhao, X.; Nagase, S. Cycloaddition of Benzyne to Armchair Single-Walled Carbon Nanotubes: [2 + 2] or [4 + 2]? *Org. Lett.* **2013**, *15* (23), 5960–5963.

(97) Martínez, J. P.; Langa, F.; Matthias Bickelhaupt, F.; Osuna, S.; Solá, M. (4 + 2) and (2 + 2) Cycloadditions of Benzyne to C60 and Zig-Zag Single-Walled Carbon Nanotubes: The Effect of the Curvature. *J. Phys. Chem. C* **2016**, *120* (3), 1716–1726.

(98) Hammouri, M.; Jha, S. K.; Vasiliev, I. First-Principles Study of Graphene and Carbon Nanotubes Functionalized with Benzyne. *J. Phys. Chem. C* **2015**, *119*, 18719–18728.

(99) Denis, P. a.; Iribarne, F. [2 + 2] Cycloadditions onto Graphene. *J. Mater. Chem.* **2012**, *22* (12), 5470–5477.

(100) Zhao, J.; Wang, H.; Gao, B.; Wang, X.; Cai, Q.; Wang, X. Chemical Functionalization of Graphene via Aryne Cycloaddition: A Theoretical Study. *J. Mol. Model.* **2012**, *18* (6), 2861–2868.

(101) Cao, Y.; Osuna, S.; Liang, Y.; Haddon, R. C.; Houk, K. N. Diels-Alder Reactions of Graphene: Computational Predictions of Prodcuts and Sites of Reactions. *J. Am. Chem. Soc.* **2013**.

(102) Denis, P. A. Organic Chemistry of Graphene: The Diels-Alder Reaction. *Chem. - A Eur. J.* **2013**, *19* (46), 15719–15725.

(103) Daukiya, L.; Mattioli, C.; Aubel, D.; Hajjar-Garreau, S.; Vonau, F.; Denys, E.; Reiter, G.; Fransson, J.; Perrin, E.; Bocquet, M.-L.; et al. Covalent Functionalization by Cycloaddition Reactions of Pristine Defect-Free Graphene. *ACS Nano* **2017**, acsnano.6b06913.

(104) García, D.; Rodriguez, L.; Herranz, M. A.; Peña, D.; Guitian, E.; Bailey, S.; Al-Galiby, Q.; Noori, M.; Lambert, C.; Perez, D.; et al. A C60-Aryne Building Block: Synthesis of a Hybrid All-Carbon Nanostructure. *Chem. Commun.* **2016**.

(105) Magedov, I. V; Frolova, L. V; Ovezmyradov, M.; Bethke, D.; Shaner, E. a; Kalugin, N. G. Benzyne-Functionalized Graphene and Graphite Characterized by Raman Spectroscopy and Energy Dispersive X-Ray Analysis. *Carbon N. Y.* **2013**, *54* (Cvd), 192–200.

(106) Lim, C. X.; Hoh, H. Y.; Ang, P. K.; Loh, K. P. Direct Voltammetric Detection of DNA and pH Sensing on Epitaxial Graphene: An Insight into the Role of Oxygenated Defects. *Anal. Chem.* **2010**, *82* (17), 7387–7393.

(107) Jung, J. H.; Cheon, D. S.; Liu, F.; Lee, K. B.; Seo, T. S. A Graphene Oxide Based Immuno-Biosensor for Pathogen Detection. *Angew. Chemie Int. Ed.* **2010**, *49* (33), 5708–5711.

(108) Xu, Y.; Bai, H.; Lu, G.; Li, C.; Shi, G. Flexible Graphene Films via the Filtration of Water-Soluble. **2008**, 5856–5857.

(109) An, X.; Butler, T. W.; Washington, M.; Nayak, S. K.; Kar, S. Optical and Sensing Properties of 1-Pyrenecarboxylic Acid-Functionalised Graphene Films Laminated on Polydimethylsiloxane Membranes. *ACS Nano* **2011**, *5* (2), 1003–1011.

(110) Kodali, V. K.; Scrimgeour, J.; Kim, S.; Hankinson, J. H.; Carroll, K. M.; De Heer, W. A.; Berger, C.; Curtis, J. E. Nonperturbative Chemical Modification of Graphene for Protein Micropatterning. *Langmuir* **2011**, *27* (3), 863–865.

(111) Güryel, S.; Alonso, M.; Hajgató, B.; Dauphin, Y.; Van Lier, G.; Geerlings, P.; De Proft, F. A Computational Study on the Role of Noncovalent Interactions in the Stability of Polymer/graphene Nanocomposites. *J. Mol. Model.* **2017**, *23* (2).

(112) Quintana, M.; Vazquez, E.; Prato, M. Organic Functionalization of Graphene in Dispersions. *Acc. Chem. Res.* **2013**, *46* (1), 138–148.

(113) Vázquez, E.; Giacalone, F.; Prato, M. Non-Conventional Methods and Media for the Activation and Manipulation of Carbon Nanoforms. *Chem. Soc. Rev.* **2014**, *43* (1), 58–69.

(114) Liu, H.; Ryu, S.; Chen, Z.; Steigerwald, M. L.; Nuckolls, C.; Brus, L. E. Photochemical Reactivity of Graphene. **2009**, 17099–17101.

(115) Chen, M.; Pekker, A.; Li, W.; Itkis, M. E.; Haddon, R. C.; Bekyarova, E. Organometallic Chemistry of Graphene: Photochemical Complexation of Graphene with Group 6 Transition Metals. *Carbon N. Y.* **2018**, *129*, 450–455.

(116) Englert, J. M.; Dotzer, C.; Yang, G.; Schmid, M.; Papp, C.; Gottfried, J. M.; Steinrück, H.-P.; Spiecker, E.; Hauke, F.; Hirsch, A. Covalent Bulk Functionalization of Graphene. *Nat. Chem.* **2011**, *3* (4), 279–286.

(117) Abellán, G.; Schirowski, M.; Edelthalhammer, K. F.; Fickert, M.; Werbach, K.; Peterlik, H.; Hauke, F.; Hirsch, A. Unifying Principles of the Reductive Covalent Graphene Functionalization. *J. Am. Chem. Soc.* **2017**, *139* (14), 5175–5182.

(118) Rubio, N.; Fabbro, C.; Herrero, M. A.; Hoz, A. De; Meneghetti, M.; Fierro, J. L. G.; Prato, M.; Vázquez, E. Ball-Milling Modifi Cation of Single-Walled Carbon Nanotubes : Purifi Cation , Cutting , and Functionalization. **2011**, 665–674.

(119) Chem, J. M.; Wu, H.; Zhao, W.; Hu, H.; Chen, G. One-Step in Situ Ball Milling Synthesis of Polymer-Functionalized Graphene Nanocomposites. **2011**, 8626–8632.

(120) Martins, M. A. P.; Frizzo, C. P.; Moreira, D. N.; Buriol, L.; Machado, P. Solvent-Free Heterocyclic Synthesis. *Chem. Rev.* **2009**, *109* (9), 4140–4182.

(121) Tanaka, K.; Toda, F. Solvent-Free Organic Synthesis. *Chem. Rev.* **2000**, *100*, 1025–1074.

(122) Seo, J.-M.; Baek, J.-B. A Solvent-Free Diels–Alder Reaction of Graphite into Functionalized Graphene Nanosheets. *Chem. Commun.* **2014**, *50* (93), 14651–14653.

(123) Li, Z.; Chen, F. Ion Beam Modification of Two-Dimensional Materials: Characterization, Properties, and Applications. *Appl. Phys. Rev.* **2017**, *4* (1).

(124) Kumar, S.; Tripathi, A.; Singh, F.; Khan, S. A.; Baranwal, V.; Avasthi, D. K. Purification/annealing of Graphene with 100-MeV Ag Ion Irradiation. *Nanoscale Res. Lett.* **2014**, *9* (1), 1–9.

(125) Willke, P.; Amani, J. A.; Thakur, S.; Weikert, S.; Druga, T.; Maiti, K.; Hofsäss, H.; Wenderoth, M. Short-Range Ordering of Ion-Implanted Nitrogen Atoms in SiC-Graphene. *Appl. Phys. Lett.* **2014**, *105* (11).

(126) Kaushik, P. D.; Ivanov, I. G.; Lin, P. C.; Kaur, G.; Eriksson, J.; Lakshmi, G. B. V. S.; Avasthi, D. K.; Gupta, V.; Aziz, A.; Siddiqui, A. M.; et al. Surface Functionalization of Epitaxial Graphene on SiC by Ion Irradiation for Gas Sensing Application. *Appl. Surf. Sci.* **2017**, *403*, 707–716.

(127) Nourbakhsh, A.; Cantoro, M.; Vosch, T.; Pourtois, G.; Clemente, F.; Van Der Veen, M. H.; Hofkens, J.; Heyns, M. M.; De Gendt, S.; Sels, B. F. Bandgap Opening in Oxygen Plasma-Treated Graphene. *Nanotechnology* **2010**, *21* (43).

(128) Xie, L.; Jiao, L.; Dai, H. Selective Etching of Graphene Edges by Hydrogen Plasma. *J. Am. Chem. Soc.* **2010**, *132* (42), 14751–14753.

(129) Walton, S. G.; Foley, B. M.; Hernández, S. C.; Boris, D. R.; Baraket, M.; Duda, J. C.; Robinson, J. T.; Hopkins, P. E. Plasma-Based Chemical Functionalization of Graphene to Control the Thermal Transport at Graphene-Metal Interfaces. *Surf. Coatings Technol.* **2017**, *314*, 148–154.

(130) Huang, W.; Ptasinska, S. Functionalization of Graphene by Atmospheric Pressure Plasma Jet in Air or H2O2environments. *Appl. Surf. Sci.* **2016**, *367*, 160–166.

(131) Gawande, M. B.; Shelke, S. N.; Zboril, R.; Varma, R. S. Microwave-Assisted Chemistry: Synthetic Applications for Rapid Assembly of Nanomaterials and Organics. *Acc. Chem. Res.* **2014**, *47* (4), 1338–1348.

(132) Cho, H. Y.; Ajaz, A.; Himali, D.; Waske, P. a; Johnson, R. P. Microwave Flash Pyrolysis. *J. Org. Chem.* **2009**, *74* (11), 4137–4142.

(133) Kim, N. D.; Metzger, A.; Hejazi, V.; Li, Y.; Kovalchuk, A.; Lee, S. K.; Ye, R.; Mann, J. A.; Kittrell, C.; Shahsavari, R.; et al. Microwave Heating of Functionalized Graphene Nanoribbons in Thermoset Polymers for Wellbore Reinforcement. *ACS Appl. Mater. Interfaces* **2016**, *8* (20), 12985–12991.

(134) Naeimi, H.; Golestanzadeh, M. Microwave-Assisted Synthesis of 6,6-(aryl(alkyl)methylene)bis(2,4-Dialkylphenol) Antioxidants Catalyzed by

Multi Sulfonated Reduced Graphene Oxide Nanosheets in Water. *New J. Chem.* **2015**.

(135) Shulga, Y. M.; Baskakov, S. a; Knerelman, E. I.; Davidova, G. I.; Badamshina, E. R.; Shulga, N. Y.; Skryleva, E. a; Agapov, a L.; Voylov, D. N.; Sokolov, a P.; et al. Carbon Nanomaterial Produced by Microwave Exfoliation of Graphite Oxide: New Insights. *Rsc Adv.* **2014**, *4*, 587–592.

(136) Matsumoto, M.; Saito, Y.; Park, C.; Fukushima, T.; Aida, T. Ultrahigh-Throughput Exfoliation of Graphite into Pristine "single-Layer" Graphene Using Microwaves and Molecularly Engineered Ionic Liquids. *Nat. Chem.* **2015**, *7* (9), 730–736.

(137) Navarro, J. J.; Leret, S.; Calleja, F.; Stradi, D.; Black, A.; Bernardo-Gavito, R.; Garnica, M.; Granados, D.; Vázquez De Parga, A. L.; Pérez, E. M.; et al. Organic Covalent Patterning of Nanostructured Graphene with Selectivity at the Atomic Level. *Nano Lett.* **2016**, *16* (1), 355–361.

(138) Navarro, J. J.; Calleja, F.; Miranda, R.; Perez, E. M.; Vazquez De Parga, A. L. High Yielding and Extremely Site-Selective Covalent Functionalization of Graphene. *Chem. Commun.* **2017**, 10418–10421.

(139) Kyhl, L.; Bisson, R.; Balog, R.; Groves, M. N.; Kolsbjerg, E. L.; Cassidy, A. M.; Jørgensen, J. H.; Halkjær, S.; Miwa, J. A.; Grubišić Čabo, A.; et al. Exciting H 2 Molecules for Graphene Functionalization. *ACS Nano* **2018**, acsnano.7b07079.

(140) Cheng, C.; Li, S.; Thomas, A.; Kotov, N. A.; Haag, R. Functional Graphene Nanomaterials Based Architectures: Biointeractions, Fabrications, and Emerging Biological Applications. *Chem. Rev.* **2017**, acs.chemrev.6b00520.

(141) Reina, G.; González-Domínguez, J. M.; Criado, A.; Vázquez, E.; Bianco, A.; Prato, M. Promises, Facts and Challenges for Graphene in Biomedical Applications. *Chem. Soc. Rev.* **2017**, 4400–4416.

(142) Eigler, S.; Hirsch, A. Chemistry with Graphene and Graphene Oxide-Challenges for Synthetic Chemists. *Angew. Chemie Int. Ed.* **2014**, *53* (30), 7720–7738.

(143) Georgakilas, V.; Tiwari, J. N.; Kemp, K. C.; Perman, J. A.; Bourlinos, A. B.; Kim, K. S.; Zboril, R. Noncovalent Functionalization of Graphene and Graphene Oxide for Energy Materials, Biosensing, Catalytic, and Biomedical Applications. *Chem. Rev.* **2016**, *116* (9), 5464–5519.

(144) Singh, M.; Holzinger, M.; Tabrizian, M.; Winters, S.; Berner, N. C.; Cosnier, S.; Duesberg, G. S. Noncovalently Functionalized Monolayer Graphene for Sensitivity Enhancement of Surface Plasmon Resonance Immunosensors. *J. Am. Chem. Soc.* **2015**, *137* (8), 2800–2803.

(145) Schneider, G. F.; Xu, Q.; Hage, S.; Luik, S.; Spoor, J. N. H.; Malladi, S.; Zandbergen, H.; Dekker, C. Tailoring the Hydrophobicity of Graphene for Its Use as Nanopores for DNA Translocation. *Nat. Commun.* **2013**, *4*, 2619.

(146) Kang, P.; Wang, M. C.; Nam, S. Bioelectronics with Two-Dimensional Materials. *Microelectron. Eng.* **2016**, *161*, 18–35.

(147) Guo, Y.; Han, Y.; Guo, Y.; Dong, C. Graphene-Orange II Composite Nanosheets with Electroactive Functions as Label-Free Aptasensing Platform for "Signal-on" Detection of Protein. *Biosens. Bioelectron.* **2013**, *45* (1), 95–101.

(148) Tiwari, J. N.; Vij, V.; Kemp, K. C.; Kim, K. S. Engineered Carbon-Nanomaterial-Based Electrochemical Sensors for Biomolecules. *ACS Nano* **2016**, *10* (1), 46–80.

(149) Cai, B.; Huang, L.; Zhang, H.; Sun, Z.; Zhang, Z.; Zhang, G. J. Gold Nanoparticles-Decorated Graphene Field-Effect Transistor Biosensor for Femtomolar MicroRNA Detection. *Biosens. Bioelectron.* **2015**, *74*, 329–334.

(150) Mijowska, E.; Onyszko, M.; Urbas, K.; Aleksandrzak, M.; Shi, X.; Moszyński, D.; Penkala, K.; Podolski, J.; El Fray, M. Palladium Nanoparticles Deposited on Graphene and Its Electrochemical Performance for Glucose Sensing. *Appl. Surf. Sci.* **2015**, *355*, 587–592.

(151) Ambrosi, A.; Chua, C. K.; Latiff, N. M.; Loo, A. H.; Wong, C. H. A.; Eng, A. Y. S.; Bonanni, A.; Pumera, M. Graphene and Its Electrochemistry – an Update. *Chem. Soc. Rev.* **2016**, *45* (9), 2458–2493.

(152) Xu, G.; Abbott, J.; Qin, L.; Yeung, K. Y. M.; Song, Y.; Yoon, H.; Kong, J.; Ham, D. Electrophoretic and Field-Effect Graphene for All-Electrical DNA Array Technology. *Nat. Commun.* **2014**, *5*, 4866.

(153) Graybill, R. M.; Bailey, R. C. Emerging Biosensing Approaches for microRNA Analysis. *Anal. Chem.* **2016**, *88* (1), 431–450.

(154) Loo, A. H.; Bonanni, A.; Pumera, M. An Insight into the Hybridization Mechanism of Hairpin DNA Physically Immobilized on Chemically Modified Graphenes. *Analyst* **2013**, *138*, 467–471.

(155) Loo, A. H.; Ambrosi, A.; Bonanni, A.; Pumera, M. CVD Graphene Based Immunosensor. *Rsc Adv.* **2014**, *4* (46), 23952–23956.

(156) Jung, H. S.; Lee, T.; Kwon, I. K.; Kim, H. S.; Hahn, S. K.; Lee, C. S. Surface Modification of Multipass Caliber-Rolled Ti Alloy with Dexamethasone-Loaded Graphene for Dental Applications. *ACS Appl. Mater. Interfaces* **2015**, *7* (18), 9598–9607.

(157) La, W.-G.; Jin, M.; Park, S.; Yoon, H.-H.; Jeong, G.-J.; Bhang, S. H.; Park, H.; Char, K.; Kim, B.-S. Delivery of Bone Morphogenetic Protein-2 and Substance P Using Graphene Oxide for Bone Regeneration. *Int. J. Nanomedicine* **2014**, *9 Suppl 1* (SUPPL.1), 107–116.

(158) Dong, H. S.; Qi, S. J. Realising the Potential of Graphene-Based Materials for Biosurfaces – A Future Perspective. *Biosurface and Biotribology* **2015**, *1* (4), 229–248.

(159) Criado, A.; Melchionna, M.; Marchesan, S.; Prato, M. The Covalent Functionalization of Graphene on Substrates. *Angew. Chemie Int. Ed.* **2015**, n/a – n/a.

(160) Itkis, M. E.; Wang, F.; Ramesh, P.; Bekyarova, E.; Niyogi, S.; Chi, X.; Berger, C.; de Heer, W. a.; Haddon, R. C. Enhanced Photosensitivity of Electro-Oxidized Epitaxial Graphene. *Appl. Phys. Lett.* **2011**, *98* (9), 093115.

(161) Hossain, M. Z.; Johns, J. E.; Bevan, K. H.; Karmel, H. J.; Liang, Y. T.; Yoshimoto, S.; Mukai, K.; Koitaya, T.; Yoshinobu, J.; Kawai, M.; et al. Chemically Homogeneous and Thermally Reversible Oxidation of Epitaxial Graphene. *Nat. Chem.* **2012**, *4* (4), 305–309.

(162) Hernández, S. C.; Wheeler, V. D.; Osofsky, M. S.; Jernigan, G. G.; Nagareddy, V. K.; Nath, a.; Lock, E. H.; Nyakiti, L. O.; Myers-Ward, R. L.; Sridhara, K.; et al. Plasma-Based Chemical Modification of Epitaxial Graphene with Oxygen Functionalities. *Surf. Coatings Technol.* **2014**, *241*, 8–12.

(163) Lerner, M. B.; Matsunaga, F.; Han, G. H.; Hong, S. J.; Xi, J.; Crook, A.; Perez-Aguilar, J. M.; Park, Y. W.; Saven, J. G.; Liu, R.; et al. Scalable Production of Highly Sensitive Nanosensors Based on Graphene Functionalized with a Designed G Protein-Coupled Receptor. *Nano Lett.* **2014**, *14* (5), 2709–2714.

(164) Eissa, S.; Jimenez, G. C.; Mahvash, F.; Guermoune, A.; Tlili, C.; Szkopek, T.; Zourob, M.; Siaj, M. Functionalized CVD Monolayer Graphene for Label-Free Impedimetric Biosensing. *Nano Res.* **2015**, *8* (5), 1698–1709.

(165) Hess, L. H.; Lyuleeva, A.; Blaschke, B. M.; Sachsenhauser, M.; Seifert, M.; Garrido, J. A.; Coulombwall, A. Graphene Transistors with Multifunctional Polymer Brushes for Biosensing Applications. *ACS Appl. Mater. Interfaces* **2014**, *6*, 9705–9710.

(166) Huisgen, R.; König, H.; Lepley, A. R. Nucleophile Aromatische Substitutionen, XVIII. Neue Ringschl??sse ??ber Arine. *Chem. Ber.* **1960**, *93* (7), 1496–1506.

(167) Scheiner, A. C.; Schaefer, H. F.; Liu, B. The x˜1A1 and ã3B2States of O-Benzyne: A Theoretical Characterization of Equilibrium Geometries, Harmonic Vibrational Frequencies, and the Singlet-Triplet Energy Gap. *J. Am. Chem. Soc.* **1989**, *111* (9), 3118–3124.

(168) Warmuth, R. O-Benzyne: Strained Alkyne or Cumulene?—NMR Characterization in a Molecular Container. *Angew. Chemie Int. Ed. English* **1997**, *36* (12), 1347–1350.

(169) Roberts, J. D.; Simmons, H. E.; Carlsmith, L. A.; Vaughan, C. W. REARRANGEMENT IN THE REACTION OF CHLOROBENZENE-1-C ^{14} WITH POTASSIUM AMIDE ^{1}. *J. Am. Chem. Soc.* **1953**, *75* (13), 3290–3291.

(170) Peña, D.; Cobas, A.; Pérez, D.; Guitián, E. An Efficient Procedure for the Synthesis of Ortho -Trialkylsilylaryl Triflates: Easy Access to Precursors of Functionalized Arynes. *Synthesis (Stuttg).* **2002**, No. 10, 1454–1458.

(171) Pérez, D.; Peña, D.; Guitián, E. Aryne Cycloaddition Reactions in the Synthesis of Large Polycyclic Aromatic Compounds. *European J. Org. Chem.* **2013**, No. 27, 5981–6013.

(172) Heaney, H. The Benzyne and Related Intermediates. *Chem. Rev.* **1962**, *62* (2), 81–97.

(173) Haberfield, P.; Seif, L. The Selectivity of Benzyne. A New Approach Using the Reaction of Benzyne with Ambident Nucleophiles. *J. Org. Chem.* **1969**, *34* (5), 1508–1510.

(174) Wittig, G.; Hoffmann. W, R. Uber Die Reversibilitat Der Dehydrobenzol-Bildung Am O-Metallierten Aryhalogeniden. *Chem. Ber.* **1962**, *95*, 2729–2734.

(175) Okuma, K.; Nojima, A.; Matsunaga, N.; Shioji, K. Reaction of Benzyne with Salicylaldehydes: General Synthesis of Xanthenes, Xanthones, and Xanthols. *Org. Lett.* **2009**, *11* (1), 169–171.

(176) Beltrán-Rodil, S.; Peña, D.; Guitián, E. Reaction of Benzyne with Styrene Oxide: Insertion of Arynes into a C-O Bond of Epoxides. *Synlett* **2007**, No. 8, 1308–1310.

(177) Wittig, G.; Pohmer, L. Intermediäre Bildung von Dehydrobenzol (Cyclohexa-Dienin). *Angew. Chem.* **1955**, *67* (13), 348–348.

(178) Hoffmann, R.; Woodward, R. B. The Conservation of Orbital Symmetry. *Acc. Chem. Res.* **1968**, *1* (1), 17–22.

(179) Kivrak, A.; Larock, R. C. Synthesis of Dihydrobenzisoxazoles by the [3 + 2] Cycloaddition of Arynes and Oxaziridines. *J. Org. Chem.* **2010**, *75* (21), 7381–7387.

(180) Fort, E. H.; Scott, L. T. Gas-Phase Diels-Alder Cycloaddition of Benzyne to an Aromatic Hydrocarbon Bay Region: Groundwork for the Selective Solvent-Free Growth of Armchair Carbon Nanotubes. *Tetrahedron Lett.* **2011**, *52* (17), 2051–2053.

(181) Miller, R. G.; Stiles, M. Reaction of Benzyne with Benzene and Naphthalene. *J. Am. Chem. Soc.* **1963**, *85* (12), 1798–1800.

(182) Friedman, L.; Logullo, F. M. **Benzynes** *via* **Aprotic Diazotization of Anthranilic Acids: A Convenient Synthesis of Triptycene and Derivatives** . *J. Am. Chem. Soc.* **1963**, *85* (10), 1549–1549.

(183) Hamilton, C. E.; Lomeda, J. R.; Sun, Z.; Tour, J. M.; Barron, A. R. High-Yield Organic Dispersions of Unfunctionalized Graphene. *Nano Lett.* **2009**, *9* (10), 3460–3462.

(184) Marcano, D. C.; Kosynkin, D. V; Berlin, J. M.; Sinitskii, A.; Sun, Z.; Slesarev, A.; Alemany, L. B.; Lu, W.; Tour, J. M. Improved Synthesis of Graphene Oxide. *ACS Nano* **2010**, *4* (8), 4806–4814.

(185) Stankovich, S.; Dikin, D. A.; Piner, R. D.; Kohlhaas, K. A.; Kleinhammes, A.; Jia, Y.; Wu, Y.; Nguyen, S. B. T.; Ruoff, R. S. Synthesis of Graphene-Based Nanosheets via Chemical Reduction of Exfoliated Graphite Oxide. *Carbon N. Y.* **2007**, *45* (7), 1558–1565.

(186) Jung, I. Y.; Lee, E. H.; Suh, A. Y.; Lee, S. J.; Lee, H. Oligonucleotide-Based Biosensors for in Vitro Diagnostics and Environmental Hazard Detection. *Anal. Bioanal. Chem.* **2016**, *408* (10), 2383–2406.

(187) Pumera, M.; Hong, C.; Wong, A.; Yong, A.; Eng, S.; Bonanni, A. Graphene and Its Electrochemistry – an Update. *Chem. Soc. Rev.* **2016**, *45* (9), 2458–2493.

(188) Gan, L.; Zhang, D.; Guo, X. Electrochemistry: An Efficient Way to Chemically Modify Individual Monolayers of Graphene. *Small* **2012**, *8* (9), 1326–1330.

(189) Rowley-Neale, S. J.; Brownson, D. A. C.; Banks, C. E. Defining the Origins of Electron Transfer at Screen-Printed Graphene-like and Graphite Electrodes: MoO 2 Nanowire Fabrication on Edge Plane Sites Reveals Electrochemical Insights. *Nanoscale* **2016**, *8* (33), 15241–15251.

(190) Minami, T. Substitution of Transparent Conducting Oxide Thin Films for Indium Tin Oxide Transparent Electrode Applications. *Thin Solid Films* **2008**, *516* (7), 1314–1321.

(191) Ambrosi, A.; Chua, C. K.; Bonanni, A.; Pumera, M. Electrochemistry of Graphene and Related Materials. *Chem. Rev.* **2014**.

(192) Zhou, M.; Zhai, Y.; Dong, S. Electrochemical Sensing and Biosensing Platform Based on Chemically Reduced Graphene Oxide. *Anal. Chem.* **2009**, *81* (14), 5603–5613.

(193) Greenwood, J.; Phan, T. H.; Fujita, Y.; Li, Z.; Ivasenko, O.; Vanderlinden, W.; Van Gorp, H.; Frederickx, W.; Lu, G.; Tahara, K.; et al. Covalent Modification of Graphene and Graphite Using Diazonium Chemistry: Tunable Grafting and Nanomanipulation. *ACS Nano* **2015**, *9* (5), 5520–5535.

(194) FITKO, A. R. and C. Polymer Formation through Diazonium Coupling. **1964**, *2* (September 1962), 1925–1940.

(195) Zhao, G.; Li, X.; Huang, M.; Zhen, Z.; Zhong, Y.; Chen, Q.; Zhao, X.; He, Y.; Hu, R.; Yang, T.; et al. The Physics and Chemistry of Graphene-on-Surfaces. *Chem. Soc. Rev.* **2017**, *46* (15), 4417–4449.

(196) Wintterlin, J.; Bocquet, M. L. Graphene on Metal Surfaces. *Surf. Sci.* **2009**, *603* (10-12), 1841–1852.

(197) Batzill, M. The Surface Science of Graphene: Metal Interfaces, CVD Synthesis, Nanoribbons, Chemical Modifications, and Defects. *Surf. Sci. Rep.* **2012**, *67* (3-4), 83–115.

(198) Li, X.; Zhu, H. The Graphene-Semiconductor Schottky Junction. *Phys. Today* **2016**, *69* (9), 46–51.

(199) Yang, Y.; Brenner, K.; Murali, R. The Influence of Atmosphere on Electrical Transport in Graphene. *Carbon N. Y.* **2012**, *50* (5), 1727–1733.

(200) Huang, C.-H.; Lin, H.-Y.; Huang, C.-W.; Liu, Y.-M.; Shih, F.-Y.; Wang, W.-H.; Chui, H.-C. Probing Substrate Influence on Graphene by Analyzing Raman Lineshapes. *Nanoscale Res. Lett.* **2014**, *9* (1), 64.

(201) Sreeprasad, T. S.; Berry, V. How Do the Electrical Properties of Graphene Change with Its Functionalization? *Small* **2013**, *9* (3), 341–350.

(202) Coletti, C.; Riedl, C.; Lee, D. S.; Krauss, B.; Patthey, L.; Von Klitzing, K.; Smet, J. H.; Starke, U. Charge Neutrality and Band-Gap Tuning of Epitaxial Graphene on SiC by Molecular Doping. *Phys. Rev. B - Condens. Matter Mater. Phys.* **2010**, *81* (23), 1–8.

(203) Das, A.; Pisana, S.; Chakraborty, B.; Piscanec, S.; Saha, S. K.; Waghmare, U. V; Novoselov, K. S.; Krishnamurthy, H. R.; Geim, a K.; Ferrari, A. C.; et al. Monitoring Dopants by Raman Scattering in an Electrochemically Top-Gated Graphene Transistor. *Nat. Nanotechnol.* **2008**, *3* (4), 210–215.

(204) Wu, Q.; Wu, Y.; Hao, Y.; Geng, J.; Charlton, M.; Chen, S.; Ren, Y.; Ji, H.; Li, H.; Boukhvalov, D. W.; et al. Selective Surface Functionalization at Regions of High Local Curvature in Graphene. *Chem. Commun.* **2013**, *49* (7), 677–679.

(205) García, D.; Rodríguez-Pérez, L.; Herranz, M. A.; Peña, D.; Guitián, E.; Bailey, S.; Al-Galiby, Q.; Noori, M.; Lambert, C. J.; Pérez, D.; et al. A C60-Aryne Building Block: Synthesis of a Hybrid All-Carbon Nanostructure. *Chem. Commun. (Camb).* **2016**, *52* (40), 6677–6680.

(206) Fagan, S. B.; Souza Filho, A. G.; Lima, J. O. G.; Mendes Filho, J.; Ferreira, O. P.; Mazali, I. O.; Alves, O. L.; Dresselhaus, M. S. 1,2-Dichlorobenzene Interacting with Carbon Nanotubes. *Nano Lett.* **2004**, *4* (7), 1285–1288.

(207) Wang, A.; Yu, W.; Huang, Z.; Zhou, F.; Song, J.; Song, Y.; Long, L.; Cifuentes, M. P.; Humphrey, M. G.; Zhang, L.; et al. Covalent Functionalization of Reduced Graphene Oxide with Porphyrin by Means of Diazonium Chemistry for Nonlinear Optical Performance. *Sci. Rep.* **2016**, *6* (1), 23325.

(208) Venkataramani, S.; Winkler, M.; Sander, W. 1,2,3-Tridehydrobenzene. *Angew. Chemie - Int. Ed.* **2005**, *44* (39), 6307–6311.

(209) Marquart, R.; Balster, A.; Sander, W.; Kraka, E.; Cremer, D. P-Benzyne. *Angew. Chem. Int. Ed.* **1998**, *37* (7), 955–958.

(210) Sato, T.; Moriyama, M.; Niino, H.; Yabe, A. Direct Observation of 1,2-Didehydronaphthalene in a Low Temperature Argon Matrix: Consecutive Photolysis of 1,2-Naphthalenedicarboxylic Anhydride. *Chem. Commun.* **1999**, No. 12, 1089–1090.

(211) Wenk, H. H.; Balster, A.; Sander, W.; Hrovat, D. a.; Borden, W. T. Matrix Isolation of Perfluorinated P-Benzyne W.S., H.H.W., and A.B. Thank the Deutsche Forschungsgemeinschaft and the Fonds Der Chemischen Industrie, W.T.B. and D.A.H. the National Science Foundation for Financial Support. The Systematic Name for Perfluor. *Angew. Chem. Int. Ed.* **2001**, *40* (12), 2295–2298.

(212) Leroi*, H.-H. N. and G. E.; Department. First Direct Observation of Pyridyne: Matrix Infrared Study of the Photolysis Products of 3,4-Pyridine Dicarboxylic Anhydride. **1988**, No. 13, 4096–4097.

(213) Sato, T.; Niino, H.; Yabe, A. Consecutive Photolyses of Naphthalenedicarboxylic Anhydrides in Low Temperature Matrixes: Experimental and Computational Studies on Naphthynes and Benzocyclopentadienylideneketenes. *J. Phys. Chem. A* **2001**, *105* (33), 7790–7798.

(214) Radziszewski, J. G.; Waluk, J.; Kaszynski, P.; Spanget-Larsen, J. High-Resolution Spectroscopic Study of Matrix-Isolated Reactive Intermediates: Vibrational Assignments for 3-Fluoro-O-Benzyne and Perfluoro-O-Benzyne. *J. Phys. Chem. A* **2002**, *106* (29), 6730–6737.

(215) Wang, Q. H.; Jin, Z.; Kim, K. K.; Hilmer, A. J.; Paulus, G. L. C.; Shih, C. J.; Ham, M. H.; Sanchez-Yamagishi, J. D.; Watanabe, K.; Taniguchi, T.; et al. Understanding and Controlling the Substrate Effect on Graphene Electron-Transfer Chemistry via Reactivity Imprint Lithography. *Nat. Chem.* **2012**, *4* (9), 724–732.

(216) Suggs, K.; Reuven, D.; Wang, X. Q. Electronic Properties of Cycloaddition-Functionalized Graphene. *J. Phys. Chem. C* **2011**, *115* (8), 3313–3317.

(217) Sulleiro, M. V; Quiroga, S.; Peña, D.; Pérez, D.; Guitian, E.; Criado, A.; Prato, M. Microwave-Induced Covalent Functionalization of Few-Layer Graphene with Arynes Under Solvent-Free Conditions. *Chem. Commun.* **2018**, 1–4.

(218) E. K. Fields and S. Meyerson. Benzyne by Pyrolysis of Phthalic Anthydride. *Chem. Commun.* **1965**, 474.

(219) Hoffman, R. W. *Dehydrobenzene and Cycloalkynes*; 1967.

(220) Barwich, S.; Khan, U.; Coleman, J. N. A Technique To Pretreat Graphite Which Allows the Rapid Dispersion of Defect-Free Graphene in Solvents at High Concentration. *J. Phys. Chem. C* **2013**, *117* (37), 19212–19218.

(221) Malard, L. M.; Pimenta, M. a.; Dresselhaus, G.; Dresselhaus, M. S. Raman Spectroscopy in Graphene. *Phys. Rep.* **2009**, *473* (5-6), 51–87.

(222) Fields, E. K.; Meyerson, S. OCTOBER 1966 ARYNES BY PYROLYSIS OF ACID ANHYDRIDES Arynes by Pyrolysis of Acid Anhydrides. *J. Am. Chem. Soc.* **1966**, *31* (October), 3307.

(223) Science, E. Microwave-Assisted Pyrolysis of Biomass Feedstocks : The Way Forward ? **2012**, 5481–5488.

(224) Kappe, C. O. Controlled Microwave Heating in Modern Organic Synthesis Angewandte. **2004**, 6250–6284.

(225) Wei, D.; Liu, Y.; Wang, Y.; Zhang, H.; Huang, L.; Yu, G. Synthesis of N-Doped Graphene by Chemical Vapor Deposition and Its Electrical Properties 2009. **2009**.

(226) Moulder, J. F.; Stickle, W. F.; Sobol, P. E.; Bomben, K. D. Handbook of X-Ray Photoelectron Spectroscopy: A Reference Book of Standard Spectra for Identification & Interpretation of XPS Data, 3rd Ed. **1995**.

(227) Kasry, A.; Ardakani, A. A.; Tulevski, G. S.; Menges, B.; Copel, M.; Vyklicky, L. Highly Efficient Fluorescence Quenching with Graphene. *J. Phys. Chem. C* **2012**, *116* (4), 2858–2862.

(228) Shen, C.; Brozena, A. H.; Wang, Y. Double-Walled Carbon Nanotubes: Challenges and Opportunities. *Nanoscale* **2011**, *3* (2), 503–518.

(229) Park, S.; Srivastava, D.; Cho, K. Generalized Chemical Reactivity of Curved Surfaces: Carbon Nanotubes. *Nano Lett.* **2003**, *3* (9), 1273–1277.

(230) León, V.; Quintana, M.; Herrero, M. A.; Fierro, J. L. G.; Hoz, A. de la; Prato, M.; Vázquez, E. Few-Layer Graphenes from Ball-Milling of Graphite with Melamine. *Chem. Commun.* **2011**, *47* (39), 10936.

(231) Zhao, W.; Fang, M.; Wu, F.; Wu, H.; Wang, L.; Chen, G. Preparation of Graphene by Exfoliation of Graphite Using Wet Ball Milling. *J. Mater. Chem.* **2010**, *20* (28), 5817.

(232) Zhang, M.; Parajuli, R. R.; Mastrogiovanni, D.; Dai, B.; Lo, P.; Cheung, W.; Brukh, R.; Chiu, P. L.; Zhou, T.; Liu, Z.; et al. Production of Graphene Sheets by Direct Dispersion with Aromatic Healing Agents. *Small* **2010**, *6* (10), 1100–1107.

(233) Yang, H.; Hernandez, Y.; Schlierf, A.; Felten, A.; Eckmann, A.; Johal, S.; Louette, P.; Pireaux, J.; Feng, X.; Mu, K.; et al. A Simple Method for Graphene Production Based on Exfoliation of Graphite in Water Using 1-Pyrenesulfonic Acid Sodium Salt. **2012**, *3* (0).

(234) Bari, R.; Tamas, G.; Irin, F.; Aquino, A. J. A.; Green, M. J.; Quitevis, E. L. Direct Exfoliation of Graphene in Ionic Liquids with Aromatic Groups. *Colloids Surfaces A Physicochem. Eng. Asp.* **2014**, *463*, 63–69.

(235) Stolle, A.; Szuppa, T.; Leonhardt, S. E. S.; Ondruschka, B. Ball Milling in Organic Synthesis: Solutions and Challenges. *Chem. Soc. Rev.* **2011**, *40* (5), 2317.

(236) Himeshima, Y.; Sonoda, T.; Kobayashi, H. Fluoride-Induced 1,2-Elimination of O-Trimethylsilylphenyl Triflate to Benzyne under Mild Conditions. *Chem. Lett.* **1983**, *12* (8), 1211–1214.